FUTURE POSSIBILITIES FOR LEP

D. Treille
CERN, Geneva, Switzerland

ABSTRACT

To go beyond the LEP 1 programme, one can

1. increase the c.m. energy;
2. increase the luminosity, an option technically related to the previous one;
3. increase the sensitivity to possible deviations from the Standard Model by polarizing the beams.

These upgrades open up the way to many possibilities for physics concerning accurate measurements as well as searches for new effects. They also require, from the theoretical and experimental points of view, several improvements and changes. These various topics and their interrelatedness are reviewed and discussed.

1 INTRODUCTION

In these lectures I would like to discuss how the standard CERN LEP programme, which started one year ago, could be developed and improved. In spite of its rich potential, which has been thoroughly explored during the course of several workshops, the LEP 1 era has limitations for several domains of interesting physics. These limitations are due either to the insufficient available energy, or to a lack of statistics, or to a non-optimal intrinsic sensitivity of the measurements.

Before embarking on physics (in Section 2), a few basic facts about the LEP machine, its present performances, and its use are reviewed, so that the problems encountered in the various options can be better understood. In Section 3, I do the same for the experimental and instrumental aspects, focusing on a few critical items.

In Section 4 the LEP 1 programme [1, 2] is summarized, with its dual aspect of accurate measurements and direct searches for new phenomena; emphasis is laid mostly on new ideas or computations that have occurred since the first Workshop [1]. The results obtained so far are briefly reviewed.

In Section 5, after giving a short description of what could be the pretzel LEP (i.e. multibunch operation), I discuss what should be the impact on physics if the luminosity were to be increased by an order of magnitude, on or near the Z peak, with respect to accurate measurements, rare decays of the Z, and fermion-antifermion physics, especially beauty-antibeauty. The experimental implications are also briefly discussed.

Section 6, inspired mostly by Ref. [3], summarizes the physics that will be accessible at LEP 200: W pairs, potential discoveries [in particular, in the supersymmetric (SUSY) Higgs sector], and accurate measurements. Some technical aspects of the required RF system are described. The effect of the actual choice of the energy end-point on the physics potential is briefly discussed.

Section 7, after recalling that spin is at the heart of electroweak interaction, describes how longitudinal polarization of LEP beams could improve the quality of our test of the Standard Model (SM) [4]. By combining different types of measurements, deviations from the SM can be unambiguously attributed to specific sources of new physics. However, building up, maintaining, rotating, and exploiting polarization properly is certainly a non-trivial enterprise: the problems encountered and their possible solutions are described, as well as the recently started R&D programme that led to a first observation of transverse polarization at LEP.

2 SOME ASPECTS OF THE LEP MACHINE

2.1 Synchrotron Radiation and its Effects

Synchrotron radiation has both positive and negative aspects for circular $e^{\pm}$ machines. The negative side is due to energy dissipation. About six photons are emitted per tesla metre and per electron, with a spectrum governed by the critical energy [5],

$$E_{\rm crit} = \frac{3}{2}\hbar c\gamma^3/\rho \ ,$$

where $\gamma \equiv E/m_e$ and ρ is the radius of curvature. For LEP at the Z peak, $E_{\rm crit} \simeq$ 100 keV. The loss per turn is $\propto \gamma^4/\rho$. Although this loss amounts to only 130 MeV at the Z peak, it becomes 2.8 GeV at $\sqrt{s} = 200$ GeV: it is therefore hopeless to think of getting much beyond this energy with a circular machine whose radius and cost would grow as E^2. Synchrotron radiation is sharply collimated ($\theta_{e\gamma} \approx 1/\gamma$), which helps when designing protection against it. A 100 keV photon flux is attenuated by a factor of $\sim$ 200 through 1 mm of lead. In 1 m of a typical gas for a time projection chamber (TPC), the probability that such a photon interacts, giving a small 'spot', is O(1%). We can go quite far in 'guesstimating' the fluxes and effects of synchrotron radiation by applying a few rules of thumb: for instance, by adopting an albedo of $\sim$ 1 for scattering at grazing angles, and of $\sim$ 1% for large-angle (more than a few milliradians) or backward scattering.

The loss of energy due to synchrotron radiation has to be compensated for. This is the role of RF cavities, which are grouped in a number of RF stations. At LEP 1, two straight sections (2 and 6) have RF stations symmetrically located on each side of the intersection point. For higher energies, the RF power will have to be more uniformly distributed around the machine; this implies the installation of cavities in the four experimental zones in order to avoid optical problems due to a local mismatch between the energies in both beams (Bassetti effect [6]).

To compensate for the energy loss, an accelerating field $E_{\rm acc}$ has to be present over a length l. For fixed l the required field scales as $\sim E_{\rm beam}^4$. The power transferred to the beam is

$$P_{\rm beam} = 2I_{\rm beam}E_{\rm acc}l\sin\phi \ ,$$

with $\sin\phi$ not far from unity. It can be seen that an increase of beam current $I_{\rm beam}$ as well as of beam energy requires more power. At present, the copper RF cavities are at room temperature, with $E_{\rm acc} \simeq 2.5$ MV/m and a total length $l \simeq$ 270 m for 128 cavities. To reach higher energies and/or current, they will have to be replaced by superconducting (SC) ones [7], and two varieties have been tested: pure niobium, and copper coated with niobium. The future set of cavities will be of the second type. We will come back to this question in Section 6. The acceleration yield $\equiv P_{\rm beam}/P_{\rm mains}$ should go from $\sim$ 10% (normal cavities) to $\sim$ 50% (SC ones).

Another important aspect of the RF cavities is their transverse impedance, which governs the way in which the beam acts on itself through its surroundings. The main limitation on the current is indeed an instability due to the transverse coupling mode, i.e. a short-range wake-field effect [8]. The instability is reached for

$$I_{\rm thresh} \propto E_{\rm beam}\frac{1}{\sum_i \beta_i K_i(\sigma)} \ ,$$

where $K_i(\sigma)$ is the factor of transverse loss for element i, and β_i is the β function at its location. The limitation occurs at the lowest energy, i.e. at the energy of injection. Of all the beam elements, the Cu warm cavities have the biggest K factor, whereas that of the SC cavities is much smaller (five to six times). To be able to reach currents that are larger than the planned one (3 mA per beam), SC cavities are required instead of warm ones.

On the other hand, synchrotron emission damps the oscillations of the beams in all three degrees of freedom. The damping times of horizontal betatron oscillations and synchrotron oscillations are coupled, and their ratio can be adjusted by varying the damping partition numbers J_x and J_s, related by $J_x + J_s = 3$. With a horizontal damping number J_x, the horizontal emittance leads to a size σ_x [9]:

$$\frac{\sigma_x^2}{\beta_x} \propto \gamma^2/Q^3J_x \ ,$$

where Q is the tune.

2.2 Luminosity

The most important factor is the luminosity, expressed by

$$L = \frac{fN^2}{4\pi k_b \sigma_x \sigma_y} ,$$

where N is the total number of particles *per beam* (which is why the number of bunches k_b appears in the denominator), $\sigma_{x,y}$ are the r.m.s. of the beam transverse dimensions (the shape is assumed to be Gaussian, x is horizontal, y vertical), and f is the revolution frequency.

In LEP 1 with four bunches, where $f = 10.8$ kHz (one turn in 92 μs, one crossing every $\sim$ 23 μs), $N = 1.71 \times 10^{12}$, $\sigma_x = 250$ μm, and $\sigma_y = 15$ μm, we find the canonical peak value of

$$L = 1.7 \times 10^{31} \text{ cm}^{-2} \text{ s}^{-1} .$$

An important parameter is the beam-beam factor $\bar{\xi}$, which measures the tune shift (change in the number of betatron oscillations) induced by one beam on the other:

$$\bar{\xi} = N r_e \beta_y^* / 2\pi k_b \gamma \sigma_x \sigma_y ,$$

where r_e is the classical electron radius.

If conditions are such that the beam-beam limit is reached, the luminosity can be re-expressed as

$$L = N f \gamma \bar{\xi} / 2 r_e \beta_y^* = \frac{k_b I_b \gamma \bar{\xi}}{2 e r_e \beta_y^*} ,$$

where I_b is the current per bunch. An interesting point is that $\bar{\xi}$ seems to have about the same value at various rings [10].

2.3 Other Parameters

With an average value for the vacuum already twice as good as the design value of 3×10^{-9} Torr, the lifetime will ultimately be dominated by beam-beam bremsstrahlung and be of the order of ~ 5 h.

The dispersion in energy is the result of an equilibrium between excitation due to synchrotron quantum emission and damping due to synchrotron radiation. This is analogous to the model of a damped harmonic oscillator with stochastic excitation. The dispersion σ_E is $\sim \gamma^2$ and reaches 200 MeV for $E_{\text{beam}} = 100$ GeV. This fact will be of deep concern when we consider the prospect for polarization.

2.4 Present situation

At the time of writing—one year after the start-up of LEP—the luminosity is $\sim 6 \times 10^{30}$ cm^{-2} s^{-1} (one third of the design). The total beam intensity has reached 4 mA. The lifetime is excellent (up to 10 h). The limitation in luminosity is due to a beam-beam effect that occurred at a lower intensity than was expected: above ~ 0.25 mA per bunch, the weakest bunch is exploded by the most intense one. There is an improvement when the current decreases, so that the intrinsic luminosity ($L/I_1 \times I_2$) increases with time. The equalization of the intensities of the various bunches, the choice of different optical tunes, etc., are possible remedies, which are being or will be tried progressively.

Another unexpected fact is the presence, all around LEP, of a weak multipolar magnetic field due to a layer of nickel which was deposited on the vacuum chamber and which unfortunately became magnetized. This may have harmful consequences, at least for polarization studies. Attempts to demagnetize the chamber are under way; meanwhile, the optics is being modified in order to make the performance less sensitive to the parasitic field.

3 THE EXPERIMENTS

It is beyond the scope of this lecture to describe here the four complicated detectors (ALEPH, DELPHI, L3, and OPAL), so I will focus on just a few points.

In the standard LEP 1, the bunches collide every 23 μs in the centre of the detectors. The size of the 'diamond' should be typically $\sigma_x = 250$ μm, $\sigma_y = 15$ μm, $\sigma_z \simeq 1.5$ cm.

3.1 Background

The background is synchronous with the bunch crossing. Synchrotron radiation, although very efficiently shielded by collimators [11], can nevertheless impinge on the vacuum chamber in the experimental region and be scattered into the detector. With the present diameter (16 cm) of the vacuum chamber and the optimal collimator setting, this background is negligible, except during particular operations such as squeezing the beam.

Another type of background is due to beam-gas interactions, i.e. electroproduction. With such a good vacuum, the rate is small, and the resulting interactions—asymmetric and involving only low-energy particles (≤ 1 GeV)—are easily identified. Electrons lost out of momentum are a potential problem for the small-angle normalization devices only.

For synchrotron radiation, however, the situation gets rapidly worse if we try to decrease the size of the vacuum chamber. A diameter of 12 cm should still be quite safe, but a further reduction in dimension, especially in the horizontal plane, would lead to a dramatic increase in the rate of synchrotron radiation into the detector. Figure 1 gives the result of an exercise made by Ritson and von Holtey [12], following earlier work by Roudeau [13]. The rate of synchrotron radiation arriving at the experimental region for standard LEP 1 running is $\sim 10^7$/s, 100 times more than with the present vacuum chamber. Whether this corresponds to the ultimate

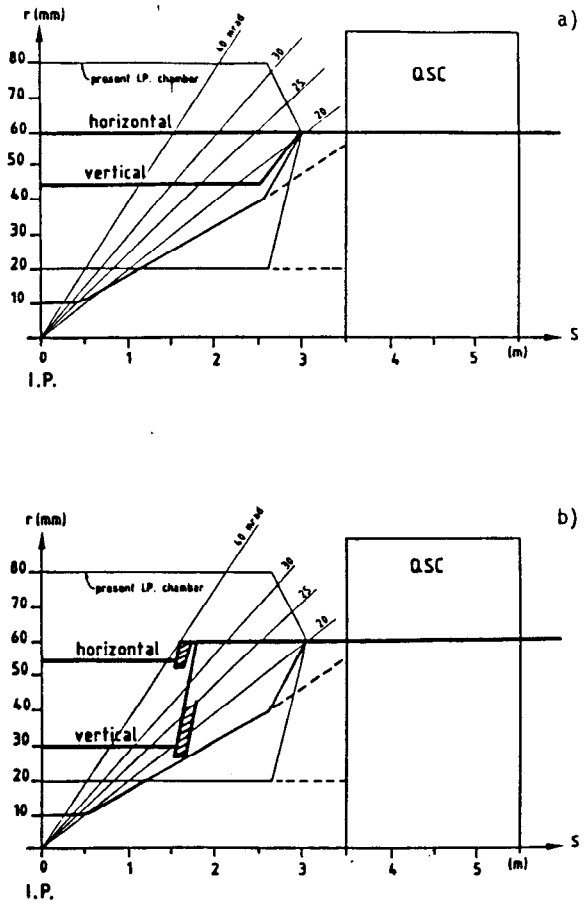

Fig. 1 Minimum radius foreseen for the vacuum chamber at LEP (from Ref. [12]): a) no mask, b) with masks.

tolerable level is certainly debatable and detector-dependent. Nevertheless, it appears that even with masks (Fig. 1b), there is no possibility of getting much below ± 3 cm vertically and ± 5 cm horizontally. For the next year of running, thin Be vacuum chambers of $r \simeq 5$ cm are being prepared. We will return to this problem in Section 5, where, having in mind bb physics, we will discuss what could be an optimal microvertex arrangement at LEP.

3.2 Normalization of the Detectors

All the detectors have a small-angle tagger (SAT) detecting Bhabha scattering in the angular region 50–150 mrad (except L3, whose SAT reaches a minimum angle of 25 mrad). The rate is about equal to the rate of Z's at the peak, so that normalization with the SAT contributes to the statistical error (by a factor of $\sqrt{2}$ for σ_{had}, except for L3). These are quite sophisticated instruments, combining segmented calorimetry and, at a later stage, accurate tracking; the absolute systematic errors have already been brought to the percent level.

The experiments usually have a very small angle tagger (VSAT) (5–10 mrad) with a much higher cross-section (20–30 times higher) and no longer any problem of statistics. However, as will be discussed in subsection 7.5, the systematic errors scale roughly as $\sim 1/\theta$, and using the VSAT will be *a priori* more tricky than using the SAT.

3.3 Long-Drift Devices

To get fine-grained space-point information from these huge barrel detectors, it is tempting to use the so-called time projection method. The principle is simple: the ionization of tracks in a gaseous volume is drifted along the axis of the barrel (which is also the $\vec{B}$ axis) by a longitudinal electric field (Fig. 2). The trajectories are thus projected onto the end-plates of the barrel, where planar detectors are located. The two transverse coordinates are obtained in the usual way (wire-pad arrangement); the longitudinal coordinate is obtained from the measured drift-time once the drift velocity is known.

This is the principle of the TPCs of ALEPH and DELPHI. In DELPHI, both the barrel electromagnetic (e.m.) calorimeter (the High-Density Projection Chamber) and the ring-imaging Cherenkov (RICH) barrel counter also use this method.

As the speed of the drift is typically 2–5 cm/μs, for a drift length of 1–2 m, the drift-time is quite substantial (~ 30 μs for the RICH). When an event candidate occurs at crossing i, crossing $i+1$ has to be lost if we are interested in the result of the full drift. With a smaller interbunch spacing, even more crossings would be lost. Since at LEP all crossings—or nearly all—are empty, this is of no importance as long as the number of candidate events (Level-1 trigger) is not too high (1 kHz would give a 2.5% dead-time). The trigger-1 decision has obviously to be made with faster detectors not involving the long-drift information itself, which can only

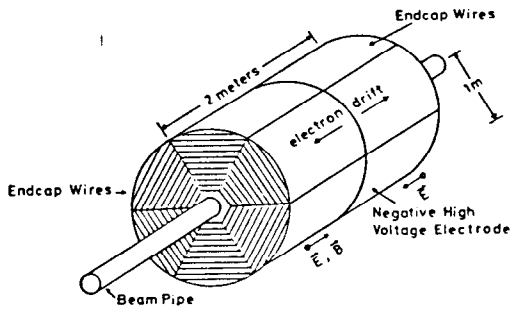

Fig. 2 The Time Projection Chamber.

be used at Level 2 to refute or confirm the previous decision. Level-1 rates are quite detector-dependent.

Long-drift devices have to be gated: this means that ionization created in them should be forbidden to enter the detector area unless it is thought to contain interesting information. This is done by acting on the E field in a transfer region. Two attitudes are possible: either i) the gate is opened before each crossing (4×10^4 times per second) and closed immediately if there is no Level-1 trigger for the crossing (the most frequent case), or ii) one waits for a Level-1 trigger to open the gate. With the first choice, the gate remains open during a substantial fraction of the time ($\sim 10\%$ under present conditions), but no information is lost because the opening has been anticipated. In the second case, the gate nearly always stays closed, but even with a very fast Level-1 answer it is not possible to avoid losing information at the edge of the detector. It may be that a third solution, in which the gating is operated as a diode, will be the right one.

The rate and speed of the Level-1 trigger and the gating methods will be of deep concern for multibunch operation at LEP.

4 THE STANDARD LEP PROGRAMME

The programme of LEP 1 is vast. Discoveries at the Z peak are possible in several domains (Higgs, supersymmetry, compositeness, etc.). Some could have been achieved with 10^3 to 10^4 Z, but up to now nothing new has been reported. Others will need $\geq 10^7$ Z. In the case of SUSY, the non-observation of at least a scalar that is lighter than or not far above the Z would be a hard blow to that theory or at least its minimal version.

Even if nothing appears directly, a whole set of accurate measurements (properties of the Z resonance, various asymmetries, τ polarization, neutrino counting, etc.) is guaranteed and will allow the SM to be tested more accurately than at present. By combining such measurements, eventual deviations from the SM expectations can be attributed unambiguously to the effect of new particles within the same gauge group SU(2) $\times$ U(1)—the so far undiscovered t-quark being the most obvious candidate—or to the effect of a different algebraic structure [14].

4.1 Accurate Measurements

4.1.1 The physical interest of accurate measurements

The physical goals of these measurements are clearly defined and thoroughly discussed, for instance in Ref. [15]. Here we will merely summarize them.

The main parameters of the SM are

$$g,\ g',\ \mu^2,\ \lambda\ ,$$

which represent, respectively, the SU(2) and the U(1) couplings and the two coefficients of the Higgs potential. Equivalently, one can choose

$$\alpha,\ m_Z,\ m_W,\ m_H.$$

In fact, while waiting for an accurate measurement of m_W, we replace it with G_μ, from μ decay.

In the minimal electroweak model, all quantities can be predicted using this set of parameters. In particular, $\sin^2\theta_w$ is no longer an independent quantity and is defined by

$$\sin^2\theta_w \equiv 1 - \frac{m_W^2}{m_Z^2}.$$

However, as a consequence of weak corrections, the prediction of some physical observables will depend also on the other parameters of the model: of these, besides the Higgs mass m_H, the most important is the t-quark mass m_t.

New physics, if any, will also influence the observables. Two classes of new phenomena can be distinguished: i) 'classical' ones, occurring within the algebraic structure of the SM, such as the existence of another family, and ii) 'genuine' new physics, implying a change of this algebraic structure (e.g. L-R symmetric models etc.).

To get information about these unknown parameters and domains, one must focus on observables that are very sensitive to them, that are not too sensitive to trivial effects such as e.m.radiative processes, that are well understood theoretically, and that can be measured with great accuracy.

Apart from m_Z, the most interesting observables are m_W—which will be accurately measured at the hadron colliders [16] and still better at LEP 2 [17]—and the left-right asymmetry A_{LR} on top of the Z [18]. These quantities are very sensitive to the weak radiative corrections corresponding to loop effects in the boson propagators (the 'oblique' corrections of Fig. 3a) governed by m_t, m_H, SUSY, etc.

There is another category of observables, involving eventually the measurement of polarized charge asymmetries A_{ch}^{pol} [19], that are ideal for sensing changes in the algebraic structure already at the tree level. These changes can result from a more complicated Higgs sector, or from the existence of new Z' bosons, compositeness, etc.—that is to say, 'genuine' new physics.

Both A_{LR} and A_{ch}^{pol} require beam polarization.

The definition and properties of these observables will be given in subsection 3.1.2. In the following subsections we shall discuss their measurement on the Z.

4.1.2 The observables

4.1.2.1 The masses of the weak bosons. The Z mass—which, from the CERN $p\bar{p}$ Collider, was known to ~ 2 GeV/c^2—is obtained with extreme accuracy at the SLAC Linear Collider (SLC) [20] and at LEP 1 [21]. The results already available are summarized in Table 1 [22]. Below, we discuss the factors that govern the uncertainties of such measurements. If transverse polarization is used through the resonant depolarization method [23], which gives an excellent absolute calibration of the beam energy, an accuracy of Δm_Z = a few MeV is foreseen. Various studies show that the uncertainty in the modification of the Z peak by radiative effects, and especially initial-state photon radiation, can be kept below this value [24].

The W mass, now known to ± 0.5 GeV/c^2, will be measured to $\sim \pm 150$–200 MeV/c^2 at the hadron colliders [16] and to ± 100 MeV/c^2 or better at LEP 200 [17]. Note, however, that this last measurement requires a substantial integrated luminosity (≥ 500 pb^{-1}).

4.1.2.2 The asymmetries. Let us now turn to the asymmetries on the Z. We start from the current

$$J_Z = \sum_f \bar{f}\gamma_\mu \left[g_L^f \frac{1+\gamma_5}{2} + g_R^f \frac{1-\gamma_5}{2} \right] f\ .$$

With

$$v_f \equiv \frac{1}{2}\left[g_L^f + g_R^f\right] = \frac{e}{2\sin\theta_w\cos\theta_w}\left[I_{3L}^f - 2Q^f\sin^2\theta_w\right],$$

$$a_f \equiv \frac{1}{2}\left[g_L^f - g_R^f\right] = \frac{e}{2\sin\theta_w\cos\theta_w}\left[I_{3L}^f\right],$$

and defining

$$A^f \equiv \frac{2v_f a_f}{a_f^2 + v_f^2} = \frac{g_L^{f^2} - g_R^{f^2}}{g_L^{f^2} + g_R^{f^2}},$$

we get for the angular distribution of the produced fermion f (Fig. 4a) a formula of the type:

$$\begin{aligned} d\sigma &\approx \left(g_L^{e^2} + g_R^{e^2}\right)\left(g_L^{f^2} + g_R^{f^2}\right) \times (1+\cos^2\theta) + \left(g_L^{e^2} - g_R^{e^2}\right)\left(g_L^{f^2} - g_R^{f^2}\right) \times (2\cos\theta) \\ &\approx 4\,(v_e^2 + a_e^2)\,(v_f^2 + a_f^2) \times (1+\cos^2\theta) \\ &\quad + 16(v_e a_e)(v_f a_f) \times (2\cos\theta)\ . \end{aligned}$$

In the case of a polarized beam, we simply have to add the contributions of the various helicity configurations (Fig. 4b):

$$g_L^{e^2} g_L^{f^2}(1+\cos\theta)^2 + g_L^{e^2} g_R^{f^2}(1-\cos\theta)^2 + \cdots.$$

a) The charge asymmetry. From the angular distribution obtained above, we easily get the front-back (FB) asymmetry, defined as

$$A_{FB} = \frac{\sigma_F - \sigma_B}{\sigma_F + \sigma_B},$$

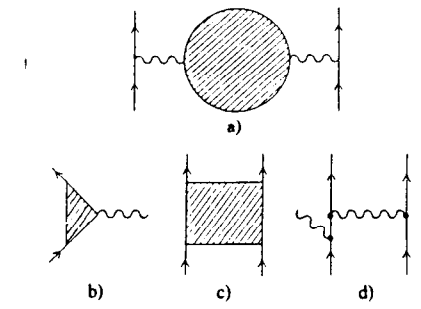

Fig. 3 Radiative corrections to the tree-level graph: a) oblique corrections; b) vertex corrections; c) box corrections; d) radiation corrections.

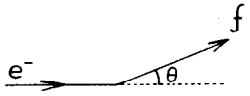

a) Conventions for $e^-e^+ \to f\bar{f}$

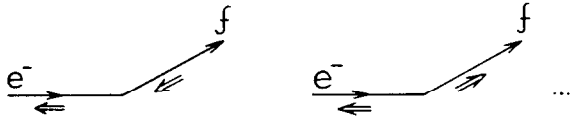

b) Various helicity configurations

Fig. 4 a) Conventions for $e^-e^+ \to f\bar{f}$ b) Various helicity configurations.

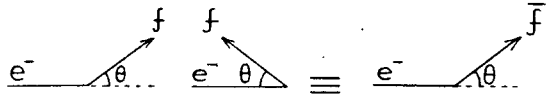

Fig. 5 The equivalence between A_{FB} and A_{ch} for $e^-e^+ \to f\bar{f}$.

where σ_F and σ_B are the fermion cross-sections in the forward and the backward hemisphere, and

$$A_{FB}^{e^-e^+ \to f\bar{f}} = \frac{\int_0^{2\pi} d\phi \left[\int_0^1 - \int_{-1}^0\right] d\cos\theta (d\sigma/d\Omega)(ee \to f\bar{f})}{\int_0^{2\pi} d\phi \left[\int_0^1 + \int_{-1}^0\right] d\cos\theta (d\sigma/d\Omega)(ee \to f\bar{f})}.$$

In the total angular domain,

$$A_{FB}^{ee \to f\bar{f}} = \frac{3}{4} A^e A^f.$$

A few remarks are relevant:

i) About an equal amount of information is obtained from the 'end-cap' ($\theta < 40°$) and 'barrel' ($\theta > 40°$) regions of the detectors.

ii) For a two-body reaction such as $ee \to f\bar{f}$, A_{FB} and the charge asymmetry A_{ch} are identical, as shown in Fig. 5. This is important for the systematics in the detector: since the measurement of A_{ch} involves the difference between acceptances for f and $\bar{f}$ (i.e. for opposite signs) in any angular region of the detector, we are dealing with only a second-order systematic effect, and the experimental problem regarding our knowledge of the acceptance is less critical.

iii) Because $A^e \simeq 2(1 - 4\sin^2\theta_w)$ is a small number, the asymmetry is itself small.

iv) The charge asymmetry A_{ch} is a rapidly varying function of $\sqrt{s}$ and is therefore strongly modified, up to a factor of 2, by initial-state radiation, the effect of which has thus to be very accurately determined to better than 10% of its value.

v) The unavoidable uncertainty in the location of the measurement relative to the pole (± 10 MeV/c^2) will, for the same reason, limit the accuracy on A_{ch} to 0.08%.

vi) Compared with the case of A_{LR}, the sensitivity of A_{ch} to $\sin^2\theta_w$, which can be written $\partial A_{ch}/\partial \sin^2\theta_w$, is small and goes to zero when $\sin^2\theta_w \to 1/4$.

vii) On the other hand, an advantage is that the measurement of A_{ch} is independent of the normalization.

b) Forward–backward asymmetry for a given polarization degree. Defining the polarization degree of the e^+e^- system as

$$P = \frac{P_{e^+} - P_{e^-}}{1 - P_{e^+}P_{e^-}},$$

$$A_{FB}^{pol.f} = \frac{\sigma_{P_F} - \sigma_{P_B}}{\sigma_{P_F} + \sigma_{P_B}},$$

we find on the Z

$$A_{FB}^{pol.f} \simeq \frac{3}{4}\frac{g_L^{f2} - g_R^{f2}}{g_L^{f2} + g_R^{f2}} \times \left[\frac{g_L^{e2}(1+P) - g_R^{e2}(1-P)}{g_L^{e2}(1+P) + g_R^{e2}(1-P)}\right].$$

For complete polarization of one beam, $P_{e^+} = 1$, $P_{e^-} = 0$:

$$A_{FB}^{pol.=1,(f)} \simeq \frac{3}{4} A^f,$$

which is a very simple expression. But in the usual case where $P_{e^+} < 1$, this asymmetry still depends on both the initial-state and the final-state couplings.

c) Polarized forward-backward asymmetry [19]. The above situation can be simplified by defining the quantity

$$A_{FB}^{pol.f} = \frac{1}{P} \frac{(\sigma_{PF} - \sigma_{-PF}) - (\sigma_{PB} - \sigma_{-PB})}{(\sigma_{PF} + \sigma_{-PF}) + (\sigma_{PB} + \sigma_{-PB})},$$

which on the Z is $\sim 3/4\ A^f$. This asymmetry has very interesting properties:

i) it depends on the nature of the final-state fermion only, and its measurement clearly calls for the individualization of the final states;

ii) it is not suppressed by the factor $(1 - 4\sin^2\theta_w)$;

iii) it is a slowly varying function of $\sqrt{s}$ around the Z, even when the γ term is included;

iv) it is quite insensitive to the experimental cuts.

d) Left–right asymmetry. Finally, let us define

$$A_{LR} \equiv \frac{1}{P} \frac{\sigma(+,-) - \sigma(-,+)}{\sigma(+,-) + \sigma(-,+)},$$

which is about equal to A^e. The sign refers to the helicity of e^- and e^+. Note that $\sigma(+,-) = 2\sigma(+,0) = 2\sigma(0,-)$, and these equalities show that various helicity configurations are equivalent. In particular, it is enough to polarize one beam, and

$$A_{LR} = \frac{\sigma_L - \sigma_R}{\sigma_L + \sigma_R},$$

where $\sigma_{L,R}$ are cross-sections for left- (right-)handed electrons.

As a function of A_{LR}, the Z cross-section for polarizations P^+ and P^- can be written as [25]

$$\sigma = \sigma_u[(1 - P^+P^-) + A_{LR}(P^+ - P^-)] .$$

A few remarks about this asymmetry:

i) It is virtually independent of the final state. Therefore, the full statistics on the Z can be used.

ii) The final-state correction is almost negligible.

iii) It is a smooth function of $\sqrt{s}$ around the Z pole, and initial-state radiation is not a problem.

iv) It is very sensitive to $\sin^2\theta_w$:

$$\Delta A_{LR} \simeq 8\Delta \sin^2\theta_w .$$

With 10^6 Z, the statistical accuracies for $P = 0.5$ are

$$\Delta A_{LR} = \pm 0.002 ,$$

$$\Delta \sin^2\theta_w = \pm 0.0003 .$$

v) This accuracy is well matched to the theoretical uncertainty in A_{LR} discussed in detail in Ref. [26].

vi) Any systematic uncertainty coming from the detector side is negligible. Small corrections to these statements can be found in Ref. [15]. All in all, the situation seems to be well under control: A_{LR} is certainly the ideal quantity for our purpose, and will be the centre of interest in Section 6.

e) Combinations of asymmetries. Asymmetries that are combinations of $A_{FB}^{pol.f}$, A_{FB}^f, and A_{LR} can also be defined and measured. As emphasized in Ref. [14], adequately chosen combinations may have interesting properties. For instance, the combination shown in Fig. 6 is sensitive specifically to changes in the algebraic structure of the gauge group [i.e. a structure that is not SU(2) × U(1)] and, on the contrary, is insensitive to effects occurring within this group structure, such as the existence of a new family.

Recent studies [27] demonstrate that combinations of accurate measurements on the Z, involving such flavour-dependent charge asymmetries, allow unambiguous discrimination between various sources of 'genuine' new physics, such as superstrings, compositeness, etc. This is illustrated by Fig. 7.

f) Summary. Figure 8 shows the main features of the various asymmetries considered: their magnitude, and their variation with the beam polarization and with energy.

Figure 9 illustrates the sensitivity of the two best observables, A_{LR} and m_W, to the main unknown parameters, m_t and m_H, once m_Z is known. It clearly shows that the information from m_W and that from A_{LR} are complementary and that, in this respect, the polarization is *not* an alternative to LEP 200. A detailed discussion of all effects that produce a dependence of A_{LR} on the final state can be found in Ref. [15]; the conclusion is indeed that these effects (or the uncertainty of how to correct for them) are well below the measurement accuracy of A_{LR}.

4.1.3 The Z parameters

4.1.3.1 The Z mass. In Table 1 [22] we gave the present results obtained at LEP, which can be compared with the $p\bar{p}$ Collider values [28].

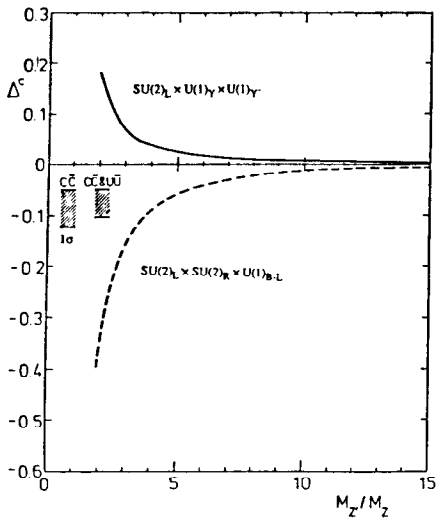

Fig. 6 Δ^u for two different gauge groups as a function of the Z′ mass, where $\Delta^u = \delta A_{RL} - (4/3)(\tilde{a}_e/\tilde{a}_u)\delta A_{FB}^{pol,u}$ (see Ref. [14] for definitions of $\tilde{a}_e, \tilde{a}_u$).

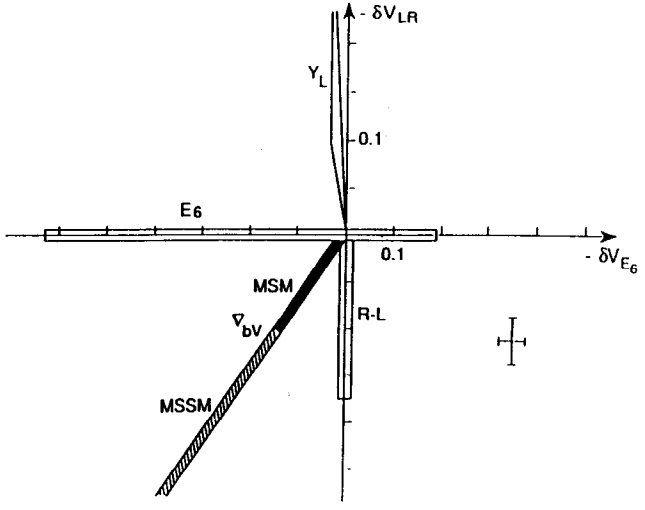

Fig. 7 The strategy to identify new physics. The δV_i are the deviations, from their Standard Model value, of quantities built up from appropriate linear combinations of LEP observables: $\Gamma_{b\bar{b}}, m_Z, m_W$, etc. The cross shows the experimental error expected from High Luminosity LEP.

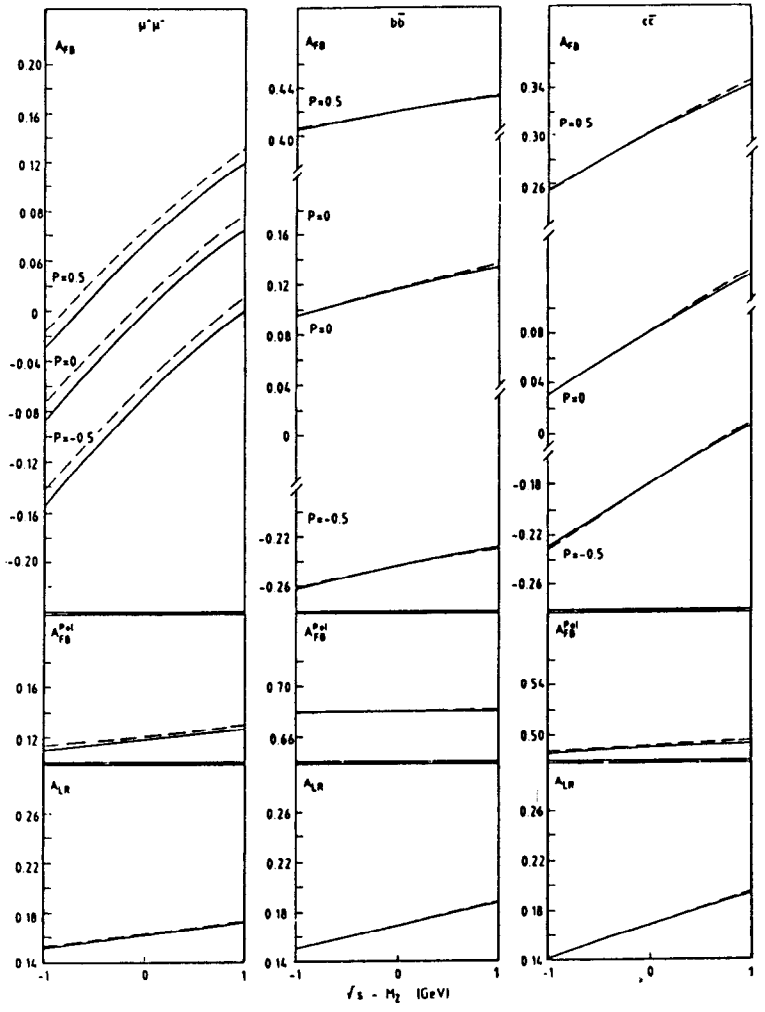

Fig. 8 The various asymmetries and their variation across the Z pole.

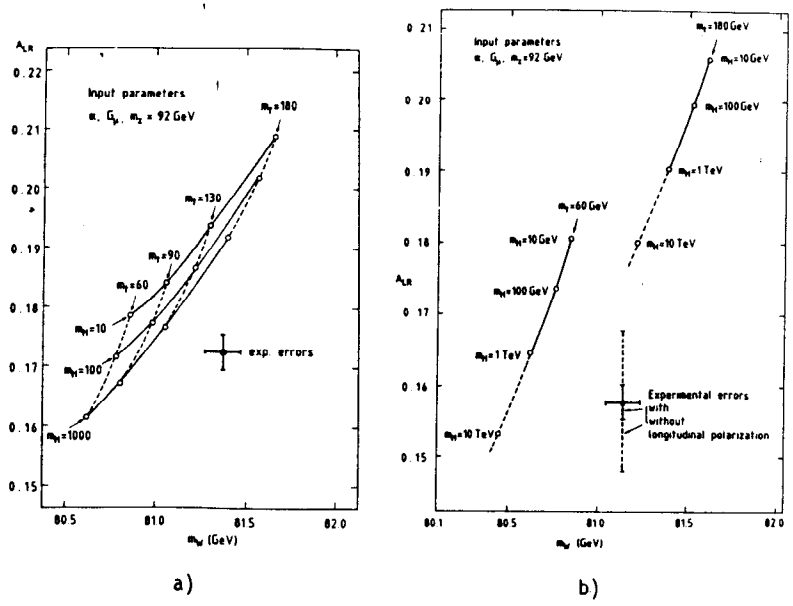

Fig. 9 Two ways of exhibiting the complementary information from A_{LR} and m_W (once m_Z is known).

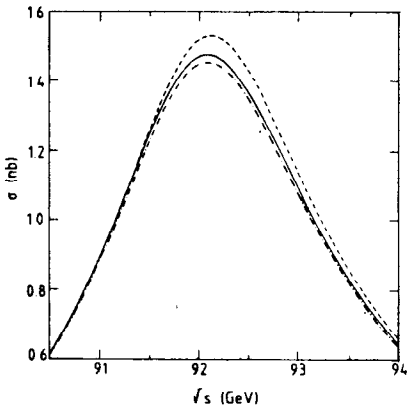

Fig. 10 Muon-pair line shape curve including all corrections. The masses are $m_Z = 91$, $m_H = 100$, and $m_t = 150$ GeV/c^2.

At LEP the mass has been obtained from a scan in energy over seven points. The statistical error is typically $\Delta m \simeq 3/\sqrt{N}$ GeV/c^2, where N is the total number of Z registered, but this error disappears rapidly.

Knowledge of the energy at which the measurements are made is clearly essential. The absolute value of the energy obtained from the B field along trajectories is not known to better than $\pm 5 \times 10^{-4}$.

Improvement can be achieved by injecting a beam of protons of well-known energy in order to calibrate the magnetic system; such a procedure has already been exploited. Protons of very well-known energy are injected into LEP and are brought into the same orbit as that of the electrons. The difference in RF between e and p, given the known proton momentum, allows us to get the LEP circumference. Then the protons are accelerated and brought to the physics energy. Again they are put on the same orbit as that of the electrons. Given the circumference, the variation in RF number allows us to obtain the momentum. However, the accuracy of the method is limited to ± 20 MeV/c^2.

Transverse polarization will allow us to perform an energy measurement by using the resonant depolarization method [23]. Without dedicated wigglers, we could only hope that the polarization would build up sufficiently for it to be detected in the polarimeter. This did indeed happen, but too late (in the last hours of 1990 LEP running) to allow for a resonant depolarization measurement to be carried out. In principle, the accuracy on absolute energy from such a measurement is $\sim 10^{-5}$. Nevertheless, unless we perform frequent calibrations, we will still be left with the problem of reproducibility and/or stability of the magnetic system ($\pm 0.5 \times 10^{-4}$). Other sources of uncertainty are:

– the relative normalization of the measurement from point to point (at the per mille level);

– the theoretical uncertainty; this is well under control to within a few MeV/c^2 (Ref. [24] and Fig. 10). In particular, the uncertainty in the mass of the t-quark and of the Higgs is of no importance here.

We can therefore assume that the uncertainty in the mass will go from the present 30 MeV/c^2 to $\sim$ 10 MeV/c^2 or better (long term). From the formula

$$\sin^2\theta = \frac{1}{2}\left[1 - \sqrt{1 - \frac{4\pi\alpha}{\sqrt{2}m_Z^2 G_\mu (1-\Delta r)}}\right],$$

we deduce $\Delta \sin^2\theta|_{m_Z} = 2.0\ (0.06) \times 10^{-4}$.

Whatever this means, I give this number to set the scale and to show the quality that is to be required from any other measurement, if we want to cross-check the coherence of the SM in a useful fashion.

4.1.3.2 Total width. For the width, the main goal is to get the number of neutrinos: a fourth light neutrino would increase the width by $\sim$ 170 MeV. In fact, more powerful methods exist, and we will discuss them later.

The statistical error is $\Delta\Gamma \simeq 6/\sqrt{N}$ GeV, but it fades away rapidly. At present the uncertainty is $\sim$ 25 MeV/c^2 per experiment. Ultimately we can ex-

pect to reach $\Delta\Gamma_Z \leq 10$ MeV, limited by the systematics on the beam and by relative normalization. Polarization here again could allow better values to be reached (ultimately 2–3 MeV). Theory is well under control, too. But here the uncertainties in the t-quark mass and in α_s are not completely negligible [29]:

$$\Delta\Gamma \text{ due to } m_t \approx 20 \text{ MeV},$$
$$\Delta\Gamma \text{ due to } \alpha_s\ (0.11 \pm 0.01) \approx 6 \text{ MeV}.$$

Present values can be read from Table 1.

4.1.3.3 Shape. The shape of the Z has been the subject of elaborate studies (see Ref. [15]) and is well understood. Moreover, there are several semi-analytical or analytical formulae that reproduce the Z shape to a good accuracy ($\leq 1\%$) and allow for a practical fitting procedure. Figure 11 gives a useful example [30].

The three measurements mentioned above require only a relative normalization, which should be achieved to a fraction of a per cent.

4.1.3.4 Hadronic absolute cross-sections and leptonic partial widths. Here, absolute normalization has to be achieved.

The goals of such measurements are important: i) to make a check of the universality in the leptonic sector, ii) to obtain the ingredients for neutrino counting, and iii) to search for the indirect effects of new objects [27].

Following the normalization procedures discussed in subsections 3.2 and 7.5, an absolute normalization error of 1.5–2% has been achieved, and we can ultimately think of $\sim 1\%$—or even better if the small-angle Bhabha cross-section is more reliably computed.

Identification of the three charged-lepton modes should be possible at the level of about a few per mille impurity and with good efficiency. In the case of τ pairs, the $e\mu$ and $h\ell$ events are characteristic: even ee and $\mu\mu$ modes can be used, provided cuts, as suggested by Fig. 12, are performed.

Acceptances for the leptonic modes are more tricky to obtain with great accuracy. The redundancy of all procedures (trigger, selection, reconstruction, etc.) should be used, instead of Monte Carlos, to *measure* the efficiency of each procedure against the others: for example, triggering $\mu\mu$ on one leg, keeping the tracking and identification of a μ independent, and so on. Since we are dealing with a measurement of the efficiency, it is clear that an increase in the statistics will also improve the systematics. Acceptances close to 100% with uncertainties of about 1% have already been achieved.

For hadronic events, no major problem with respect to acceptance is foreseen. Two-photon physics is easily removed by mild cuts. Here again the main uncertainty comes from normalization.

Existing results for the hadronic cross-sections and leptonic widths are given in Table 2 [22].

Fits to the hadronic cross-section in absolute value give access to the number of neutrinos, as we shall see in subsection 4.1.5.

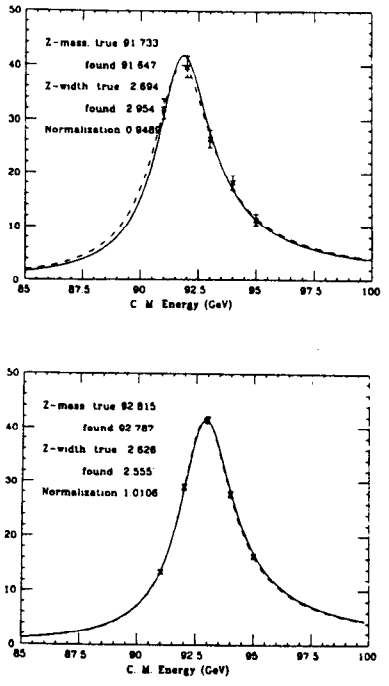

Fig. 11 Results of a simulation of total cross-section measurements near the Z, with the cross-section given in nanobarns. Data were generated corresponding to 10 nb^{-1} at each of five energies. A fit (dashed) was made to the simulated data using the known radiatively corrected line shape, but allowing the overall normalization to float. The second figure shows an analogous simulation with 100 nb^{-1} at each point. The solid curves show the true line shapes for the simulated masses and widths.

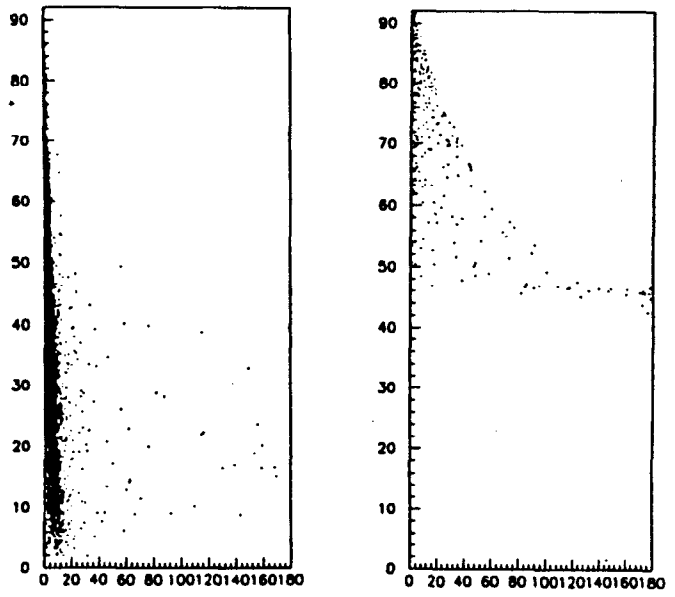

Fig. 12 Acoplanarity versus visible momentum for different Z decays: a) $Z \rightarrow \tau\tau$, b) $Z \rightarrow \mu\mu$.

4.1.4 Asymmetry measurements without polarization

Here we consider the measurement of the A_{ch} asymmetry and of the polarization of the τ.

4.1.4.1 Charge asymmetry for the $f\bar{f}$ final state. We saw that A_{ch} is a steep function of $\sqrt{s}$ (Fig. 8) and is therefore quite sensitive to the initial-state radiative corrections. This is especially critical for the $\mu^+\mu^-$ final state.

Recent and on-going work on radiative corrections [31], incorporating multiple photon emission and interference, will probably reach the level of accuracy that is required in order to match other sources of uncertainty.

The ignorance of the exact location relative to m_Z (± 10 MeV/c^2) is, however, an unavoidable source of uncertainty and, for $\mu\mu$, will contribute to limiting the accuracy that can be achieved.

Systematic errors are of different natures. For the $\mu\mu$ final state, the problem is to know the relative acceptances for positive and negative leptons to an accuracy of $\sim 1‰$, and this can be achieved using appropriate methods based on the principle of redundant procedures. For $q\bar{q}$ states, the main problem is quark identification and the estimate of the uncertainties in tagging efficiency and tagging purity: this will be discussed in subsection 7.7. From the information about fragmentation obtained in a preliminary exposure on the Z, it seems that quark identification can be reliable enough to allow excellent asymmetry measurements for the various flavours.

The statistical accuracy, which for $q\bar{q}$ is linked to the tagging efficiency, will be the dominant one for a long period. The increase in LEP luminosity (Section 5) will allow it to be reduced and in some cases made negligible in comparison with systematic errors.

The uncertainties expected for A_{ch} are summarized in Table 3a [32]. Although the systematic errors may look quite small, they are not so different from those quoted for the measurements of $\mu\mu$ or $q\bar{q}$ asymmetries done at PEP and PETRA [33]. Furthermore, we should take into account the much larger statistics available on the Z, which allow the systematic errors to be decreased as well, and the fact that various sources of instrumental problems (confusion of signs, mixing of e and μ, cosmic rays, etc.), still present at PEP and PETRA energies, are non-existent on the Z with the LEP detectors.

Nevertheless, it is clear that the information obtained from A_{ch} at LEP 1 is far less accurate than that from A_{LR}, as shown in Table 4. In particular, $A_{b,c}$ obtained from $A_{ch,b,c} = 3/4\ A_e A_{b,c}$ suffers from the uncertainty in A_e.

The results obtained so far for $A_{ch}^{b\bar{b}}$ are given in Table 3b: they should be compared with the possible ultimate achievements through A_{LR} or unpolarized asymmetries with higher luminosity (see subsection 5.3). An improvement of an order of magnitude is still to come.

For $A_{ch}^{\mu\mu}$ the present uncertainty is $\Delta A \sim 2 \times 10^{-2}$, dominated by statistics.

4.1.4.2 Tau polarization. Another way of determining $\sin^2\theta_w$ is by measuring the polarization of the τ, in $e^+e^- \rightarrow \tau^+\tau^-$.

On the Z,

$$\tilde{P}^{\tau}(\theta) = \frac{A^{\tau} + P(2\cos\theta/1+\cos^2\theta)}{1 + A^{\tau}P(2\cos\theta/1+\cos^2\theta)},$$

where

$$P \equiv \frac{P_e + A^e}{1 + P_e A^e}.$$

It can be seen that the mean value is equal to

$$A^{\tau}(\equiv A^e \text{ if universality holds}),$$

and therefore, in principle, the same information as that from A_{LR} can be obtained. However, if the observable is the energy distribution of the $\pi^{\pm}$ from the $\tau \to \pi\nu$ decay mode, the statistics are rather limited (6‰ of the Z final state is used), and some systematic error sources, mostly related to the background mode $\tau \to \rho\nu$, are present [34]. Again, Table 3 shows that the accuracy on $\sin^2\theta_w$ expected at LEP 1 is much (five times) worse than that obtained from A_{LR}.

In fact, τ leptonic decays, and especially $\tau \to \rho\nu$, $A_1\nu$, can be usefully exploited as well. Theoretical studies and preliminary results indicate that a global (but experimentally tricky) treatment of several final states could improve the accuracy by a factor of ~ 2.

Up to now, ALEPH has given the best results on P_τ through the leptonic, $\tau \to \pi\nu$ and $\tau \to \rho\nu$ channels. The values given in Table 3c are still far from the goal.

Putting together the information from all quantities obtained without beam polarization ($A_{ch}^{ff}, P_\tau, \Gamma^{ff}$) one can get an accuracy on $\sin^2\bar{\theta}_w$ which is presently ± 0.0023(ALEPH). With 4M (25M) Z it should reach ± 0.0008 (± 0.0004)per experiment.

4.1.5 The number of neutrinos

This is a crucial measurement. Moreover, since several theories [35] predict that at LEP it could be possible to obtain a non-integer number, we should try to get the best possible accuracy. Such theories can be supersymmetry, with a contribution to N_ν from sneutrinos, or various ideas involving mixing.

We have already discussed the limitation on N_ν from the direct width measurement. A more refined treatment has allowed us to do better. The invisible width method [36] rests on the exploitation of the obvious identity:

$$\Gamma_{invis} = \Gamma - \Gamma_{vis} = \Gamma - \Gamma_{had} - \Gamma_\ell.$$

Partial widths and cross-sections are related by

$$\sigma_X = \frac{12\pi}{m_Z^2}\,\frac{\Gamma_{ee}\Gamma_X}{\Gamma_{tot}^2}.$$

For instance,

$$\sigma_{\mu\mu} = \frac{12\pi}{m_Z^2}\,\frac{\Gamma_{ee}\Gamma_{\mu\mu}}{\Gamma_{tot}^2} \quad \text{and} \quad \sigma_{had} = \frac{12\pi}{m_Z^2}\,\frac{\Gamma_{ee}\Gamma_{had}}{\Gamma_{tot}^2}.$$

The idea, then, is to take, for some partial widths, the standard theoretical value. In the original proposal,

$$\Gamma_\ell = \Gamma_\ell^{stand}$$

was adopted. The widths Γ and Γ_{had} are extracted from the equations giving $\sigma_{\mu\mu}$ and σ_{had}: this implies the measurement of these two quantities and therefore a good knowledge of acceptances and radiative corrections for the $\mu\mu$ and hadronic channels. The use of the $\mu\mu$ channel leads to a limitation in statistics.

Another way is to take both Γ_{had} and Γ_ℓ as the standard values. We have only to measure σ_{had}. For $\sin^2\theta_w = 0.23$, the number of neutrinos can then be expressed as

$$N_\nu = \frac{2983}{\sqrt{\sigma_{had}(\text{pb})}} - 11.68,$$

or

$$\Delta N_\nu = \frac{N_\nu + 11.68}{2}\,\frac{\Delta\sigma_{had}}{\sigma_{had}}.$$

A 1% relative error on σ_{had} gives $\Delta N_\nu = 0.075$. In both methods the important fact is that cancellations occur in the error propagation, so that for a given luminosity the uncertainty is smaller than for Γ_{tot} measurements.

Figure 13 shows the present results as a function of the number of recorded Z, and also what one can expect from these methods. The limitation is clearly of a systematic nature related to normalization, and it ranges around $\Delta N_\nu = 0.1$.

This is quite excellent, and a number of people consider that the problem of the light-neutrino counting is solved.

Nevertheless, in the long term the radiative method [37] could be as accurate, with less dependence on standard assumptions. The idea is to sit somewhat higher than the Z peak and to measure

$$e^+e^- \to \gamma Z$$
$$\qquad\quad \llcorner\!\!\to \nu\bar{\nu},$$

i.e. a final state with a single γ. We can simply understand the observed γ spectrum as the product of a bremsstrahlung distribution by the Z resonance curve.

Elaborate calculations treating the graphs of Fig. 14 exist: Fig. 15 [38] shows how the γ spectrum and the cross-section are modified relative to the Born term. To obtain a sufficiently high cross-section, it is necessary to stay close to the Z peak. On the contrary, a larger $\sqrt{s}$ will give a harder photon spectrum, with a better known reconstruction efficiency as well as a safer theoretical picture.

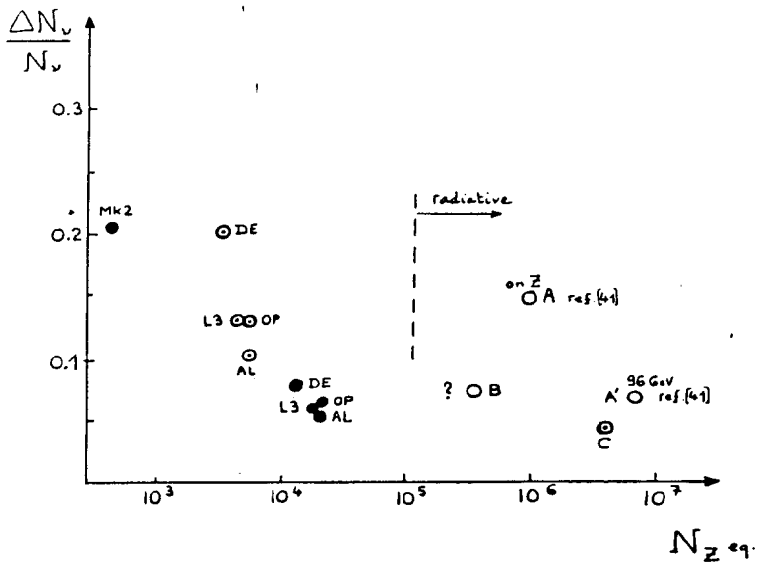

Fig. 13 $\Delta N_\nu/N_\nu$ obtained from width and invisible width measurements and expected from the radiative method (the points A, A', B, C are explained in the text).

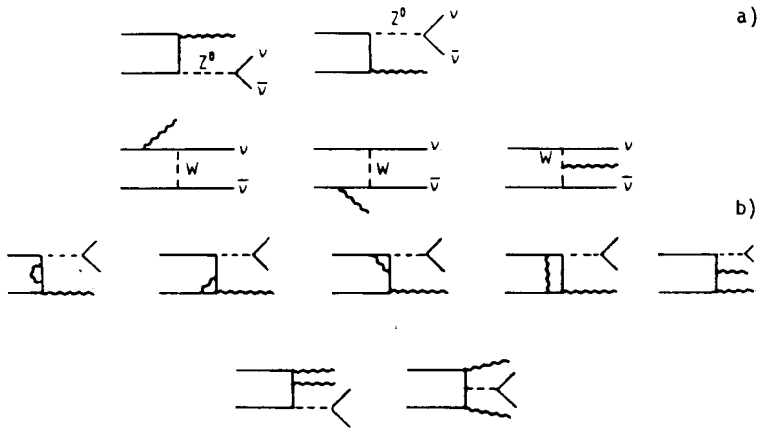

Fig. 14 a) Lowest-order diagrams contributing to $e^+e^- \to \nu\bar{\nu}\gamma$. b) $O(\alpha)$ radiative corrections.

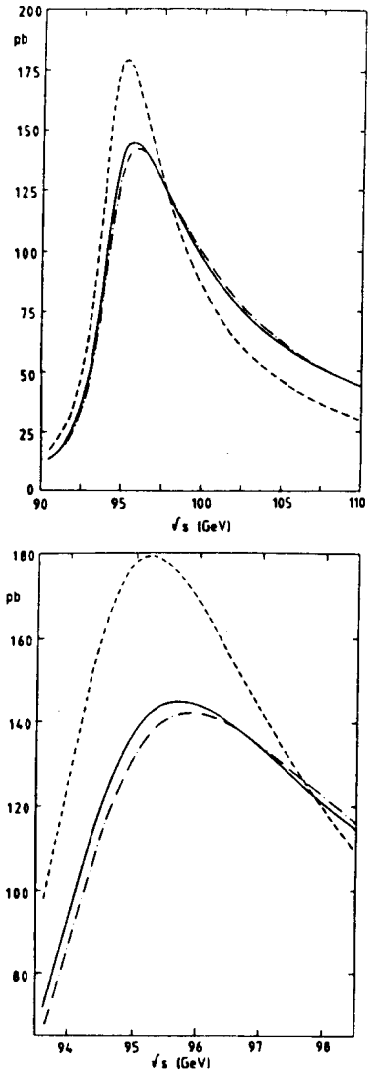

Fig. 15a, b Total cross-section (a) and blow-up (b) in the Born approximation (dashed line), fully corrected (solid line), and $O(\alpha)$-corrected (dash-dotted line) (from Ref. [38]).

The main background is ee → (ee)γ, with the final $e^{\pm}$ disappearing: it can be decreased by selecting γ at larger angles (> θ_{min} of Fig. 16) and vetoing $e^{\pm}$ down to very small angles (θ_{veto} of Fig. 16). Figure 17 gives an idea of the signal and the signal-to-background ratio as a function of θ_{min} and $\sqrt{s}$: the trend is clear.

In Fig. 13 we give an estimate of the power of the radiative method. The number of Z's should now be understood as the number that would be obtained by spending the same $\int L\, dt$ on the peak. Point A shows what can be obtained from an exposure of 10^6 Z at the peak [39]. This is, however, quite experiment-dependent since on the Z we must cope with fairly low energy photons. Only appropriate e.m. detectors (resolution at low energy, coverage) can effect such a measurement.

Point B shows what can be expected from 3×10^5 equivalent Z (about two weeks of nominal LEP) in the region 96–104 GeV [1]: this, however, looks optimistic.

From what we have said above, it is clear that an increase in luminosity should be quite profitable for radiative neutrino counting. We will come back to this topic in subsection 5.3. Anticipating the result, we show (point C) our estimate of what the pretzel LEP could bring to N_ν. Point A′ [39] is higher because the assumption about normalization is more conservative.

4.2 The 'Discoveries'

Perhaps the genuine role of LEP will be to provide a set of extremely accurate measurements, leading eventually to indirect discoveries. Nevertheless, it is legitimate to search first for all possible direct effects that have not yet been ruled out by previous experiments. They are numerous, so we shall focus on

i) the classical Higgs;
ii) supersymmetry:
- SUSY Higgses,
- charged Higgses and the t-quark problem,
- chargino and neutralino sectors;
iii) compositeness.

4.2.1 The classical Higgs

The search for the classical Higgs through the Bjorken reaction

$$ee \to ZH,$$

where the Z is either virtual (LEP 1) or real (LEP 200) and decays into $\ell^+\ell^-$ or $\nu\bar{\nu}$, has been studied *ad satietam* [40] (Fig. 18).

A recent development [41] concerns a possible source of background that was not fully considered in the past, namely

$$e^+e^- \to Z \to 4\text{fermions}.$$

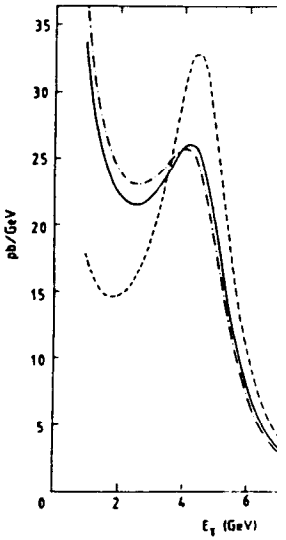

Fig. 15c Energy spectrum of the observed ph
line), fully corrected (solid-line), and O(α)-
Ref. [38]).

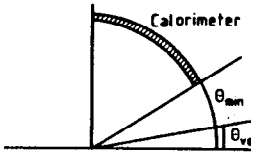

Fig. 16 Experimental set-up: θ_{veto} is the ve
detectable angle.

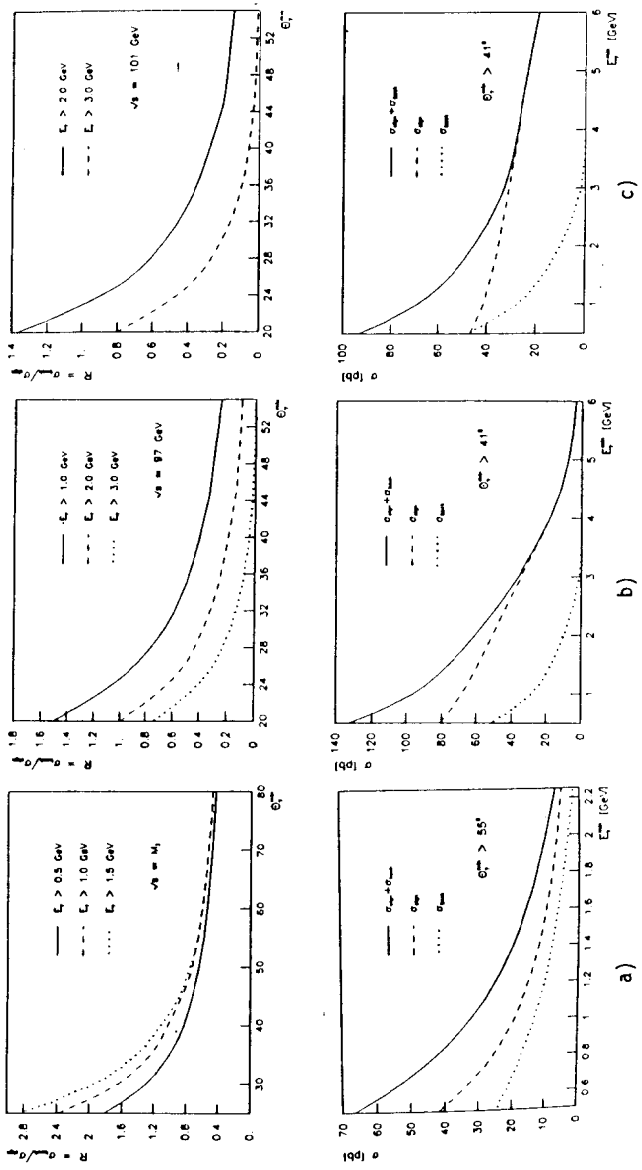

Fig. 17 The top part is the ratio of the cross-sections depending on the minimum polar angle at $E_{cm} = m_Z$ (a), $E_{cm} = m_Z + 4$ GeV (b), and $E_{cm} = m_Z + 8$ GeV (c). The bottom part shows the cross-sections of signal and background, depending on the energy cut at the same respective values of E_{cm}. (From E. Lieb, Ph.D. thesis, Univ. Wuppertal, 1989).

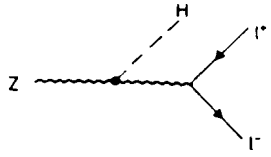

Fig. 18 Feynman diagram for the decay $Z \rightarrow H\ell^+\ell^-$.

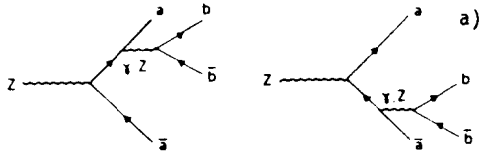

Fig. 19a Feynman diagrams for the decay $Z \rightarrow a\bar{a}b\bar{b}$. Four other diagrams are obtained by exchanging both fermions and antifermions ($a \leftrightarrow b, \bar{a} \leftrightarrow \bar{b}$).

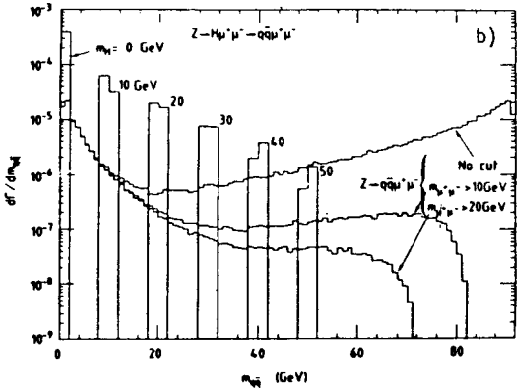

Fig. 19b The invariant mass distribution of the quark pair, $m_{q\bar{q}}$, produced in both $Z \rightarrow q\bar{q}\mu^+\mu^-$ decay and $Z \rightarrow H\mu^+\mu^- \rightarrow q\bar{q}\mu^+\mu^-$ decay for m_H = 0, 10, 20, 30, 40, 50, and 60 GeV/c^2. We show also the effect of a cut on the invariant mass of the muon pair, $m_{\mu^+\mu^-} > 10$ GeV/c^2 and $m_{\mu^+\mu^-} > 20$ GeV/c^2.

The process is shown in Fig. 19a and the cross-section is given in Table 5. This cross-section is large but, owing to the dominance of quasi-real γ exchange, the kinematics of the four-fermion state is quite peculiar: a pair at high mass and a pair at low mass, as shown by Fig. 19b; therefore, for the safe channels in the Higgs search, i.e. $Z \rightarrow \ell^+\ell^- b\bar{b}$, a cut on the dilepton mass eliminates this background.

The reach of LEP 1 to the 'safe' channel $Z \rightarrow H\mu^+\mu^-$ can be deduced from Fig. 20. A signal of 10 events for a Higgs of 50 GeV/c^2 would require 10^6 Z.

In fact, things went much faster through the exploitation of the channel $Z \rightarrow H\nu\bar{\nu}$, which is supposed to be six times more abundant [42]. Provided a good hermeticity prevents the occurrence of background, for instance from $ee \rightarrow q\bar{q}(\gamma)$, the γ being lost, one can, in the absence of any candidate, put quite strong limits. With $\sim$ 100,000 Z, ALEPH was, for example, able to exclude the Standard Higgs up to 42 GeV/c^2. Combining all four experiments, 48 GeV/c^2 can be reached. Provided the background situation stays the same, an order of magnitude in the number of Z would provide a gain of 10 GeV/c^2 on the limit.

4.2.2 Supersymmetry

Present results from e^+e^- machines and from the CERN $p\bar{p}$ Collider had already almost completely excluded the domain accessible to LEP 1, as far as sfermions are concerned (Fig. 21). This has been checked directly by the LEP experiments. LEP 200, on the contrary, will offer the possibility of pushing the mass limits to values approaching $\sqrt{s}/2$ (Fig. 22).

Nevertheless, it is now admitted that the two aspects of SUSY that are the most likely to reveal themselves at LEP are the SUSY Higgs sector and its chargino/neutralino sector.

4.2.2.1 SUSY Higgses. It took some time to realize how much this sector is constrained in minimal SUSY. Starting from the two complex doublets, after symmetry breaking we are left with two neutral scalars h^0 and H^0, a pseudoscalar A^0, and two charged Higgses H^+ and H^- (h^0 and A^0 are often called H_2, H_3 in the literature). The properties of the Higgses depend in particular on $\mathrm{tg}\,\beta \equiv v_2/v_1$, the ratio of vacuum expectation values.

Figure 23 [43] summarizes the situation in minimal SUSY:

At tree level:

i) There always exists at least one neutral scalar h^0 lighter than the Z (on the contrary, charged Higgses are heavier than the W);

ii) there is always a neutral scalar close to the Z mass (Fig. 23e,f);

On the Z:

iii) if $v_2/v_1 \leq 2$–3 (Fig. 23b), the lightest scalar h^0 is essentially produced like the standard Higgs;

iv) if v_2/v_1 is large, h^0 is produced in association with the pseudoscalar A^0 (Fig. 23c),

$$ee \rightarrow h^0A^0;$$

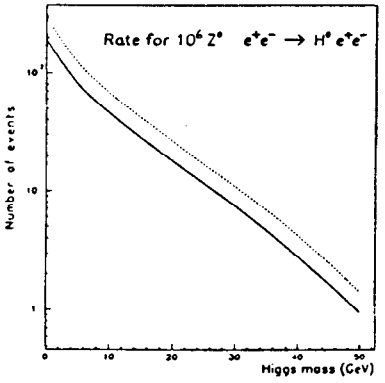

Fig. 20 Event rate with (solid) and without (dashed) radiative corrections versus Higgs mass, using $\alpha = 1/137$, $\sin^2\theta_w = 0.23$, $m_Z = 92$ GeV, $\Gamma_Z = 2.5$ GeV, and $\mathrm{BR}(Z \rightarrow \mu^+\mu^-) = 3\%$ (for 10^6 'tree-level' Z's).

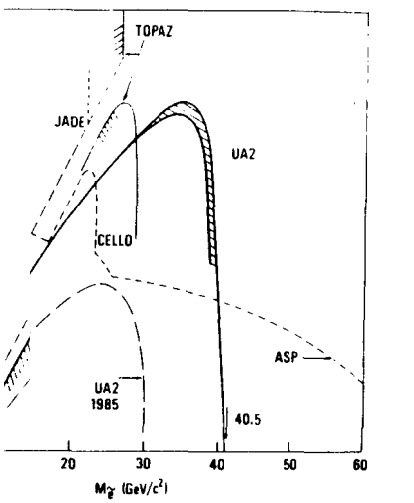

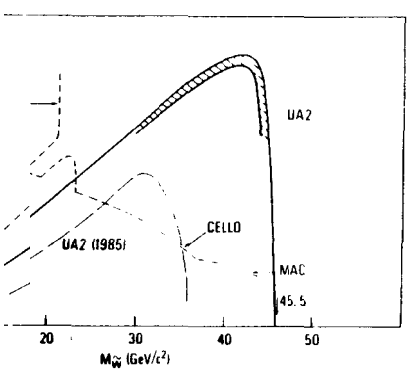

s lis for selectrons (top) and Winos (bottom) (pre-LEP).

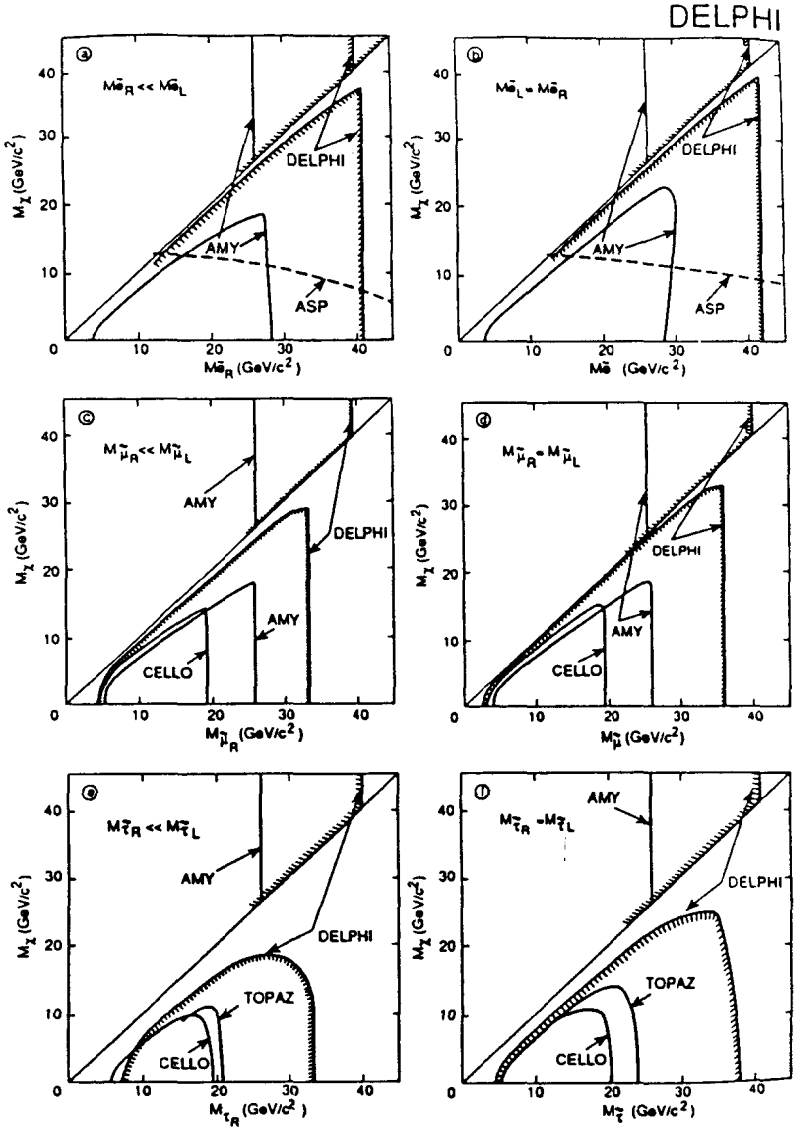

Fig. 21b LEP results on sleptons (DELPHI).

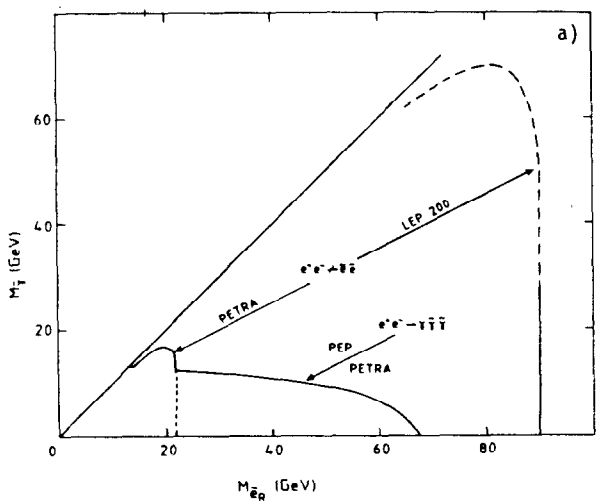

Fig. 22a Excluded $m_{\tilde{\gamma}}$–$m_{\tilde{e}}$ domain for stable photinos (Monte Carlo for LEP 200).

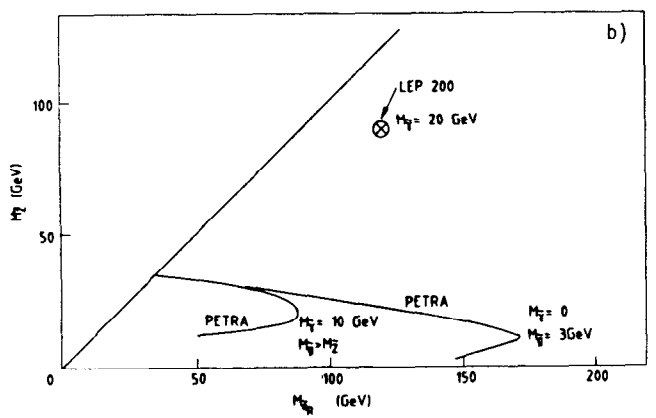

Fig. 22b Excluded $m_{\tilde{\gamma}}$–$m_{\tilde{e}}$ plane (Monte Carlo for LEP 200).

the relation between the masses of the two objects is given by Fig. 23a, which shows that they rapidly degenerate when v_2/v_1 increases. One sees that the associated production can be substantial, reaching a few per cent of the Z final state.

Furthermore, Figs. 24 [44] indicate that the decay into τ pairs is always copious (for $v_2/v_1 > 1$), giving a useful experimental handle to the selection of such a final state through $\tau\tau$ jet-jet, or even quadri-taus. Charm can play a role as well (inclusive D's).

Other possible Higgs channels around that theme should also be kept in mind.

All the 'theorems' stated above are valid for minimal SUSY and for several of its extensions. They are not completely unavoidable in a general model, but SUSY specialists agree that the non-existence of a light neutral scalar would make the theory appear quite contrived and unattractive. However loop diagrams involving the top and its spartners may modify the tree- level mass of the Higgses and in particular push m_{h^0} somewhat above m_Z. This shift critically depends on the top mass.

Whilst the large associated cross-section [which varies merely as (velocity)^3] and branching ratio into τ pairs have allowed us to explore rapidly a substantial region of the parameter space for large v_2/v_1, it will take much more effort, at LEP 1 and 200, to get an answer regarding the crucial assessment of point (i). One can visualize this from Fig. 25 giving the LEP results, and from Fig. 26 locating them within the allowed domain. In fact, the size of the region which is left open varies with the couple of parameters adopted! Although (tg β, m_h) emphasizes the road already covered, the choice (tg β, m_A) rather illustrates how far one has still to go.

4.2.2.2 Charged Higgses and the t-quark problem. In minimal SUSY, the $H^{\pm}$ are heavier than the W. Nevertheless, this sector should be explored systematically.

The present limit from CELLO [45] is $\sim$ 19 GeV/c^2. TRISTAN and LEP 1 have allowed us to push it to close to the respective kinematical limits, and LEP 200 will do the same.

It is interesting to examine this problem in conjunction with the mystery of the elusive t-quark. Figure 27a [46] shows the various possible regions in the $m_{H^{\pm}}$–m_t plane, as well as the existing experimental bounds. In region I the t-quark can only decay through $H^{\pm}$:

$$t \rightarrow Hb\ .$$

In region II there is competition between

$$t \rightarrow W^*b \qquad \text{and} \qquad t \rightarrow H^*b\ .$$

The relative importance expected for these decays is shown in Fig. 27b for the two models described in the caption.

Here again, decays through taus (Fig. 27c) will play an important role by providing a good means of identifying the state under scrutiny.

Figure 27d gives the present UA1 limit.

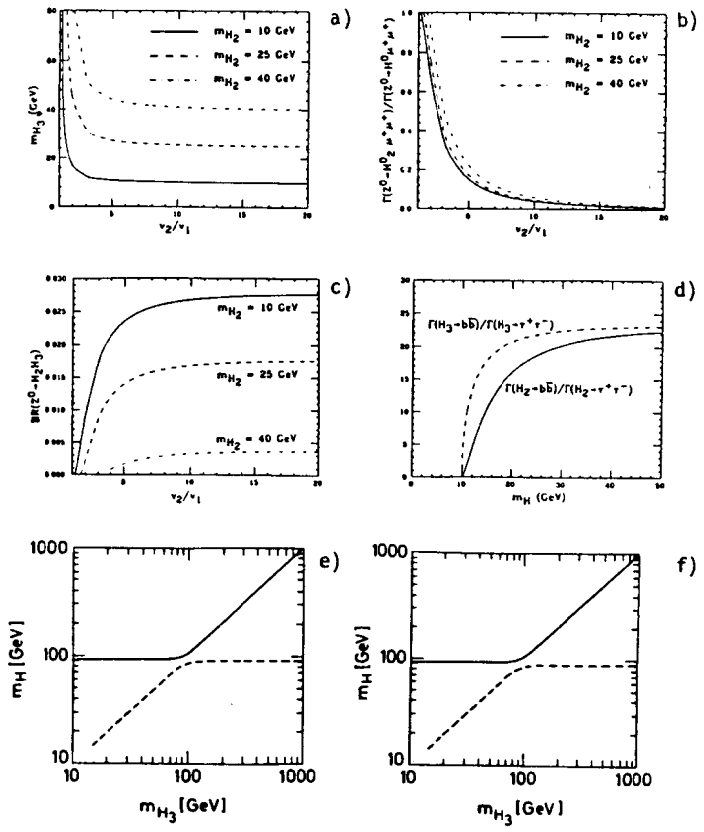

Fig. 23 The neutral Higgs system in minimal SUSY (from Ref. [43]): a) m_{H_3} versus v_2/v_1; b) BR of the $Z \to H_2\mu\mu$ versus v_2/v_1; c) BR of the $Z \to H_2H_3$; d) decays of H_2H_3. e, f) The relation between masses showing that one Higgs is close to the Z mass: the upper curve is for H^0, the lower one for h^0 (see Rutherford report RAL 89-077, 1989).

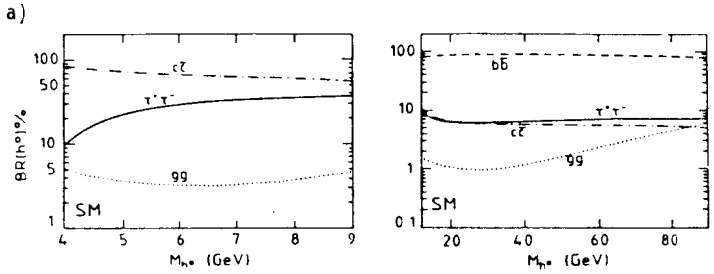

Fig. 24a Branching ratios for a scalar Higgs in the Standard Model.

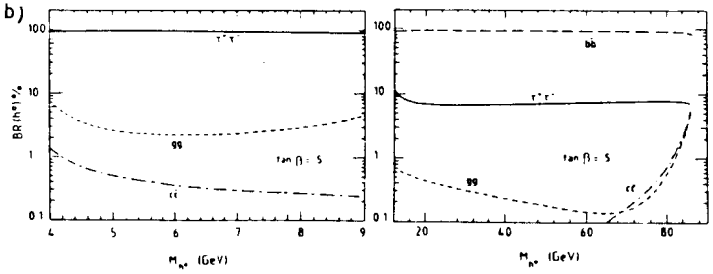

Fig. 24b Branching ratios for a scalar Higgs in the Minimal Supersymmetric Standard Model with $\tan\beta = 5$.

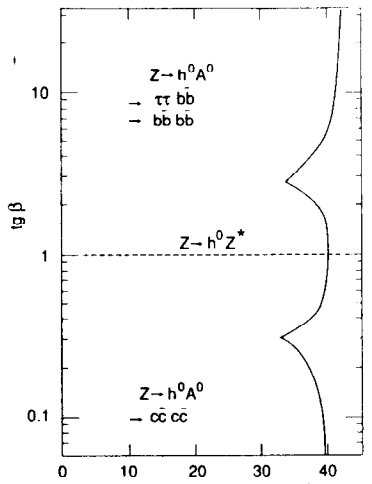

Fig. 25 The LEP results on SUSY Higgs (all experiments combined): tan β versus m_{h^0}.

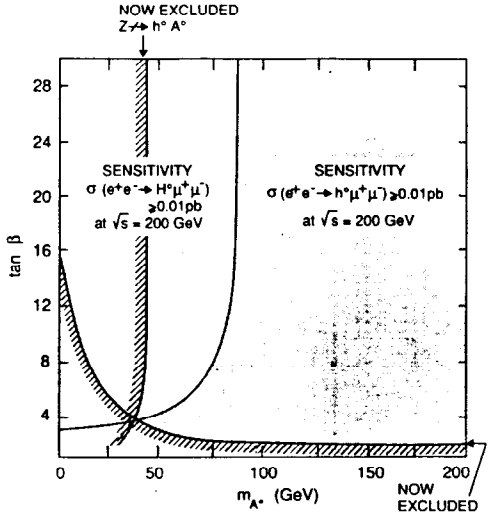

Fig. 26 The domain of SUSY Higgs parameter visualized: in tan β, m_A planes; the present limit is shown; a sensivity of 500 pb^{-1} at LEP 200 gives access to the full domain.

Figures 27 should help to define the possible search procedures. LEP 1 has already pushed the mass limit of $H^{\pm}$ to ~ 40 GeV/c^2, depending on the $\tau\nu$ branching ratio Fig. 28 [47]. This automatically set a model-independent limit of $\sim m_H^{\pm} + m_b$ on the t-quark mass. A still better model-independent limit is obtained for the t-quark—and for any heavy quark—by a direct study of the acoplanarity of $Z \to q\bar{q}$ events [48] (Fig. 29).

4.2.2.3 Charginos and neutralinos. The charginos $\tilde{\chi}_i$, $i = 1, 2$, are the superposition of Wino and Higgsino states which diagonalize the mass matrix

$$M^{(c)} = \begin{pmatrix} M & \sqrt{2} m_W \sin\beta \\ \sqrt{2} m_W \cos\beta & \mu \end{pmatrix},$$

where M, μ, and β (tg $\beta = v_2/v_1$) are the parameters of the Lagrangian in the Minimum Supersymmetric Standard Model (MSSM). The cross-section is dominated by the Z exchange diagram. With the signature

$$e e \to \tilde{\chi}^+ \tilde{\chi}^- \to \ell^+ \ell^- + p_T^{miss},$$

the lightest charginos should be detected up to the border of phase space.

Neutralinos $\tilde{\chi}_i$ are Majorana fermions, superpositions of the neutral gauginos and Higgsinos. Their masses and compositions are determined by the diagonalization of a mass matrix $M^{(0)}$ defined by the same parameters as those occurring in $M^{(c)}$ in the case of the MSSM. The best hope of detecting them at LEP 1 comes from the associated production

$$e e \to \tilde{\chi}\tilde{\chi}',$$

where $\tilde{\chi}$ is the lightest neutralino. The decay of the heaviest neutralino $\tilde{\chi}'$ can be

$$\text{i)} \quad \tilde{\chi}' \to \tilde{\chi} H_2 \quad \text{or} \quad \tilde{\chi}' \to \tilde{\chi}^{\pm} q\bar{q}', \quad \tilde{\chi}^{\pm} \ell\nu ,$$

if the Higgs H_2 and/or the chargino are light enough; otherwise:

$$\text{ii)} \quad \tilde{\chi}' \to \tilde{\chi} q\bar{q}, \quad \tilde{\chi}\ell\bar{\ell}, \quad \tilde{\chi}' \to \tilde{\chi}\gamma ,$$

giving very striking signatures. Contour plots are given in Fig. 30.

A systematic exploration of the kinematically allowed regions for neutralinos requires a sensitivity to cross-sections of less than a picobarn. However, within the MSSM, a large fraction of the domain of naturalness can be excluded also by the non-observation of charginos at LEP 1 and 200.

The most recent exclusion contours given by LEP are shown in Fig. 31 [49]. Such figures are very complicated because of the many sources of information used. If the origin of the limits is not taken into account, we get the overall picture of Fig. 32. The physical content is made clearer if we remember that the

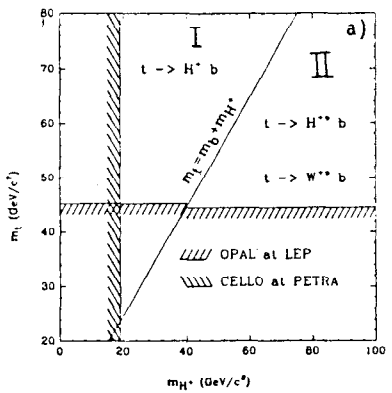

Fig. 27a The plane (m_{H^+}, m_t) and the regions excluded at present by experimental lower limits on m_{H^+} and m_t from e^+e^- collider experiments. Also shown are the kinematical regions accessible to on-shell $t \to H^+b$ and to off-shell $t \to H^{+*}b$ decay on the left- and right-hand side of the line $m_t = m_{H^+} + m_b$, respectively.

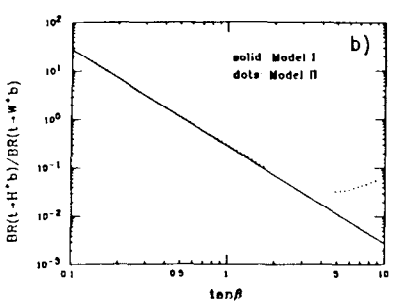

Fig. 27b Plot of $BR(t \to H^+b)/BR(t \to W^+b)$ as a function of $\tan\beta$ for m_t = 100 GeV, m_b = 4.5 GeV, and $m_{H^+} = m_W$. Results for both Model I (all $f\bar{f}$ couple to only one of the two doublets) and Model II (up-$f\bar{f}$ couple to ϕ_2, down-$f\bar{f}$ couple to ϕ_1) fermion couplings are displayed.

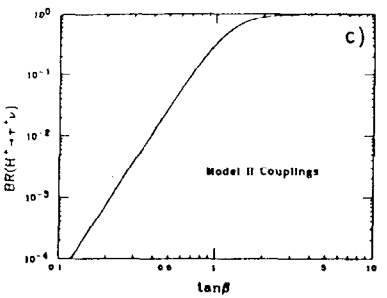

Fig. 27c The branching ratio for $H^+ \to \tau^+\nu$ as a function of $\tan\beta$. The CKM mixing angles were neglected, and values of m_{H^+} = 50 GeV, m_e = 1.5 GeV, and m_s = 0.15 GeV were taken. Results are for Model II couplings. The Model I result corresponds to the $\tan\beta$ = 1 value.

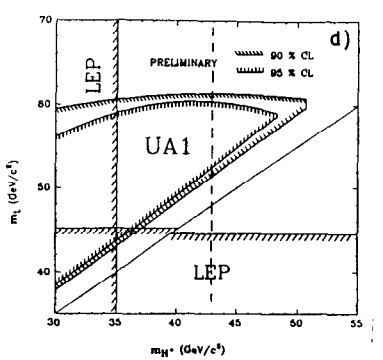

Fig. 27d The present UA1 limits.

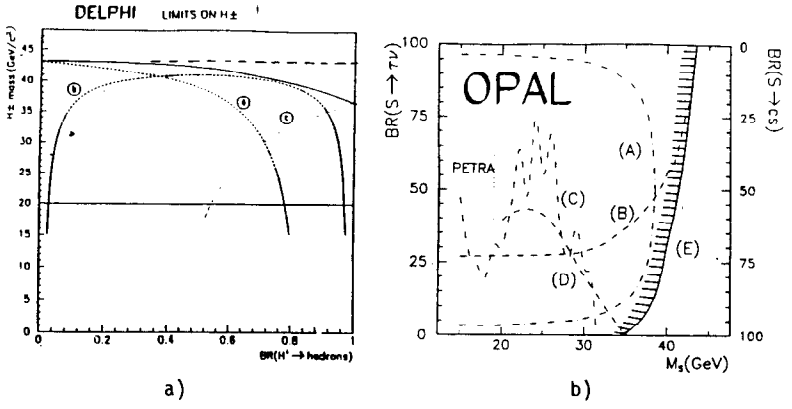

Fig. 28 The LEP mass limit for charged Higgs (DELPHI).

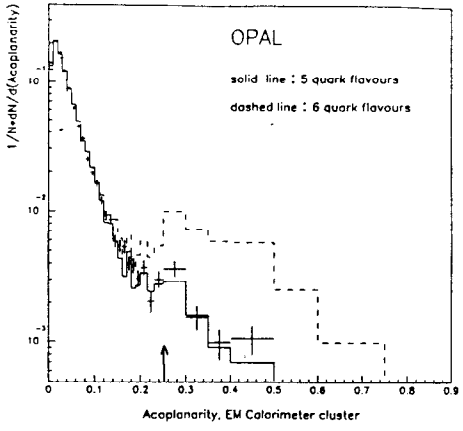

Fig. 29 The acoplanarity distribution expected from a t-quark or any heavy quark (OPAL).

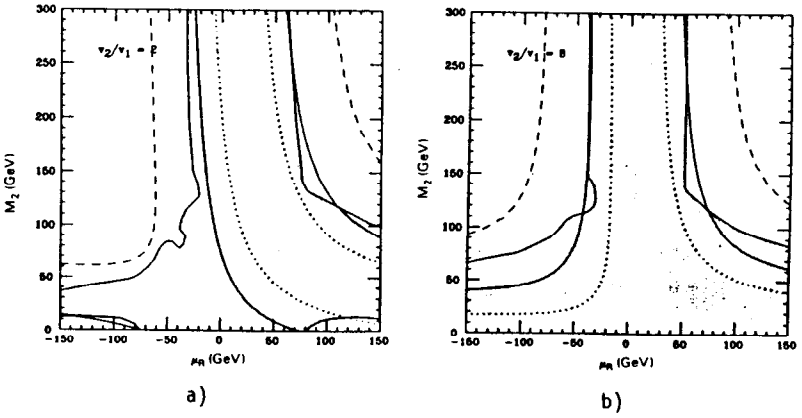

Fig. 30 Contour plots in the parameter plane of the MSSM for two values of v_2/v_1 (a, b), showing (shaded area) the region inside which $ee \to Z \to \chi\chi'$ has a BR $> 10^{-5}$, as well as the exclusion areas corresponding to the non-discovery of $\chi^+\chi^-$ at LEP 1 (between the full lines) and LEP 200 (between the dashed lines).

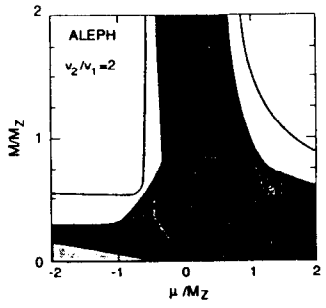

Fig. 31 The LEP limits on neutralinos (ALEPH).

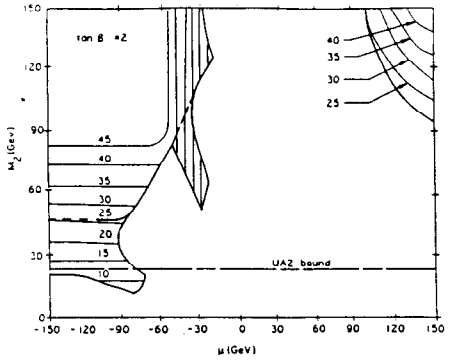

Fig. 32 Sketch of the excluded region in the M, μ plane and iso- LSP mass curves.

vertical scale M is in fact related to the gluino mass and, for small M values, to the mass of the lightest neutral SUSY particle $\tilde{\chi}$. For tg $\beta > 2$ we are in fact excluding $m_{\tilde{g}} < 100$ GeV/c^2 and $m_{\tilde{\chi}} < 17$ GeV/c^2. By the way, the latter would have important consequences for cosmology, since $\tilde{\chi}$ is usually considered as a good candidate for non-baryonic dark matter. Unfortunately one has not yet shown that tg $\beta > 2$.

4.2.3 Compositeness

This is a radical issue of the problems left open by the SM. Particles are assumed to be made of subconstituents (preons, rishons, etc.) linked by a new interaction. At the compositeness scale, constituent hard scattering would be observed. At energies well below that scale, compositeness is described by an effective interaction, the intensity of which is governed by g/Λ, the ratio of its specific coupling to the scale; therefore the notion of scale is ambiguous as long as the nature of the coupling assumed for the underlying interaction is not made explicit.

Usual compositeness assumes that quarks and leptons are composite. The main effects to be looked for are contact terms in fermion scattering, excited objects, etc.

Contact terms can be parametrized à la Eichten–Lane–Peskin (ELP) [50]: strong coupling, strong scale Λ, various helicity combinations. Contact terms are mostly felt by their interference with usual amplitudes. On the Z, unfortunately, their real contribution does not interfere with the imaginary resonant term. This explains the dip observed in the curves of Fig. 33a at the Z mass. On the wings of the Z and at LEP 200 the sensitivity is restored. Limits on Λ, depending on the helicity configuration and under the assumption of strong coupling, are given in Fig. 33b.

The most promising excited object is the e*. It can be pair-produced (limit: $\sqrt{s}/2$), singly produced through γ exchange (limit $\sim \sqrt{s}$), or exchanged in ee $\rightarrow \gamma\gamma$. A thorough study can be found in Ref. [51].

As expected, LEP has set strict limits up to $\sim \sqrt{s}/2$ through the non-observation of pair production. It has excluded also excited leptons up to ~ 80 GeV, and for a sufficiently large magnetic coupling, through the non-observation of single production.

Another fascinating issue would be nearby compositeness, i.e. compositeness of the IVB. The scale, under the assumption of electroweak coupling, would then be of the order of the Fermi scale. A good example is the strongly coupled Standard Model (SCSM) [52], built from 72 left-handed fermion doublets ψ_L and a complex scalar doublet ϕ with the same SU(2) $\times$ U(1) as in the SM. However, SU(2) is assumed to be confining, and the objects above are preons which, by their combinations, give the known particles, as well as new ones: leptoquarks, isoscalar vector bosons, etc. Nearby compositeness induces, for instance, rare decay modes of the Z (Fig. 34) [53] and departures from the SM for many observables such as

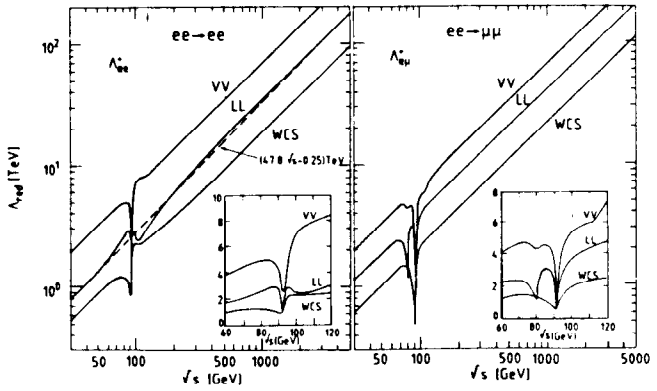

Fig. 33a The 'reach' of e^+e^- colliders, $\Lambda^{\rm red}$ = limit $(\Lambda_c)\cdot\{[s/(190\ {\rm GeV})^2]\cdot(500\ {\rm pb}^{-1}/\int L\ {\rm d}t)\}^{1/4}$, as a function of $\sqrt{s}$, showing approximate scaling (dashed line). For details, see Ref. [54].

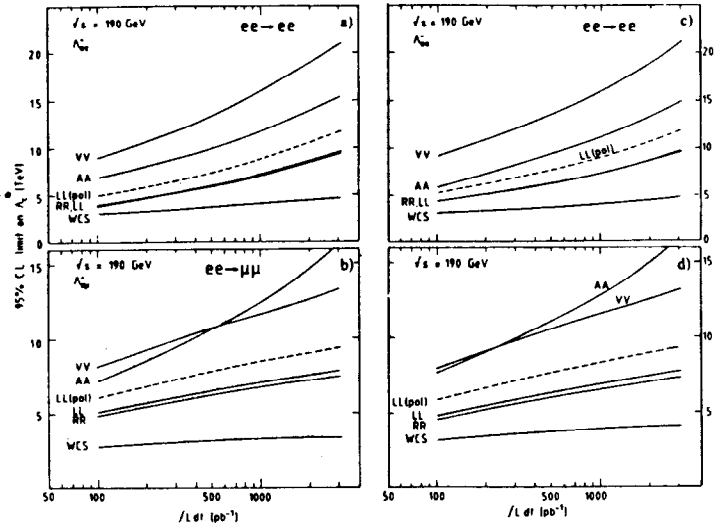

Fig. 33b Lower bounds on the compositeness scale Λ_c for $e^+e^- \to e^+e^-$ [(a), (c)] and for $e^+e^- \to \mu^+\mu^-$ [(b), (d)], as a function of the integrated luminosity at $\sqrt{s}$ = 190 GeV. For details, see Ref. [54].

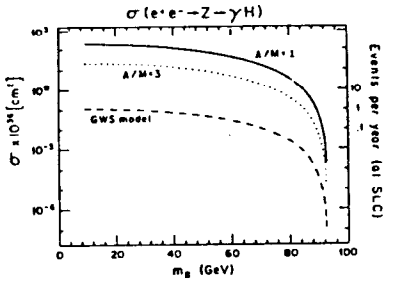

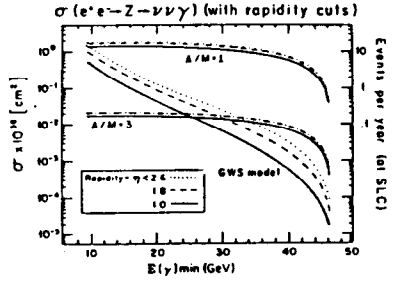

Fig. 34 Enhancement of cross-sections in the SCSM (from Ref. [53]); 1 event per year at the SLC ($L = 10^{30}$ assumed) means 100 events per year at the pretzel LEP. See also Ref. [57].

asymmetries. The mass and width of the Z can be modified by the presence of higher bosons. In the SCSM, the channels ee $\rightarrow$ ff at LEP 200 are modified in a correlated way (Fig. 35) [54].

On the Z, the most spectacular mode would be $Z \rightarrow 3\gamma$. In the SM this is unobservably small ($\sim 5 \times 10^{-10}$). Compositeness can boost it to a branching ratio of $\sim 5 \times 10^{-4} Q^6$, where Q is the mean electric charge of the preons. In the absence of an underlying model, phase space is used to evaluate the visibility of such a channel, over a background due to radiative ee $\rightarrow \gamma\gamma$. In Ref. [51] it is shown that, with 100 pb^{-1}, a branching ratio $\geq 1.1 \times 10^{-5}$ would be visible. Scaling up in luminosity, we deduce that the pretzel scheme should allow us to reach 2×10^{-6}. This would be a meaningful measurement if we refer to the guessed-at number given above. The present limit from OPAL is 5.2×10^{-5} (95% CL). Observing such a channel would be a major result. However, on the contrary, its non-observation would not produce any information since the guess does not rely on any firm consideration.

In Table 6 a few useful scaling laws are given, which allow us to see at once the effect of $\int L\, dt$ and $\sqrt{s}$ on the sensitivity to compositeness. In the search for contact terms and excited electrons, it turns out that to increase $\sqrt{s}$ is more rewarding than to insist on increasing the luminosity.

5 INCREASING THE LUMINOSITY = THE PRETZEL LEP

A new option was recently proposed for LEP [55]: multibunch operation on the Z, providing a tenfold increase in luminosity. This is known as the pretzel[1] scheme [56]. Physicswise, a thorough study, such as was done for LEP 200 and for polarization on the Z, has been carried out at a Workshop [57].

With the pretzel scheme (see subsection 5.1), if it can be successfully implemented, one could imagine an exposure on the Z leading to $\sim 10^8$ such particles. Clearly, many experimental and organizational problems would have to be solved in order to cope with such a flux and with the total amount of information. They are briefly discussed in subsection 5.2. The output of physics from 10^8 Z is then explored along three directions:

i) the improvement of accurate measurements on or near the Z (subsection 5.3);

ii) the detection of rare modes of the Z, with branching ratios $\leq 10^{-5}$ (subsection 5.4);

iii) the physics of beauty that one can hope to perform (Section 6) on the Z resonance.

[1]This is the English name of a biscuit called Pretze by the Bavarians (and Brezel by the Germans), and which can be described as 'ein Backwerk, etwa in Form einer Acht' (i.e. a biscuit, resembling somewhat the shape of an eight).

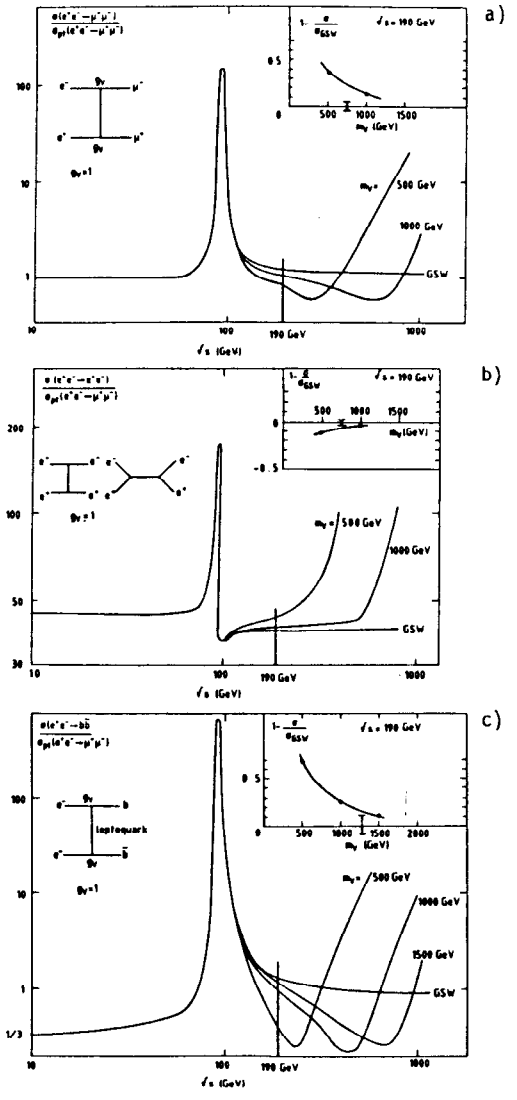

Fig. 35 Correlated effects of exotic isoscalar vector bosons on $\mu^+\mu^-$ (a), e^+e^- (b), and $b\bar{b}$ (c) final states, as expected in the SCSM, assuming a coupling $g = 1$. The insets show the experimental sensitivity at $\sqrt{s} = 190$ GeV (Ref. [54]).

There are also other potentially interesting fields (e.g. tau physics).

An important remark should now be made (it will be substantiated later): high luminosity on the Z, however interesting it may be, is physicswise not an alternative to an increase in LEP energy (giving access to the W-pair domain) or to the exploitation of longitudinal polarization and to searches for heavier objects on the Z: these two options contribute specific irreplaceable information.

On the other hand, it will rapidly become apparent that technically (RF powerwise) the increase in the energy and in the luminosity is strongly coupled.

5.1 The Pretzel Scheme

The formula for the luminosity, given in Section 1,

$$L = \frac{k_b I_b (E_0/mc^2)\bar{\xi}}{2er_e\beta_y^*},$$

exhibits the main parameters governing its value. With $k_b \equiv$ number of bunches $= 4$, $I_b \equiv$ current per bunch $= 0.75$ mA, $\beta_y^* \equiv$ beta function at the interaction point (IP) $= 7$ cm, and $\bar{\xi} \equiv$ beam-beam limit factor $= 0.04$, we get the canonical value of $L = 1.7 \times 10^{31}$ cm^{-2} s^{-1} at the Z mass, which hopefully will be reached in the near future.

To go beyond this value, we can think of increasing the bunch current (by a factor of 2?) and decreasing β_y^* (by a factor of 1.5), and we can hope that a larger beam-beam limit (a factor of 1.5) can be tolerated. However, any such attempt has its unknown features.

A radical approach is to increase the number of bunches, whilst avoiding unwanted bunch-bunch collisions. The best idea would be to have a second ring on top of the first one, but occupancy of that location is already foreseen! An alternative method is the pretzel scheme: its principle is to give opposite wavy patterns to the e^+ and e^- closed orbits (Fig. 36), so that the bunches avoid each other. These patterns cannot be tolerated in the RF section because synchro-betatron resonances would be excited; this imposes an upper limit on the number of bunches, namely:

$$n_{max} = \frac{\text{circumference}}{2 \times \text{distance IP to end of RF}} \simeq 54.$$

Furthermore, the number of bunches should divide the RF harmonic number of the machine, so that proper acceleration is ensured. And obviously there must be encounters at even intersection points. If $k_b \neq p \times 4$, there are no collisions in the odd pits. This gives the following possibilities:

$$k_b = 2, 4, 8, ..., 18, ..., 36, 40\ .$$

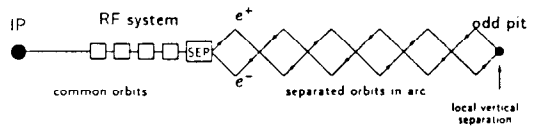

Fig. 36 Basic idea for a pretzel scheme (showing one octant) (from Ref. [56]).

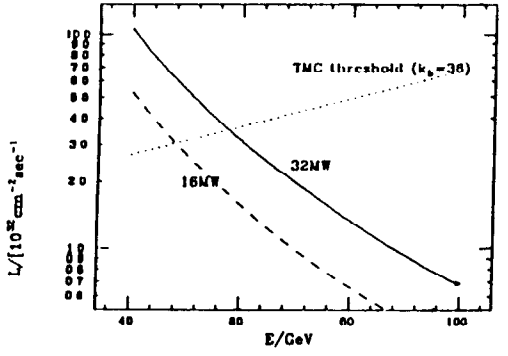

Fig. 37 Power-limited luminosity at LEP [56]. The transverse-mode coupling threshold is indicated.

For several reasons, the choice would be to separate the beams in the horizontal plane, in particular because there the aperture is larger. The residual beam-beam tune shift resulting from the close encounter of opposite bunches has been studied [57], using separators (electrostatic or RF magnetic) in place of the last half-cell of the RF cavities. With $l = 8$ m and $E_x = 0.8$ MV/m, this tune shift would still be acceptable for a 36-bunch solution. The resulting luminosity would be of the order of $L = 1.4 \times 10^{32}$ cm^{-2} s^{-1}.

However, it is necessary to have sufficient RF power ($\sim$ 7.5 MW to get the quoted luminosity at the Z mass), and such a scheme can only be possible if some of the copper cavities are already replaced by superconducting (SC) ones (also, room is needed for the separators); in 1991, 32 SC cavities could be installed.

With an RF power of $P_{\rm beam} \approx 10$ MW, the scheme could be used up to $\sqrt{s} = 100$ GeV. With more RF power it could allow us to increase the luminosity at higher energies. This would be welcome, because of the smallness of the cross-sections in that domain.

To fix the ideas about the maximum amount of RF needed at LEP 200, we could, for instance, have the following aim: to get enough power to be able to double the luminosity in a useful region above the W-pair threshold (eight bunches or more current). With the luminosity behaving as $L \propto 1/E_{\rm b}^3$, a larger gain would be obtainable at more modest energies (Fig. 37).

It is premature to make any prediction about polarization: however, the choice of a horizontal separation does not *a priori* compromise the chances of maintaining the polarization (if there is any) in a pretzel scheme.

A simpler way to increase the luminosity by a factor of 2—modest but safe—is to provide a scheme for eight bunches. The pretzel is not needed; we just have to ensure the separation of bunches which would otherwise cross in the middle of the areas. Eight pairs of vertical separators can do the job. However, being bound to vertical separation would prevent any further step in the direction of a pretzel and would also make the eight-bunch scheme useless for polarization.

5.2 Experimental Problems

As we saw in Section 2, LEP experiments have been prepared having in mind an interval of 23 μs mind an interval of 23 μs between crossings and for a peak luminosity of 1.7×10^{31} cm^{-2} s^{-1}. The 36-bunch solution would bring this interval to 2.5 μs and increase the luminosity by an order of magnitude; provided the vacuum can be kept at around the same value, the background would probably scale with the number of bunches. Finally, 10^8 Z represents at least an order of magnitude increase in the volume of data foreseen. Let us note first that the Z rate is approximately four per second: therefore physicswise, all—or nearly all—of the $\sim$ 400,000 crossings per second are empty, and the two-photon interaction does not change this picture.

The argument that the existence of long-drift devices (e.g. TPC, RICH) would preclude the use of such a bunch spacing is not a valid one. What has to be done is to abandon the gating mode that leads to a systematic opening at each crossing. One could use an externally triggered mode: the elements of such a fast trigger have to be provided, but whatever its rapidity, a few centimetres of information will be lost on the edges of the drift volume. It is difficult to see what could prevent us from having such an efficient trigger at a rate of 1 kHz or less. Probably better, however, would be a permanent gating mode of the 'diode' type: preliminary tests have been performed.

Another effect of long-drift devices would be to integrate the background of several crossings. For the nominal LEP conditions, with a vacuum chamber of radius $r = 8$ cm, the background conditions [11] are not severe; the detectors should be able to stand two orders of magnitude more. However, if at the same time we try to decrease the radius of the chamber, things get rapidly worse, as we have seen in Section 3. In fact, we can act only in the vertical plane. From the point of view of background, a chamber profile, as shown in Fig. 1 [12], seems to represent the ultimate tolerable limit for the nominal luminosity. Therefore, it is hardly possible to run the pretzel and at the same time use such a chamber. My guess is that instead of struggling to approach the interaction point below $r = 5$–6 cm in order to improve the extrapolation accuracy, we should rather act in such a way as to decrease the effect of Coulomb scattering by using thinner microvertex detectors, possibly installed in a pre-vacuum region. We will come back to this discussion in subsubsection 5.4.5.

More problematic is the fact that the various detectors, because they were prepared for a large interbunch spacing, have, for some aspects of their electronics and readout, been 'taking their time'. None of them would find it a problem to accept eight bunches. Beyond that, non-negligible modifications would have to be performed in some cases. This would need time, effort, and money, but such outlay would anyway remain at the level of a few per cent of the total project investment. Detailed studies have now been made for each experiment [57].

The problem of acquiring about four Z per second (assuming that we know how to avoid triggering on the background) is not a major one. The idea of processing 100 million Z appears to be challenging. As we will see, quite rare and unusual events are being searched for, and therefore we have to avoid the systematic use of fast but biasing filters for speeding up the production.

The problems of mass storage, fast link, and manpower are probably more severe than the question of CPU availability. However, relying on the rapid evolution of techniques, we can envisage that these problems will be manageable in the near future, as has been concluded in Ref. [57]. Furthermore, it is quite likely that a collider such as the LHC will, several years after the pretzel is introduced, require even more computing power, and therefore we should be prepared for this eventuality.

5.3 Accurate Measurements

The interest of doing accurate measurements on the Z in order to test the Standard Model in depth and possibly reveal new physics, has been studied with great care in the past and was reviewed in Section 4.

The obvious tendency here is for the statistical errors—which in many cases were still dominating—to fade away. The measurement is thus more exposed to experimental systematic errors and theoretical uncertainties.

Another aspect is that, with abundant statistics, we can also act on the systematic errors in order to decrease them: cuts can be made tighter so as to avoid doubtful kinematical regions; acceptances can be measured by comparing redundant procedures; our knowledge improves with the statistics, and so on.

The $\mu\mu$ (or $\ell\ell$) charge asymmetry (Table 7) will then be dominated by the error due to the uncertainty in the position of the measurement relative to the Z pole: here I have assumed that it is ± 10 MeV/c^2, limited by reproducibility of the machine. Systematic scanning and/or the frequent use of resonant depolarization to get the scale could even lead to a more favourable value. The value quoted in Table 7 for the uncertainty in the radiative correction ($\sim$ 5–6% of the correction) can probably be reached, but first there will have to be a lot of progress with respect to the present state of the art, which, for unessential reasons, shows much dispersion of the results between the various programs. The experimental error (built up from the difference between the acceptances for + and − integrated over the detector) is an example of a quantity that can benefit from an increase in the statistics, since it can be measured from the data.

For the τ-polarization measurement, the statistical error, which still dominates at the level of a few 10^6 Z (the signal is only 6‰ of the Z rate if the $\tau \to \pi\nu$ mode is used), disappears, and we are left with the dominating systematic errors: for instance, in the case of $\tau \to \pi\nu$, it is the confusion with $\tau \to \rho\nu$. Our improved knowledge of the detectors, the increased statistics that allow tighter cuts to be made, the likely exploitation of $\tau \to \ell\nu\nu$ modes, and the possible combined exploitation of the $\tau \to \pi\nu$ and $\tau \to \rho\nu$ modes, could finally lead to numbers below those quoted in Table 8.

It is certainly in the exploitation of hadronic modes that the improvement is mostly felt. Indeed, owing to the severity of cuts at the tagging level, the statistics were always considered to be the limiting factor. Moreover, information obtained on the Z peak is essential to our having confidence in the 'stability' of programs describing fragmentation—in particular for quarks such as the s, which were 'minority carriers' at PEP and PETRA, and in deep-inelastic scattering. It is likely that this information, and therefore the quality of tagging, will gradually improve in the LEP era. The availability of large statistics also allows us to make use of double-tag procedures, in which several quantities such as tagging efficiencies, poorly known branching ratios, etc., cancel out. Expected numbers for the single-tag method are given in Table 9, as derived from Table 3. Included in the systematic errors are: QED, with uncertainty on the position relative to the Z pole; QCD corrections, which seem to be well under control; and the dominating instrumental and tagging errors. We should note that such measurements are not the privilege of detectors with powerful hadron identification. For instance, the promising c-tagging procedure [58] of the third column requires only the good measurement of a 2–3 GeV pion, and its ultimate systematic error, which is still uncertain, will depend on the quality of such a measurement and on the reliability of background subtraction (Fig. 38). The number given for the u-quark (fast proton tag) is obviously a very shaky one because of our present ignorance about such fragmentation.

Table 9 shows a set of impressive numbers which would be obtained from quark tagging. However, the amount of work and of further understanding that will be necessary in order to reach this level is impressive too!

Therefore the polarization asymmetry ($A_{\rm LR}$) measurement offered by longitudinal polarization keeps its invaluable quality. With a modest 50 pb^{-1}, and provided the conditions quoted in Table 10 are fulfilled, an experimental accuracy of $\Delta \sin^2\theta = \pm 0.0003$ can be obtained [4]. Reaching this accuracy, without polarization, would require the combined information ($A_{\rm CH}^{\rm ff}, P_\tau, \ldots$) extracted from an exposure of $\sim$ 25 M Z. The systematic errors are of a totally different nature compared with the charge asymmetry $A_{\rm ch}$, and the amount of data to be processed is quite limited. The experimental accuracy matches well with the theoretical uncertainty of ± 0.0004. The polarization option is more interesting than ever. Compared with the SLC, in which polarized beams should be easier to obtain, LEP has the vital advantages of luminosity and of the four-bunch scheme (see Section 7).

As mentioned in Section 4, another accurate measurement, where abundant luminosity can make an impact, is neutrino counting, using the classical radiative method. Luminosity allows us to go higher above the Z (say around 100 GeV, since the pretzel is still operative there), and to select photons of higher energy (> 3 GeV) and wider angle ($> 45°$), keeping a large signal ($\sim$ 3000 events for 100 pb^{-1}, i.e. two weeks of running time). This transverse energy ($E_{\rm T}$) cut, combined with the quite low angle tagging foreseen with a second-generation SAT ($< 2°$), almost eliminates the eeγ background; if necessary, this can be subtracted, using a measurement below the Z. If an experimental problem of acceptance to $E_\gamma > 3$ GeV still exists, then by triggering on photons we can measure the ratio of $\nu\nu\gamma$ to $\mu\mu\gamma$, which in principle eliminates such uncertainty, but at the expense of statistical limitations with $\mu\mu\gamma$. Normalization problems limited to $\sim \pm 1\%$ in the SAT could be still improved by the use of forward e.m. calorimeters counting about one tenth of the Z (300,000 e^+e^- for 100 pb^{-1}) and with hopefully lower and different systematics. If a month of pretzel is devoted to ν counting, it is difficult to see why an experimental error of $\Delta N_\nu/N_\nu \leq 4\%$ should not be obtained, as shown in Fig. 13 (point C). We saw that on the theoretical side [40] the situation, within such an acceptance, is also quite favourable. Admittedly the results on N_ν obtained from the total cross-section measurement are already of

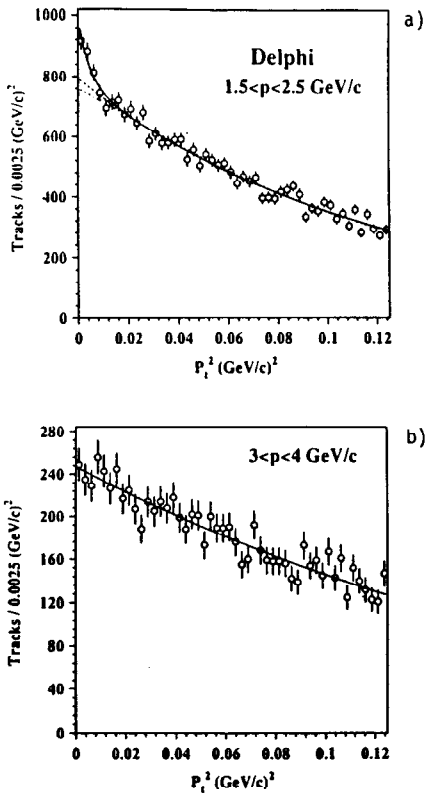

Fig. 38 Spectrum of the p_T^2 of single π relative to the jet axis: a) non-charm, b) all events. (Data from DELPHI, Ref. [58]).

an equivalent quality and do not seem to present any ambiguity of interpretation. The motivation for a radiative measurement is therefore weaker, although there may be both safety and satisfaction in getting a second measurement of high accuracy with totally different systematic errors.

In principle, 'fast' measurements such as those of m_Z and Γ_Z do not improve with statistics, whilst Γ_{had} and $\Gamma_{\ell\ell}$ should become somewhat better, in particular if the absolute normalization error is decreased. However, some people argue that the study of ee $\rightarrow$ ee at large angle ($> 15°$), through the interference between Z and γ contributions, should in the long term produce revolutionary accuracies for total and partial width measurements [59], provided the problem of radiative corrections is treated adequately.

5.4 Rare Modes of the Z

Non-standard phenomena reviewed in Section 3 should lead to the existence of new decay modes for the Z. Such phenomena should also slightly modify the accurate measurements on the Z (or at higher energy). However, whenever a direct effect has a chance of being observed, we should certainly look for it. Here we enter a domain where, most of the time, detailed Monte Carlo work is missing.

Intuitive arguments tell us, however, that whenever a channel with a branching ratio of 10^{-5} or smaller is proposed, an increase in luminosity can only strengthen the chances of revealing this channel in a significant way.

Let us see how the conclusions drawn in Section 4 would be modified if an exposure of 10^8 Z could be obtained.

5.4.1 Standard Higgs

Figure 39 shows that in the standard channel Z $\rightarrow$ H$\mu\mu$, and keeping our criterion of 10 events as a meaningful discovery signal, the mass limit can in principle be pushed to ~ 65 GeV/c^2. In the absence of $t\bar{t}$ and with the favourable features of the background four-fermion final state, there is a possibility that this can be exploited. As has already been mentioned, if the background could still be eliminated, the channel Z $\rightarrow$ H$\nu\bar{\nu}$ could allow the limit to be pushed even higher. One can, however, have legitimate doubts about an everlasting absence of background even in the best detector. In this mass range the channel Z $\rightarrow$ Hγ [2] would be more favourable. It corresponds to a set of diagrams, among which those of Fig. 40 are the most remarkable. The rate does not depend appreciably on the unknown t-quark mass. On the experimental side, the visibility of such a mode is unfortunately ruined by the final-state radiation ee $\rightarrow$ q$\bar{\text{q}}\gamma$, which under the most favourable experimental assumptions is two orders of magnitude above the standard signal.

Another remark is that LEP 200 provides an alternative way of producing such high Higgs masses through the Bjorken mechanism ee $\rightarrow$ Z (real) + H. The corresponding cross-section varies smoothly with the Higgs mass. The cross-over

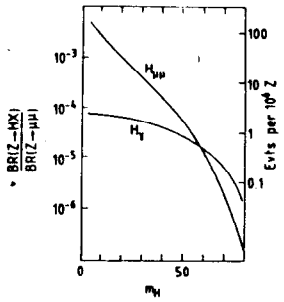

Fig. 39 Standard Higgs cross-section.

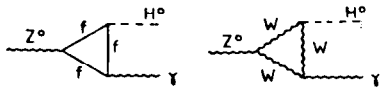

Fig. 40 Triangle diagrams for $Z \to H^0\gamma$.

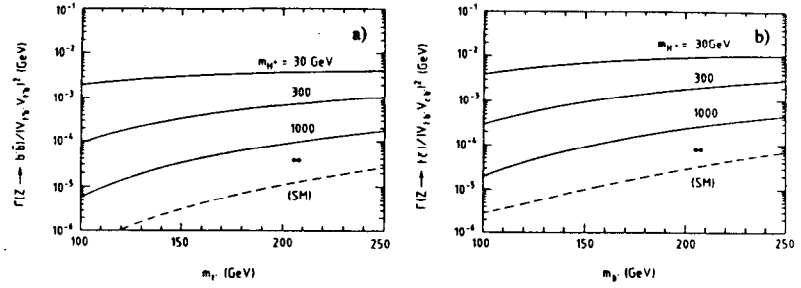

Fig. 41 FCNC cross-sections for the extended Higgs model (from Ref. [60]).

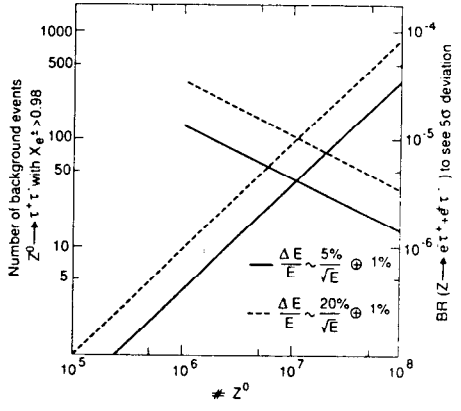

Fig. 42 Limits accessible for $Z \to \tau\mu, \tau e$ (Ref. [57]).

point between the pretzel LEP 1 and the standard LEP 200 (the mass at which we get the same rate per unit time) is $\sim$ 60 GeV/c^2. How high in mass we can hope to go with LEP 200 will be the subject of a discussion in Section 6.

5.4.2 Compositeness

In Section 4 we saw that for the contact terms, e* search etc., 'patience', i.e. accumulating luminosity, does not pay very much: rather, we should move to higher $\sqrt{s}$.

On the contrary, compositeness can induce rare modes of the Z or boost their branching ratio to observable values. For instance, the $Z \to 3\gamma$ mode (see Ref. [51]), from a 100 million Z equivalent exposure, would then be revealed down to a branching ratio of $\sim 2 \times 10^{-6}$. If there is some truth in the guessed-at branching ratio presented in Section 4, then this gain of an order of magnitude could be crucial for revealing the phenomenon.

5.4.3 SUSY

In Section 4 we reviewed the ways of producing and observing SUSY Higgs. For large v_2/v_1, the rate of associated production ee $\to$ hA (the two being mass-degenerate) falls relatively smoothly [like (velocity)^3]. For tg $\beta = 5$, $m_{h^0} \simeq m_{A^0} = 40$ GeV/c^2, the branching ratio is 10^{-4} for one of them into $\tau\tau$, 7×10^{-6} for both of them into $\tau\tau$. LEP 1 should get close to the kinematic limit. For larger masses ($> m_Z/2$) an increase in energy is necessary, as well as high luminosity (see Section 6).

For tg β not far from 1, the lightest scalar is produced in the standard way, albeit at a reduced rate. For tg $\beta \ll 1$, the $\tau\tau$ mode of h and A is no longer available as a signature: the search must be performed in quadri-jets. High luminosity on the Z (as well as above it) will be very useful.

The same is true for the neutralinos search (Figs. 31, 32), although, as we have said, the SSM suggests exploring rather the chargino domain at LEP 1 and 200.

5.4.4 Flavour-changing neutral currents

The existence of a fourth generation and of further new physics (such as two Higgs doublets) predicts flavour-changing neutral currents (FCNC), leading to unconventional final states [60] (Fig. 41) if they are kinematically accessible:

$$Z \to b\bar{s}\,, \quad Z \to b'\bar{b}\,, \quad Z \to t'\bar{c}\,, \quad \text{etc.}$$

There may be doubts about the occurrence of the last two.

The same can happen for leptonic decays [61]:

$$Z \to e\tau\,, \quad Z \to \mu\tau\,, \quad \text{etc.}$$

The predicted branching ratios vary widely but may reach accessible values.

For the leptonic modes, the most obvious background is $Z \rightarrow \tau\tau$, with one τ decaying into $\ell\nu\nu$, the lepton carrying most of the momentum. The momentum spectrum is nearly linear in that region, and under the width of the peak at the beam energy (given by the momentum resolution ϵ) the background is roughly ϵ^2. Putting in numbers [$\epsilon \approx 2\%$, BR($\tau \rightarrow \mu\nu\nu$) $\approx 20\%$], one can expect that, with large statistics ($\sim 10^8$ Z), branching ratios of a few 10^{-6} should be accessible. Before and during this Workshop, Monte Carlos have been run on these processes. The results are shown in Fig. 47 [62, 57].

From the hadronic FCNC, only the $Z \rightarrow b\bar{s}$ has been carefully studied at the High Luminosity Workshop [57]. The s-quark is identified through $\phi \rightarrow K^+K^-$, the b-quark through its secondary vertex. The results of the simulation are given in Fig. 43.

5.4.5 The Z as a $b\bar{b}$ factory

The Z is a democratic source of all fermion pairs. For instance, the physics that could be extracted from a few million τ pairs is to be studied; and whilst information on the ν_τ mass is probably the domain of dedicated τ factories, we should learn much about the Lorentz couplings of the τ on the Z, for example.

For $b\bar{b}$ physics, the prospects are the following. From 100 million Z (visible), about 19 million events of the $b\bar{b}$ type are available, i.e. 38 million 'B' particles. According to the Lund fragmentation model, their distribution by population should be as indicated in Table 11.

One can say that a single exposure (to be compared with the situation at threshold $b\bar{b}$ factories) provides an abundance and a variety of beauty species. Table 11 and Fig. 44 give the main characteristics of $b\bar{b}$ events [63] according to the Lund program. Various properties allow such events to be tagged in a very efficient manner (leptons, offsets in a microvertex detector, leading particles, etc.). However, the impressive results of Table 12 [64] should be viewed with caution since we will be looking for rare and peculiar b-decay modes, whilst the tagging results are obtained for typical events. One way out would be to tag on one jet only, leaving the other jet free. The effect of this procedure has yet to be evaluated in detail, but the efficiency should still be high.

A *sine qua non* condition for performing good b physics is the implementation of a high-performance vertex detector. Table 13 compares, for instance, the characteristics of the present DELPHI vertex detector with those of an ideal one [63]. We should go from two to three layers; the inner radius should be decreased—but remember subsection 5.2—and the lever arm possibly increased. In order to limit the Coulomb scattering, the vacuum chamber and microvertex layers should be kept as thin as possible. [If this is achieved, and if the main vacuum chamber represents a large fraction of the remaining thickness, we should try to push it outward (near the third layer). This means that the first two layers should be in a pre-vacuum region, just separated from the ultravacuum of the machine by a thin window. This is quite challenging technically (and may be impossible), since

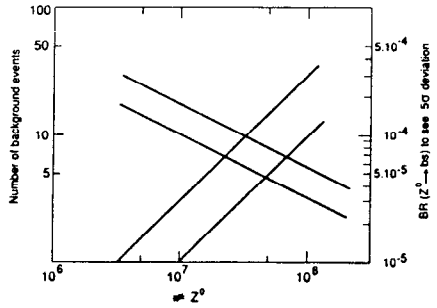

Fig. 43 Limits accessible for $Z \rightarrow b\bar{s}$ (Ref. [57]).

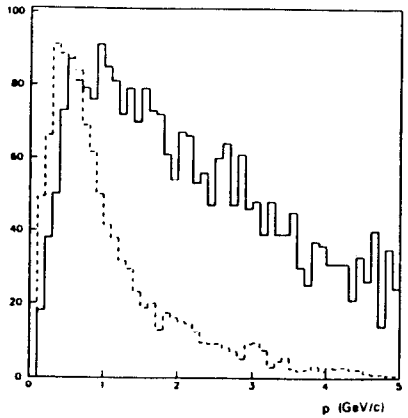

Fig. 44 Momentum of tracks from $b\bar{b}$ events at the Z: — — from B, $\bar{B}$; - - - at the main vertex (from Ref. [63]).

cooling, as well as shielding against electromagnetic noise, has to be achieved.] It is also likely that the inner layer, at least, would provide both coordinates with good accuracy, although 5 μm is not mandatory. All these conditions imply a major technological step forward, compared with present achievements. But we could then safely expect a longitudinal resolution of typically 150 μm on the decay vertex of B particles, with minimal confusion and wrong attribution of B tracks to the main vertex (Fig. 45), a source of error in the determination of the charge of the decaying beauty particle. Beauty physics can be obtained from an exposure on the Z at various levels of integrated luminosity. We give four examples.

5.4.5.1 The measurement of the lifetimes of individual beauty states. There are two possible ways of doing this. One is to use semileptonic decays,

$$B^0 \rightarrow \ell\nu D\ , \quad (1)$$

$$B^{\pm} \rightarrow \ell\nu D\ , \quad (2)$$

$$B_s \rightarrow \ell\nu D_s\ , \quad (3)$$

and to identify the D states produced. The flight length is obtained from the intersection of the lepton and the D trajectories. The rate per million Z should be 200–300 for processes (1) and (2), and 20–30 for process (3). As we shall see later, the knowledge of the B momentum can be improved by various constraints and should be at the $\sim$ 10% level.

Another way is to reconstruct exclusive decays; for instance,

$$B^0 \rightarrow \psi K\pi\ , \quad B^{\pm} \rightarrow \psi K\ .$$

The rates depend on the branching ratios [65], which in most cases are poorly known. More information should come from CESR (Cornell) before beauty physics really starts at LEP.

From the already available information and using guidelines from theory, one can draw up Table 14, giving for various channels the number of events produced, and —when details are to hand— the expected number of reconstructed ones, from Monte Carlo simulation. One should reasonably foresee that with 10 million Z the lifetimes of individual species will be measured to $\sim$ 3% or so.

Serious competition is to be expected from fixed-target and hadron collider data.

5.4.5.2 Rare modes of the B. These 'precious rarities' [66] should give access to the V(b $\rightarrow$ u) Kobayashi-Maskawa (KM) matrix element (B $\rightarrow$ $\pi\pi$, $p\bar{p}$, $\tau\nu$, etc.), and can open windows on new physics (b $\rightarrow$ sγ, B $\rightarrow$ K$\ell\bar{\ell}$).

Figure 46 recalls that whilst such branching ratios are small—or even inaccessible—within the Standard Model, new phenomena such as SUSY could boost them to quite observable values.

A threshold B-factory has well-known advantages; the main one is its excellent mass resolution of reconstructed channels (of a few MeV), obtained with the help of beam constraints. At LEP, on the other hand, whilst the mass resolution

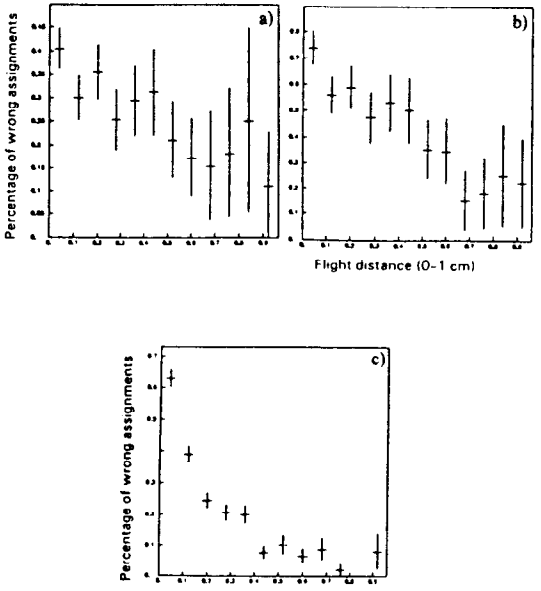

Fig. 45 Probability of wrong assignment of B tracks to the main vertex as a function of flight distance: a) microvertex 1 of DELPHI; b) microvertex 2 with one coordinate; c) ideal micro vertex 2 (from Ref. [63]).

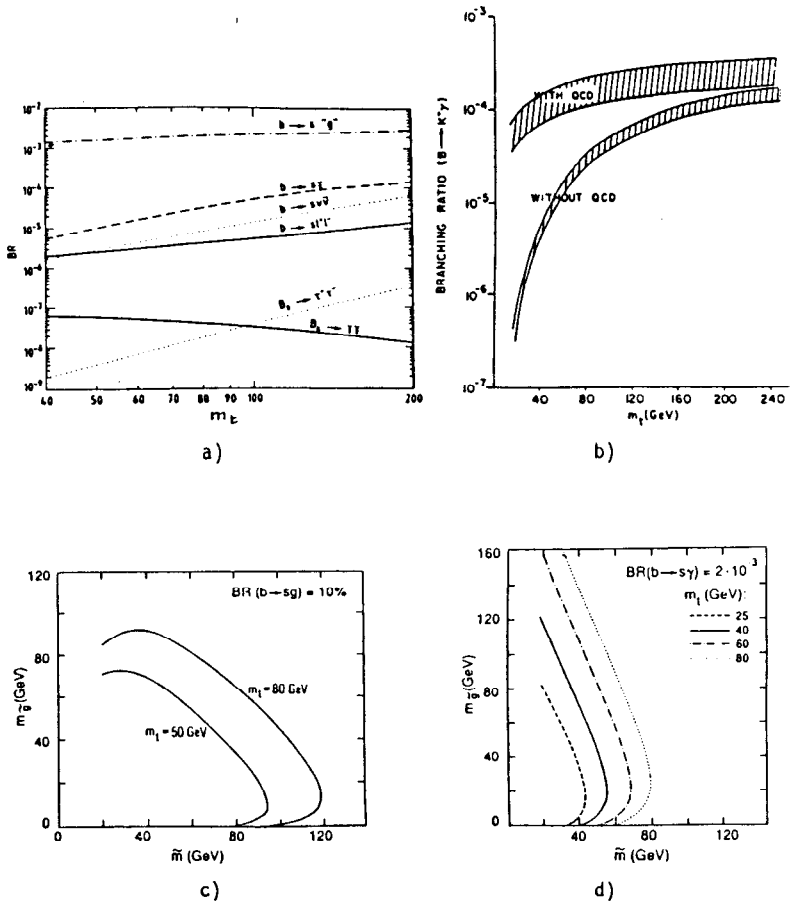

Fig. 46 SM predictions for rare B decays (a, b) and possible deviations due to SUSY (c, d).

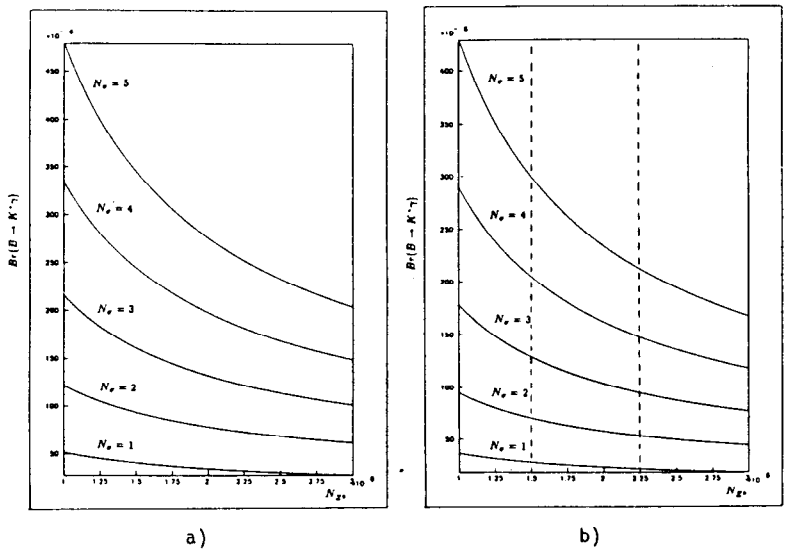

Fig. 47 Number of standard deviations N_σ for observing $B(\rightarrow K^*\gamma)$ versus the number of Z analysed (from Ref. [67]): a) all events, b) full tag of $b\bar{b}$ (100% efficient).

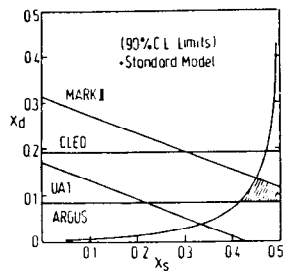

Fig. 48 Limits on χ_s versus χ_d; $\chi = r/(1+r)$, where $r = x^2/(2+x^2)$.

is somewhat worse (typically $\sigma \approx$ 40–50 MeV), the natural boost ensures the visibility of the B decay vertex, which is the only secondary vertex for charmless decay modes. It also guarantees that the decay products of the two b's are in opposite hemispheres, with no possible confusion: for a 'meagre' final state such as $B \to \tau\nu$, this is certainly a major advantage, compared with threshold $B\bar{B}$ physics.

A few exercises have been done along these lines [67] (see Fig. 47). So far it has not been demonstrated that $B \to \tau\nu$, for instance, can be specifically explored down to the expected rate.

5.4.5.3 The mixing of B_s. We can admit that the mixing of ordinary B's will be well measured at the time of pretzel LEP. Inspection of the KM matrix (see Table 14 for notation) shows that the measurement of x_s ($x = \Delta M/\Gamma$), once x_d, ρ, and λ are known, gives access to the phase of the matrix:

$$\frac{x_s}{x_d} = \frac{1}{\lambda^2(1+\rho^2-2\rho\cos\delta)}.$$

Experimentally (Fig. 48), we know that x_s is larger than ~ 3. Therefore, for B_s states we can expect quite fast time-oscillations.

We can readily state the resolution that is required from a vertex device in order to give access to a measurement of these oscillations. The period is $T = (2\pi/x)\tau$, and it corresponds to a spatial distance of $(2\pi/x)\gamma c\tau$. If we say, for instance, that we should resolve a third of a period, then the required resolution on the flight path (which in fact means the resolution on the secondary vertex, see Table 13) is

$$\Delta l = 4.4/x \qquad \text{(in mm)}.$$

The formula giving the resolution in proper time can be written as

$$\left(\frac{\sigma_t}{\tau}\right)^2 = \left(\frac{\tau_\ell}{L_0}\right)^2 + \left(\frac{t}{\tau}\,\frac{\sigma_E}{E}\right)^2 .$$

The first term is geometrical; the second one comes from the uncertainty on the energy of the B, and its contribution increases with proper time.

Attempts to see B_s oscillations by fully reconstructing B_s final states are too demanding in statistics. Work has been carried out along the lines of semi-exclusive processes such as

$$B_s \to \ell\nu D_s ,$$

where only the charged tracks of the D_s (containing either zero or two K's) are used. In spite of incomplete reconstruction, the intersection of the ℓ and D lines of flight gives a proper measure of the secondary vertex: Fig. 49 [63] shows that according to the estimate made above, x-values as large as ~ 20 are accessible. However, we also need the γ factor of the decaying B_s, and incomplete reconstruction could be a problem. In fact, the peaked fragmentation function of the b-quark (Fig. 50) gives, by itself, a good indication of the B momentum. The situation can

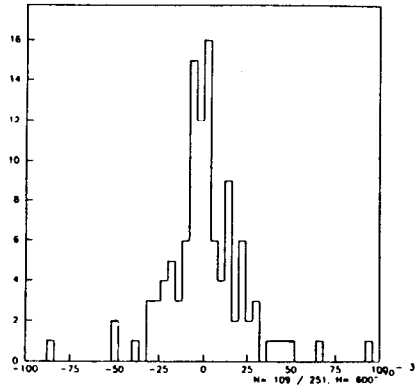

Fig. 49 Accuracy on the B_s decay vertex using semileptonic decays.

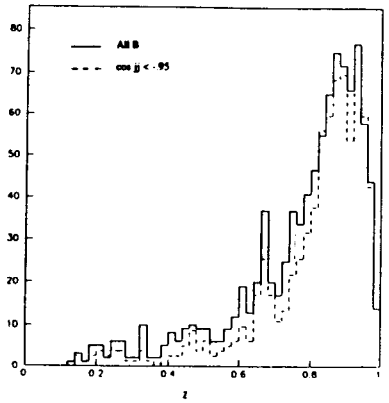

Fig. 50 Fraction of beam energy taken by the B particle (Lund MC).

be improved by getting rid of the low-energy tail of this distribution, using the measurement of particles accompanying the B. In Ref. [68] the best exploitation of constraints due to partial measurements (vertex, etc.) has been performed for processes such as $B_s \to \ell_\nu D_s$, $B_s \to$ hadrons + D_s, with the D_s measured only through ≥ 3 charged and identified prongs. The results shown in Fig. 51 confirm that we end up with proper time resolution of the order of 7–10%. The uncertainty on energy has no effect for short flight times, but precludes exploitation of the distributions for too long flights. Tagging of the other B proceeds as shown in Table 12b [63].

Another nice study [69] uses a Fourier transform of the time distribution to extract the mixing parameter. Through the convolution theorem, the resolution curve thus enters as a multiplicative function.

In Ref. [63] a synthetic and transparent formula is derived, which gives the number of B and thus the number of B_s needed to measure x_s with a given accuracy

$$N_s^0 = \left(\frac{x_s}{\sigma_{x_s}}\right)^2 \frac{1}{8P^2\rho A} ,$$

where A is the asymmetry, ρ is the factor by which the oscillation is damped due to finite resolution, etc., and P is the purity of the B_s sample.

All the three studies conclude that oscillations can be measured up to $\sim$ 10 with $\sim$ 5 million Z (provided the microvertices are in operation during the exposure) and up to $\sim$ 18–20 with the pretzel exposure ($\geq$ 25 million Z) (Fig. 52).

Compared with B factories, the Z seems to be more efficient at large x_s values (> 5) as shown by Fig. 53, which gives the damping factor of the oscillations: a constant for B factories (on the left) since $\Delta l/L_0$ is the only contribution ($\beta_\gamma = 0.4$ and 50 μm resolution were taken); a factor decreasing with t/τ for LEP (on the right) because of the uncertainty in the B energy.

The oscillation pattern Ref. [68] is shown in Fig. 54.

As illustrated by Fig. 55, the measurement of x_s combined with others such as $|V_{bu}/V_{bc}|$ will give access to the phase of the KM matrix, a quantity which probably governs CP violation: it is therefore a crucial measurement.

5.4.5.4 CP violation in the B system. This is the most ambitious goal of beauty physics.

CP violation in the mass matrix, which is to be searched for using dileptons, is totally out of reach within the framework of the Standard Model (10^{-3} expected); conversely, an exposure of 10^8 Z could give access to the observation of CP violation with a non-standard level of a few per cent.

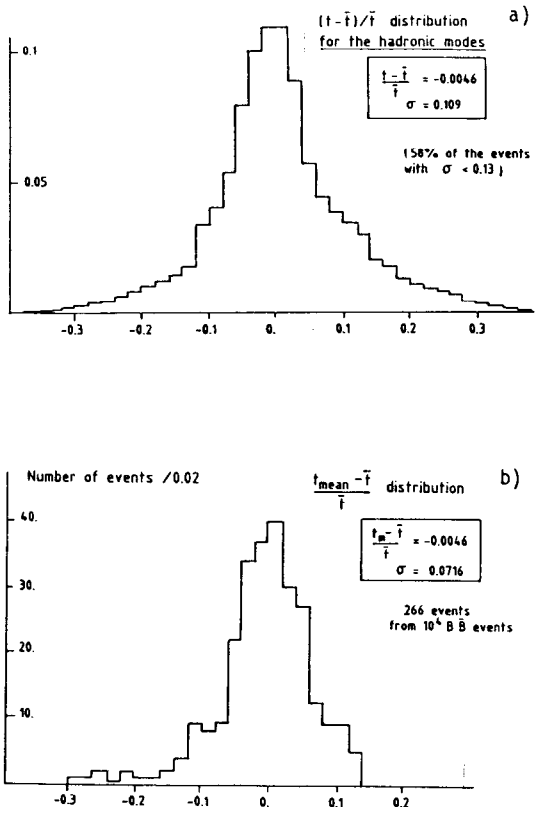

Fig. 51 The resolution on proper time achievable for inclusive B_s channels (Ref. [68]).

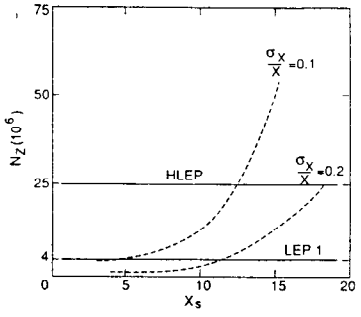

Fig. 52 The X_s measurement achievable versus N_Z.

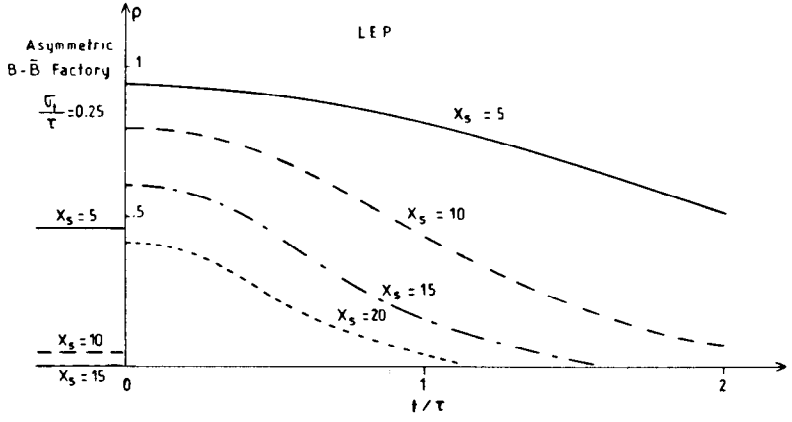

Fig. 53 The damping factor of B_s oscillations at LEP and in a B factory (Ref. [63]).

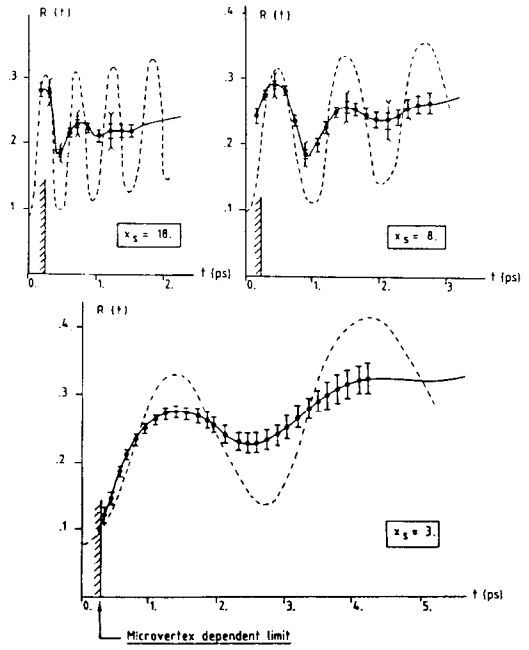

Fig. 54 The expected oscillation pattern for B_s from Ref. [68]. Error bars are for 10^8 Z; some bigger ones are shown for 25×10^6.

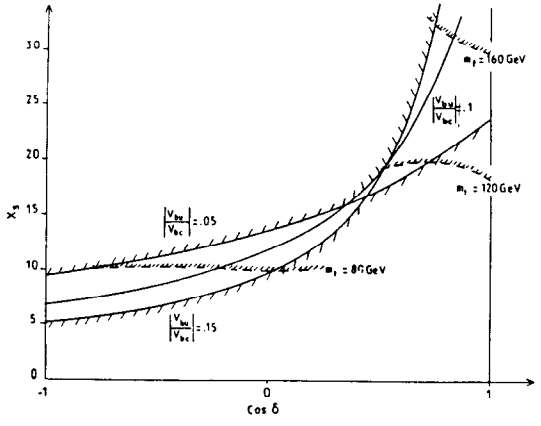

Fig. 55 The measurement of the KM phase through X_s (Ref. [63]).

The most promising way is to consider decays to a CP eigenstate that are accessible from two different paths, such as

$$\begin{array}{ccc} & \mathrm{B^0} \to \psi \mathrm{K} & \\ & \searrow \quad \nearrow & \\ & \mathrm{\bar{B}^0} & \end{array}$$

Other final states could be considered as well (ψK^*, $D^{*+}D^-$, ...). Clearly, it is imperative that detectors should be able to isolate such channels clearly; for instance, they should not mix ψK^0_S and ψK^{0*} by missing the extra π^0: this is a *sine qua non* requirement.

A naive calculation of the number of $b\bar{b}$ needed to give an n_σ effect gives

$$N_{b\bar{b}} = \frac{n_\sigma^2}{A^2} \frac{1}{2\mathrm{BR}} \frac{1}{\epsilon_{\mathrm{tag}}} \frac{1}{\epsilon_{\mathrm{det}}} \frac{1}{\epsilon_{\mathrm{B^0}}} .$$

For $n_\sigma = 3$, $A = 0.2$, BR $= 5 \times 10^{-5}$, $\epsilon_{\mathrm{tag}} = 0.2$, $\epsilon_{\mathrm{det}} = 0.3$, and $\epsilon_{\mathrm{B^0}} = 0.35$, we obtain

$$N_{b\bar{b}} \approx 10^8 \text{ events} .$$

Figures 56a, b show that with a good vertex detector, the time evolution of the effect can be exploited. Figure 56a represents the most favourable asymmetry for the ψK^0_S mode between B^0 and $\bar{B}^0$:

$$\mathrm{B^0} \to \psi \mathrm{K^0_S} \propto \mathrm{e}^{-\Gamma t}(1 + \sin\phi \sin x\Gamma t) ,$$

$$\mathrm{\bar{B}^0} \to \psi \mathrm{K^0_S} \propto \mathrm{e}^{-\Gamma t}(1 - \sin\phi \sin x\Gamma t) ,$$

for the largest possible value of $\sin\phi \simeq 0.6$. Figure 56b indicates that on the tagging side a cut against long flight times can limit the unwanted mixing.

A more serious evaluation has been done at Snowmass [70], where all types of $b\bar{b}$ factories have been compared. Table 15 shows the following interesting features:

- The next-to-last line demonstrates that still within the Standard Model the uncertainty in the expected asymmetry is quite large. Only the most favourable side of the domain can give rise to observable effects.
- Even then, the task is difficult. On the Z without polarization, the required integrated luminosity is 0.5×10^{40} cm^{-2}; this corresponds to a quantum of 1.7×10^8 Z, which is larger than the one we considered. An OPAL study indeed shows that the number of tagged and reconstructed B^0_s is unfortunately quite limited. ($\sim$ one per 10^6 Z Our only hope to have a good chance of reaching the SM-level CP violation is through a very luminous asymmetric $B\bar{B}$ factory ($\beta\gamma \geq 0.4, L \approx 10^{34}$ cm^{-2} s^{-1}), which is not easy to build and exploit. The idea of a pretzel should not compromise the efforts to

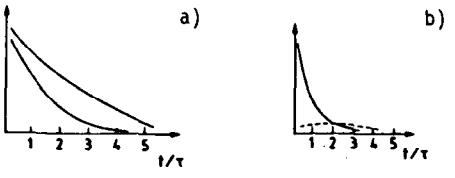

Fig. 56 a) B_d (top) and $\bar{B}_d$ (bottom) decay into ψK^0_S ($\sin\phi = 0.6$); b) $B^0 \to (\ell^- X)$ (full line) and B^0 ($\ell^+ X$) (dotted line).

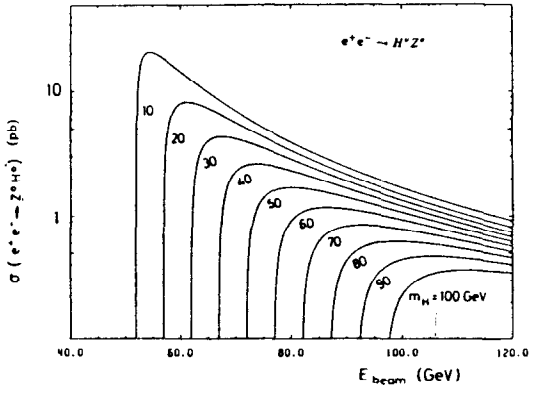

Fig. 57 Total cross-section for HZ production as a function of E_{beam} for a range of Higgs masses. The curves corrected for initial-state bremsstrahlung values of $m_Z = 93.8$ GeV/c^2 and $\sin^2\theta_w = 0.22$ were used.

design such a threshold machine. We should not forget that the world could be non-standard and that the search for CP violation should in any case be performed systematically at LEP. A substantial amount of polarization [71], providing an automatic tagging of b (versus $\bar{b}$), would greatly help. We have seen that such polarization is not *a priori* incompatible with the pretzel scheme, although we enter a domain of wild speculation.

5.4.6 Conclusions on the high-intensity option

The exploitation of high intensity at LEP 1, which increases the speed of Z physics and offers the possibility of an exposure of 10^8 such particles, is certainly a very interesting option.

- It is not an alternative to LEP 200, nor to the use of polarization at the Z.
- It can provide very accurate measurements of essential quantities, such as the number of neutrinos, obtained by the radiative method.
- It will make it possible to substantially improve the accuracy of the tests of the SM through the well-known methods (e.g. lepton and quark width and asymmetries, τ polarization, etc.). High statistics allows us to get hadronic partial widths such as $\Gamma_{b\bar{b}}$ with great accuracy. However, for the determination of $\sin^2\theta$ through asymmetries, compared with a measurement of A_{LR} with polarized beams, the volume of work and the number of problems to be solved are much greater for a result of somewhat lower quality.
- High luminosity may reveal rare decay modes of the Z that are of considerable interest, and many of these channels should be studied carefully.
- The pretzel LEP is a factory for $f\bar{f}$ states. The prospect of identifying $q\bar{q}$ states is good. In particular, for $b\bar{b}$, the pretzel represents a very promising approach with a large amount of physics output, part of which would already appear at the level of 10^7 Z. The measurement of χ_s through the mixing of tagged B_s can be performed under very good conditions (at the different hadron colliders), and it is a crucial one since it gives access to the KM phase. The success of the most ambitious goal, i.e. CP violation, is not guaranteed, and nature will decide. This statement is true for all the facilities being considered at present. I think that the implementation of the pretzel should not preclude the continuing effort to conceive an 'ideal' threshold $B\bar{B}$ programme.

6 LEP 200

LEP 200 has been thoroughly studied in Ref. [3], so here I will focus on only a few particular points.

6.1 How to get there?

A *sine qua non* condition is to have a sufficient number of appropriate superconducting RF cavities. The present state of the art is well described in Ref. [7], and results seem quite promising. Pure Nb cavities have exceeded the design field of 5 MV/m and reached Q-values between 2 and 3×10^9. Niobium-coated copper cavities (1 μm Nb layer deposited by magnetron sputtering) have been shown to be free of thermal breakdown and insensitive to small external static magnetic fields. Accelerating fields up to 9 MV/m have in some cases been reached, as well as quality factors of $5\text{–}7 \times 10^9$. The low transverse impedance of the SC cavities offers the possibility of storing higher currents, besides increasing the power.

Table 16 [72] shows the number of cavities needed to reach various energies, and the approximate date when the exploitation could start. In principle, up to 2×192 cavities could be arranged around the LEP tunnel, although this would be a heavy financial and technical burden. It would be interesting to have *a priori* clear physical guide-lines about the maximum RF power that we would like to see ultimately installed.

To implement the pretzel scheme, room should be provided for the separators. The same is true for the rotators providing longitudinal polarization: it seems that technically the coexistence of all these requirements could be achieved [73] in a peaceful manner.

Table 17 describes another aspect of the energy increase, namely a set of scaling laws that are valid under given assumptions [9]. They lead to the expectation of an increase in luminosity, at least as γ (constant current), and may even be faster if more than 3 mA per beam can be stored. A reasonable guess is

$$L \simeq 5 \times 10^{31}\ \mathrm{cm}^{-2}\ \mathrm{s}^{-1}(\mathrm{peak})\ ,$$

which means that we need two to three years in which to accumulate 500 pb^{-1}, the 'Aachen quantum'. It is clear that any further gain in luminosity would be welcome, and this implies more RF power.

6.2 WW Pair Physics

We will not repeat the physical arguments in detail (see Ref. [3]).

With 500 pb^{-1}, the W-pair sample is still meagre, as indicated in Table 18. The main objective is an accurate measurement of the W mass. Three methods would allow us to reach $\sim \pm 100$ MeV/c^2, namely

i) the threshold dependence of σ_{WW},

ii) the end-point of the lepton spectrum $W \rightarrow \ell\nu$,

iii) the reconstruction of $WW \rightarrow 4$ jets and dijet mass.

It is important to disentangle the statistical and systematic errors so as to know what would be the impact of an increase in luminosity. It turns out that only the first method would benefit from it: with twice as much data, the uncertainty on m_W could probably be decreased to ± 70 MeV/c^2. If further study were to support

this conclusion, this would be an argument in favour of our attempt to fix ideas about the amount of RF power needed. Other aspects of W-pair physics may benefit also from the increased luminosity. In principle, the RF power needed to run LEP at $\sqrt{s} = 200$ GeV and normal current could allow the storage of twice as many bunches or twice as much current at 170 GeV.

6.3 Fermion–Antifermion

The various asymmetries A_{FB}^{ff} at LEP 200 are important factors in the hunt for new physics and in disentangling the origin of possible effects (we speak of unpolarized asymmetries, since we are unlikely to get polarization at high energy).

The accuracy on these asymmetries is statistically limited and would also benefit from an increase in luminosity.

In particular, we recall the typical correlated pattern of deviations that could be found if the strongly coupled Standard Model is a reality (Fig. 35).

6.4 Searches

In the case of the Higgs it is important to get clear ideas about the influence of the energy end-point on the physics reach. The Higgs production cross-section at LEP 200 is given by Fig. 57: we can see a smooth dependence with mass and energy above the threshold. Previous studies have shown that the classical Higgs can be discovered up to ~ 80 GeV/c^2. If the mass were higher, i.e. in the vicinity of m_Z, then it was felt that the ee $\rightarrow$ ZZ background would preclude observation of the Higgs. However, if an efficient tagging of the $b\bar{b}$ final state is performed, this may not be the case. Tthe rate of ee $\rightarrow$ $b\bar{b}ff$ is significantly modified if the Higgs is present, and preliminary studies show that the presence of a Higgs, even having the same mass as the Z, can be revealed through an excess of $b\bar{b}\ell\bar{\ell}$ and $b\bar{b}q\bar{q}$ events with an integrated luminosity of 500 pb^{-1} and $\sqrt{s} \geq 190$ GeV, provided b tagging with an efficiency of $\sim 50\%$ and a purity of $\sim 2/3$ is achieved.

For a classical SM Higgs, this mass range has nothing magic about it. However, for the Higgses of minimal SUSY, the vicinity of m_Z is a singular point as already stated. At tree level the h^0 is always lighter than the Z, and its mass is quite close to m_Z for a large region of the parameter space (Fig. 58). The other scalar, H^0, is always heavier than the Z, but again, in a large complementary region of the parameter space, its mass is within a few GeV/c^2 of the Z mass. The sum of the cross-sections of the two processes

$$ee \rightarrow h^0Z$$
$$ee \rightarrow H^0Z$$

is always, at a given $\sqrt{s}$, larger than the cross-section of the classical process

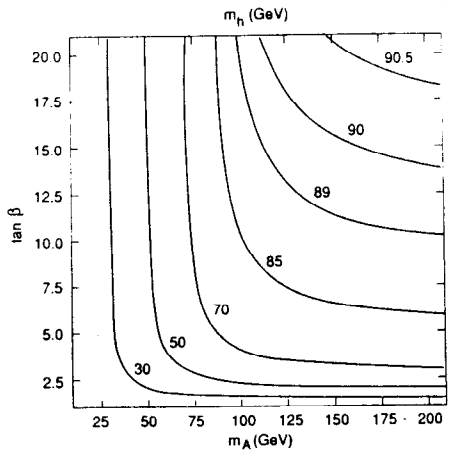

Fig. 58 Iso-m_{h^0} curves in the tan $\beta - m_{A^0}$ plane

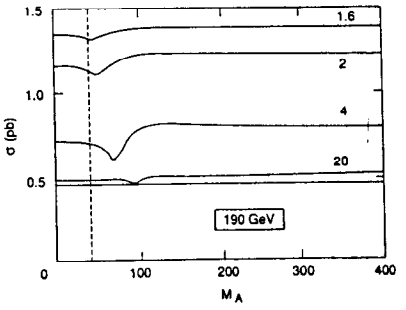

Fig. 59 The sum of cross-section for ee$\rightarrow$ h^0Z and ee$\rightarrow$ H^0Z as a function of tan β (valid at tree level).

$$e\bar{e} \to H(m_H = m_Z)Z \quad \text{(Fig. 59)} ,$$

assuring *a fortiori* the visibility of the SUSY Higgs [74]. However, the available energy has to be $\geq$ 190 GeV; at 180 GeV the exclusion region in the plane $(tg\beta, m_A)$ would be incomplete.

This picture is valid at tree level. As we said one expects however that loops involving the top will raise the masses: h^0 may become heavier than the Z. By how much depends critically on the top mass. If the shift is not too large one can hope that the maximum $\sqrt{s}$ can be raised accordingly.

The exploration of the SUSY Higgs sector, which can lead to the falsification of the minimal SUSY model, is a crucial point that should be considered when one defines the maximum $\sqrt{s}$ and the integrated luminosity at LEP 200.

Figure 60 shows that for SUSY Higgses the associated production mechanism quoted for the Z [43] is present at LEP 200 with rates which should allow their observation [75] but only up to a certain mass well below m_Z. It has been shown [76] that LEP 200 would allow the observation of many other new objects up to the kinematical limit, or close to it, and I refer the reader to these studies [3].

7 POLARIZATION AT LEP

7.1 The Prospects for Polarization

These are developed in Ref. [4], and I will merely summarize the main features and conclusions.

At the SLC [77] the method is to inject polarized e^-, extracted from a GaAs crystal illuminated by a circularly polarized laser. A mean value of $\sim 45\%$ is expected for the polarization. Clearly, only e^- can be polarized this way.

At LEP, the Sokolov–Ternov [78] effect builds up a transverse polarization with the spin of e^- antiparallel to $\vec{B}$. The build-up rate is exponential:

$$P(t) = P_\infty^{\text{ideal}} \left(1 - e^{-t/\tau_P}\right) .$$

The natural values for LEP at the Z are $P_\infty^{\text{ideal}} = 0.924$, $\tau_P = 5$ h. Previously designed wigglers would give $P_\infty = 0.74$, $\tau_P = 90$ min.

Dedicated wigglers have recently been proposed [81] for decreasing the polarization time while keeping the ideal polarization at a high level; we would then obtain

$$P_\infty = 0.88 , \qquad \tau_P = 36 \text{ min} .$$

The overall cost of these wigglers is 2–2.5 MSF. They dominate the machine as far as polarizing and depolarizing effects are concerned. Unfortunately, they strongly enhance the beam energy spread.

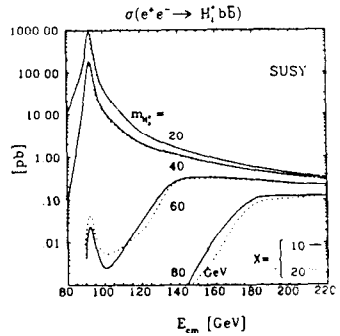

Fig. 60 The cross-section for $e^+e^- \to H_2 b\bar{b}$ in the SUSY model for $v_2/v_1 = 10$ and 20, for different values of m_{H_2}.

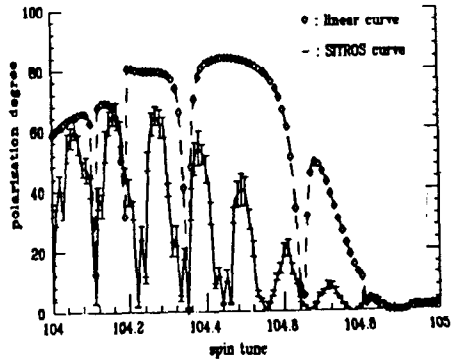

Fig. 61 The expected level of polarization after corrections, including partial harmonic correction (Ref. [80]).

These wigglers have been found, by simulations, to simplify polarization optimization procedures even when higher-order effects are included [79]. An asymptotic polarization degree of $\sim$ 65%, leading to an effective polarization of 50%, seems to be obtainable (Fig. 61). These wigglers lead to much synchrotron emission, a cause of depolarization. The key to spin matching is thus to decrease, at the location of the wigglers, the spin-orbit coupling, which governs the spin rotation due to a change in energy. This has been satisfactorily performed theoretically [80].

But what is needed for physics is longitudinal polarization, which will necessitate having spin rotators on both sides of each experiment. Two types of rotators (Fig. 62) are being studied: Montague rotators [81] incorporated in the arcs and involving both vertical and horizontal bends, and Richter-Schwitters (RS) rotators [82] installed in the straight sections and with vertical bends only.

It is now admitted that the latter type is the only practical one. It is simpler and cheaper. But the main reason is that RS rotators can be properly spin matched [83] and will not lead to depolarization. However, they will force the experiments to be tilted longitudinally by $\sim 1^\circ$ and will be an abundant source of extra synchrotron radiation. Various collimators have been proposed in order to decrease this background, but they will very likely be insufficient, and each experiment will have to foresee further masking so as to protect itself.

7.2 The Bunch Configuration

Once the rotators are active, the natural configuration of helicities is such that colliding e^+ and e^- have equal helicities (Fig. 63a). For full polarization, this corresponds to a null cross-section in the approximation of a vanishing electron mass! Therefore, one of the two colliding bunches needs to be depolarized selectively. This is technically feasible with high efficiency, with a negligible increase in emittance, and using the existing equipment [84].

7.2.1 The classical scheme [85]

In a two-bunch situation we are therefore led to the spin configuration shown in Fig. 63b, which is obtained by depolarizing every other bunch in each beam. This configuration is equivalent to that of the SLC, where successive e^- bunches have opposite helicities (Fig. 63c). We get two types of crossings:

$$\text{type 1 with } \sigma_1 = \sigma_u - P\sigma_\ell \ ,$$

$$\text{type 2 with } \sigma_2 = \sigma_u + P\sigma_\ell \ .$$

The respective cross-sections give us the asymmetry

$$A = \frac{\sigma_2 - \sigma_1}{\sigma_2 + \sigma_1} = P\frac{\sigma_\ell}{\sigma_u} = PA_{LR} \ ,$$

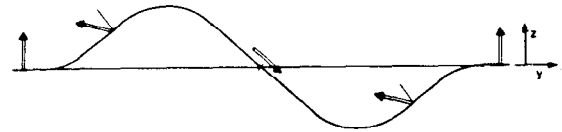

a) Vertical bend rotator

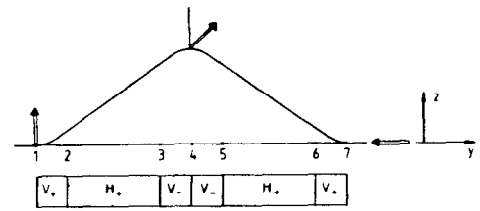

b) Montague's combined bend rotator

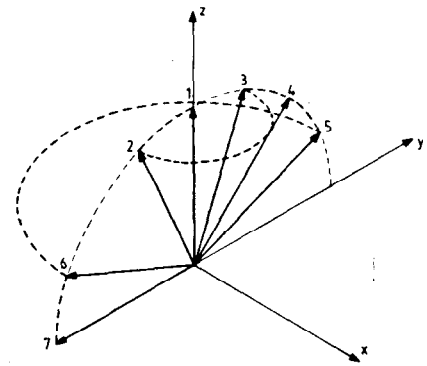

c) The movement of the spin vector in Montague's rotator

Fig. 62 Two types of rotators: a) Vertical bend rotator. b) Montague's combined bend rotator. c) The movement of the spin vector in Montague's rotator.

with

$$A_{LR} = \frac{A}{P} ,$$

which again shows that an excellent knowledge of the polarization is needed: better than 1% in absolute value. At the SLC, measurements of Compton back-scattering and Møller scattering [77] will be combined to obtain the value of the polarization. It is not yet clear whether the figure of 1% is a completely realistic goal for such types of measurements. This uncertainty was casting a serious doubt on the potentiality of polarization until the four-bunch scheme, specific to LEP, was proposed by Blondel [86].

7.2.2 The four-bunch scheme

With four circulating bunches in each beam, and with the possibility of selectively depolarizing any of them, the configuration of Fig. 63d can be realized. There are now four types of crossing, with the corresponding cross-sections:

$$\begin{aligned}
\sigma_1 &= \sigma_u - P_L^- \sigma_\ell , \\
\sigma_2 &= \sigma_u + P_L^+ \sigma_\ell , \\
\sigma_3 &= \sigma_u , \\
\sigma_4 &= (1 - P_L^+ P_L^-)\sigma_u + (P_L^+ - P_L^-)\sigma_\ell .
\end{aligned}$$

In an ideal machine, where all P_L are equal and depolarization is complete, it can be seen that the measurements of σ_1 and σ_2 give A_{LR}, as before, whilst σ_3 and σ_4 give P_L, the absolute value of the polarization, which is now obtained from the data themselves. The desired statistical accuracy on P_L requires, in principle, of the order of only 10^5 Z events.

7.3 The Experimental Requirements

In spite of the help afforded by this scheme, an accurate measurement of A_{LR} poses two serious problems. In practice, the following integrated luminosities will be registered: L_1 with $P_{e^+} \equiv P^+$ and $P_{e^-} = 0$, giving N_1 events; L_2 with $P_{e^+} = 0$ and $P_{e^-} = P^-$, giving N_2 events. We will have

$$P^+ \simeq P^- = P , \qquad L_1 \simeq L_2 = L .$$

Defining

$$A_{exp} = \frac{N_1 - N_2}{N_1 + N_2} ,$$

we obtain

$$A_{LR} \simeq \frac{1}{P}\left[A_{exp}\left(1 + A_{exp}\frac{P^+ - P^-}{2P}\right) + \frac{L_2 - L_1}{L_2 + L_1}\right] ,$$

which shows that

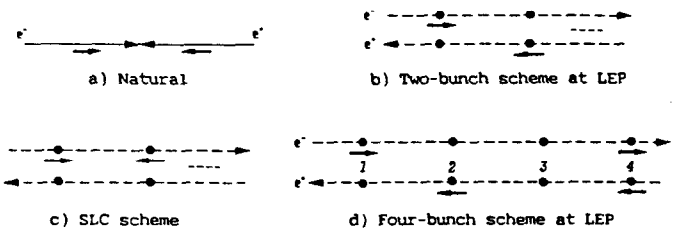

Fig. 63 The helicity configurations.

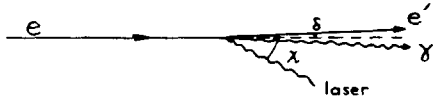

Fig. 64 Compton back-scattering (schematic). The recoiling e' and γ in the laboratory follow the direction of the incoming e^- within a few microradians.

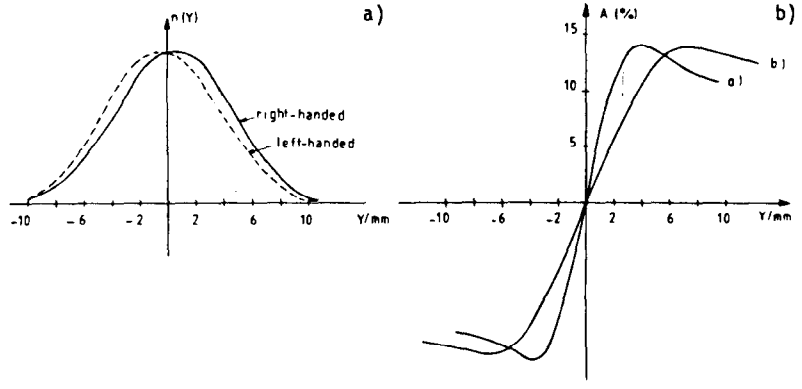

Fig. 65 Up/down asymmetry in transverse polarization measurement (from Ref. [88]).

i) the uncertainty due to lack of knowledge of the polarization is

$$\Delta A_{LR} \simeq A_{LR} \frac{\Delta P}{P} ,$$

thus a 1% relative error on P gives 1.6‰ on A_{LR};

ii) the uncertainty due to lack of knowledge of the relative luminosity is

$$\Delta A_{LR} \simeq \frac{1}{P} \frac{\Delta(L_2 - L_1)}{L_2 + L_1} ,$$

and a 2‰ error on the relative luminosity $\Delta(L_1/L_2) = \Delta L/L$ gives 2‰ on A_{LR} for $P = 0.5$.

These are the typical performances that must be achieved if the systematic error on A_{LR} is to match the statistical error corresponding to 10^6 Z.

7.4 Polarimetry

7.4.1 Remaining requirements on polarimetry

In reality, the situation regarding polarization is more complex than in the ideal case. Depolarization may not be complete. Polarization of bunches 1 and 4 for e^-, and 2 and 4 for e^+, may be unequal. Polarization in the e^- beam can be different from that in the e^+ beam. This last effect can also be measured directly from the cross-sections

$$\Delta P^{\pm} = \frac{\sigma_1 + \sigma_2 - 2\sigma_3}{A_{LR}\sigma_3} .$$

To cope with the former possibilities, we still need polarimetry for monitoring the polarization in both e^+ and e^- beams. Polarimeters are therefore needed in both beams. Their answers must be fast and precise; specifications are discussed in detail in the papers on Polarimetry in Ref. [87]. Because of the possibility of measuring $\Delta P^{\pm}$, the polarimeters fortunately do not have to be calibrated against one another.

Even if the absolute value of polarization is obtained from the detector itself, the requirements on polarimetry are still quite severe, particularly with respect to the bunch-to-bunch systematic effects. To achieve an accuracy of $A_{LR} = 0.025$ with about 10^6 Z events, the polarization measurements should reach the following precision:

i) $\delta P_e \simeq (1\text{–}2) \times 10^{-2}$ obtained in several minutes, to average cross-sections taken with different polarizations;

ii) $\delta(\Delta P_e) \simeq 3\times10^{-3}$, where ΔP_e is the difference in level between two polarized like-sign bunches;

iii) $\delta P_e \simeq 5 \times 10^{-3}$ for 'unpolarized' bunches. It seems that these requirements are likely to be met: Ref. [87] concludes that, including systematic effects, the electron polarization can be measured to $\sim 0.3\%$ in less than 20 minutes of LEP operation.

7.4.2 The two schemes for polarimetry

For such critical measurements, redundancy is certainly welcome, and besides the transverse polarimetry foreseen by the LEP group [88], there is the necessity to provide also measurements obtained at locations where the polarization is longitudinal [87].

Both types of measurements should be equivalent if the spin rotation is well controlled. However, the sources of systematic errors are quite different in the two cases.

The two schemes use a common method: namely, Compton back-scattering of a laser beam (Fig. 64), shot at a small angle onto the $e^{\pm}$ beam, and the detection of recoiling photons. But the observables are different: flipping the circular polarization of the laser leads

– in the case of transverse polarization of $e^{\pm}$, to the inversion of an up–down asymmetry in the distribution of back-scattered γ (or e) (Fig. 65);

– in the case of longitudinal polarization of $e^{\pm}$, to a change in the shape of the energy spectrum of the recoiling γ (or e) (Fig. 66).

In both methods, considerations of background lead to a preference for a multiphoton mode of operation in which, at each shot of the laser, a large number of photons are back-scattered and detected.

In the first method the ratio of the signals is measured in the up and down parts of a calorimeter (Fig. 65). The luminosity of the laser–beam interaction does not matter: on the contrary, the quality of the geometrical alignment of the set-up is crucial and has to be achieved by exploiting symmetry properties. Beam divergence also has to be accurately controlled.

In the second method, if gammas are detected as such, the knowledge of the luminosity of the laser–beam interaction is crucial. This is a very unattractive feature, and a conversion method (Fig. 67) has to be used: gammas are converted into e^+e^- pairs, which are analysed by a magnet, and the observables are ratios of energy deposits in a set of calorimeters, located symmetrically downstream from the magnet. The loss in rate, compared with that in the direct method, is severe (~ 30) but is compensated by the increase in sensitivity, and the dependence on the properties of the laser–beam interaction disappears.

In the case of straight-section rotators, polarimetry is also being considered: it could involve the detection of recoiling e and γ.

7.5 Normalization

7.5.1 Requirements

We recall that in the measurement of A_{ch}, without polarization, the normal-

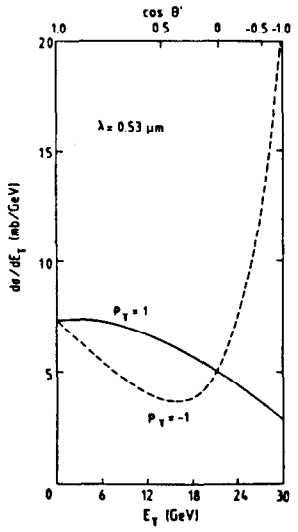

Fig. 66 The modification of the energy spectrum of back-scattered photons from longitudinally polarized electrons when the circular laser polarization is reversed.

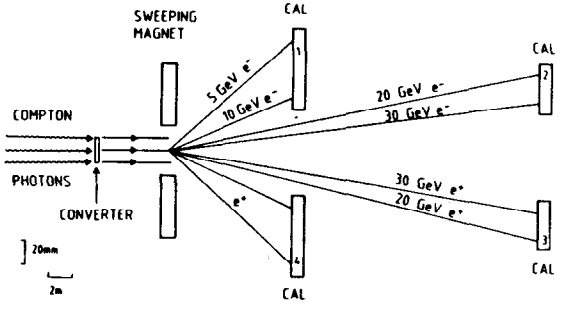

Fig. 67 The conversion method for detecting the back-scattered photons.

ization of the exposure is not important.

For A_{LR}, on the contrary, we saw that the relative normalization between the exposures taken with each type of helicity configuration must be known with an accuracy of at most 2‰: this seems to be a severe requirement, but we emphasize that it involves only a *relative* comparison between two types of crossings following each other at an interval of 23 μs.

For A_{ch}^{pol} the requirements on normalization are less severe: if the conditions are acceptable for A_{LR}, the error on A_{ch}^{pol} will be negligible.

7.5.2 Method

To reach the accuracy of 2‰, only one process can be exploited: Bhabha scattering at small angles. The rate increases very quickly in the very forward region ($\propto 1/\theta^2$). The weak effect on the cross-section is very small in this angular domain and can be corrected for. There is no dependence of the rates on polarization.

In Section 3 we have said that all four LEP experiments have a SAT, generally spanning the domain between $\sim$ 50 and 150 mrad (except for L3, which reaches smaller angles, $\theta_{min} \approx 25$ mrad). The Bhabha cross-section in that region is

$$\sigma_{e^+e^-} \approx \sigma_Z \approx 25\text{–}30 \text{ nb } (\sim 100 \text{ nb in the case of L3}) .$$

In a typical run the statistical accuracy is 2% (1% in L3). Approximately one year (10^7 s) at nominal luminosity (1.3×10^{31} peak, 0.70×10^{31} average) is needed in order to reach the desired figure ($\sim$ 1.6‰ statistical, which leaves room for 1‰ systematic error to reach $\sim$ 2‰ overall). This is already longer than the time needed to register the required amount of data in the optimized four-bunch scheme, and we can see that because of the normalization, the statistical error is increased by $\sim \sqrt{2}$. Furthermore, owing to the low counting rate in the SAT, the systematics of the luminosity measurement cannot be controlled on a short-term basis.

Small-angle taggers are quite elaborate detectors, having both tracking and calorimetric functions and good energy resolution and segmentation: this sophistication is needed for reaching the excellent absolute accuracy (2% or better) required for cross-section measurements. As the SATs are located at relatively large angles (compared with the beam divergence, for instance) they are not affected—if used carefully (see below)—by systematic effects related to the geometry of the interaction region. A satisfactory solution to our problem would be to decrease the lower limit of the angular acceptance of such detectors, so as to be able to register about three to four times more Bhabha events.

In fact, all four experiments have already decided to reduce the radius of their beam pipe. The motivation is generally to improve the performance of the microvertex coverage. But the SAT arrangement will benefit from such a modification if the use of masks (against synchrotron background) close to the crossing point—which is a likely condition—does not jeopardize the possibility of accepting $e^{\pm}$ in the angular region of interest (20–50 mrad).

Besides the SAT, experiments are also exploiting a VSAT with typically $\sigma_{e^+e^-} \sim$ 10–20 $\times$ σ_Z. The problem of statistics disappears. But these detectors, being located at angles between 5 and 10 mrad, are more sensitive to a set of systematic effects, which have to be identified and controlled with great care.

7.5.3 Control of systematic errors

After the first year of experimentation, all the experiments consider that an absolute value below 1% is a reasonable expectation from the SAT but, as already mentioned, this depends on the quality and elaboration of these devices (see Ref. [89]). Reaching this figure also requires a very accurate treatment of radiative corrections to small-angle Bhabha scattering [90].

In fact, we are interested here in the relative aspect of normalization. Because of the fast alternance of crossings of both helicity configurations, most of the effects (radiative corrections, detector position, efficiency, etc.) just cancel, and it is difficult to see what can contribute to a relative shift except

i) the background, and

ii) the shape and the position of the luminous region,

all of which can be different from one crossing to the other since the intensities and emittances of bunches can vary. If such variations occur, they will have different effects depending on whether they happen randomly or are systematically different from one bunch type to another.

The possible strategies foreseen are the following:

1) To measure the background, which can be due to off-momentum e^-, beam–gas interactions, etc. It has been shown (Ref. [89]) that by designing a complete set of measurements of various random coincidence rates on a bunch-to-bunch basis, the problem of background subtraction can be treated correctly.

2) To decrease the sensitivity of the detectors to the features of the luminous region [91]. The SAT and the VSAT are symmetric detectors, with both arms identical. However, whenever there exists in them a mask or a position-measuring device, it is possible to get an asymmetric acceptance *de facto* or off line (Fig. 68). Intuition and simulations show that the sensitivity of the normalization procedure to parameters such as the centroid displacement or the divergence of the beams in the collision region is much decreased, without appreciable loss in rate. Since the dependence of the rates on these parameters cannot be completely suppressed, a correction must still be performed.

3) To be informed of such variations so that they can be corrected for.

One source of information will be the measurements of the machine-surveying instruments. Each interaction point will be equipped with a luminosity monitor [92], which is located at ± 15 m from the interaction point; it is similar in conception to the proposed VSAT and is operated by the LEP team. Its expected performances can be deduced from Fig. 69 and will afford an interesting cross-check.

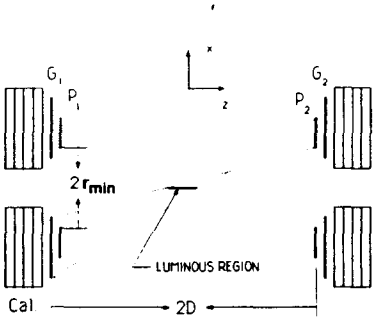

Fig. 68 The principle of an asymmetric acceptance for a luminosity detector.

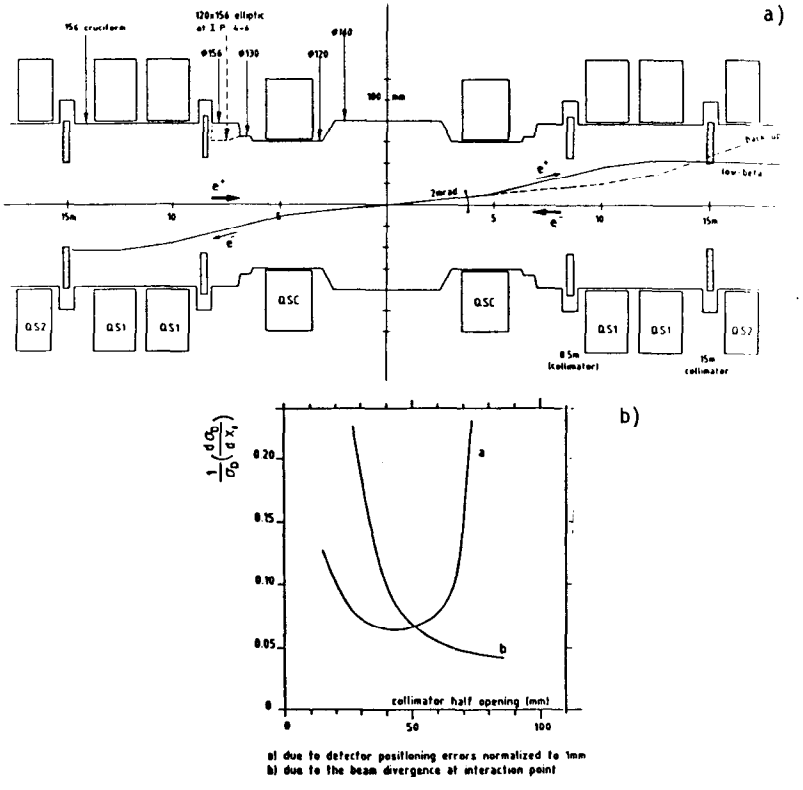

Fig. 69 The LEP luminosity monitor and its performance (from Ref. [92]).

Moreover, a whole set of measurements will be performed for each crossing and will be made available to the experiments: the bunch intensities (which are supposed to stay equal between e^+ and e^- bunches to better than 1%) and their emittance, angular divergence, lateral displacement, etc. These measurements are shown in Table 19, which contains the nominal values, possible displacements, and uncertainties in the relevant quantities.

To substantiate and improve the numbers in Table 19, much information will have to be obtained from the experiments themselves. This cannot be on a bunch-to-bunch basis; but in short periods—of the order of a filling—and with the required accuracy, measurements of the mean parameters of one bunch type relative to another will be obtained.

One class of such measurements is linked to the vertex reconstruction, and is quite accurate when a microvertex is available (typically ~ 25 μm transverse accuracy).

Another source of information about the behaviour of the beams comes from the SAT—or rather from its tracking part, if it exists—and from the VSAT with its position detector. This is quantitatively discussed in Ref. [87].

The result is that—contrary to what one could fear in view of the limited rate of e^+e^- in the SAT—an experiment can be quickly informed of possible relative systematic effects at the 1‰ to 2‰ level: it is not necessary to wait until the SAT has reached the equivalent statistical accuracy.

Another interesting device, as far as the measurement of the beam divergence is concerned, is the divergence monitor proposed in Ref. [93].

For the Polarization Workshop [4], a group carefully studied the systematic effects in the relative normalization procedure for the two-monitor scheme (SAT and VSAT, to which one can add the LEP monitor). With the asymmetric acceptance technique and with the accuracy of the information on the luminous region, we are certainly not far from achieving the required accuracy. But it is difficult to foresee exactly what the systematics of VSAT-type detectors will be, and we need to have some experience of their use.

However, it is likely that by the time polarization is achieved, a new generation of SATs at smaller angles will be in operation, so that the statistical and the systematic problem will be solved by a single device. This is already the case for L3. We can also note that the SATs are already not far from achieving in absolute value the level of relative accuracy needed.

7.6 The scenario and the factor of merit of the measurement of A_{LR}

The expression giving the statistical error on A_{LR},

$$\Delta A_{LR}^{stat} = \sqrt{\frac{1}{P^2(N_1+N_2)} + \cdots},$$

shows that the figure of merit of the measurement is

$$F = \int P^2 L \, dt \, .$$

Figure 70 gives the time dependence expected for polarization in a run. Figure 71, drawn under a set of likely assumptions, indicates that the optimization of this quantity does not correspond exactly to an optimization of the integrated luminosity; it reflects the fact that for polarization measurements, longer runs are preferred. However, the effect is small: of the order of 7%, with the dedicated wigglers. It is fair to define *a priori* which factor of merit should be our aim. It seems to us that a figure of $\int P^2 L \, dt \simeq 10$ pb^{-1} makes sense, because, as indicated in Table 4, it brings about the dramatic improvement of a factor of 4 in the accuracy, compared with the improvement that could be obtained in a much longer exposure (a factor of 4 for $P = 0.5$) without polarization. If at some time it is demonstrated that this goal cannot be reached in a reasonable period, say of the order of one year, this probably means that the whole polarization programme would have to be reconsidered.

However, following in the discussion of the preceding section, we must realize that the above figure of merit, corresponding to 40 pb^{-1} with $P = 0.5$, will be sufficient only if some improvement in normalization has been made with respect to the present situation, so that the statistical error linked to the SAT is no longer a limiting factor: as we have said, this could be achieved by bringing its coverage down to 25 mrad. If the SAT acceptance were to stay at its present value, then 65 pb^{-1} would have to be registered instead. Table 20 summarizes these numbers. The impossibility of reaching a level of polarization of 30% would also indicate that the programme should not be pursued, since systematic errors behave as $1/P$.

7.7 Systematic Errors in the Detector

7.7.1 The case of A_{LR}

To measure A_{LR}, in principle one simply flips the helicity of the beam and nothing is changed in the experimental procedure.

One has to distinguish Z events from two-photon and background events. This has been shown not to be a serious problem. What really matters is only the stability of the selection from one bunch type to another. Since A_{LR} is independent of the final state in first approximation, the efficiency of the selection of the various fermion-antifermion pairs in the Z decay is irrelevant as long as it stays constant.

The only possibility of error could come from a large variation in the background (not related to the luminosity) from one bunch type to another, if a small fraction of this background creeps in at the selection level. Such a change in the background level is unlikely to happen, and it can be monitored. The probability that a machine background event can be registered as a Z decay is found to be

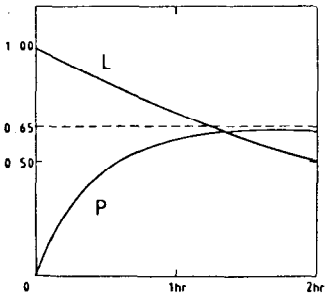

Fig. 70 The time dependence expected for polarization in a run.

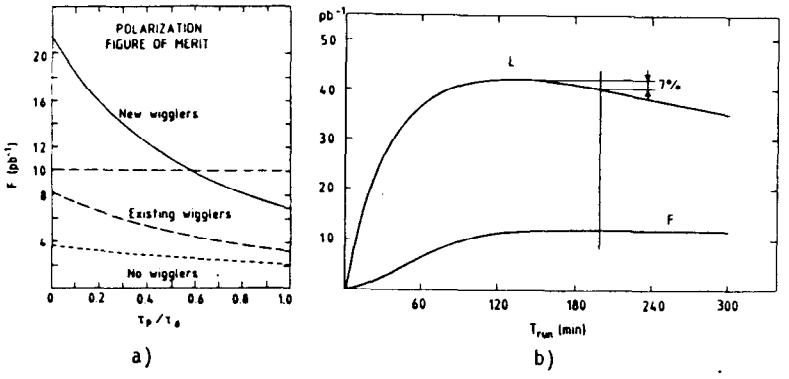

Fig. 71 The figure of merit (a); the comparison between its optimization and the optimization of the integrated luminosity (b). Assumptions: dedicated wigglers on luminosity lifetime: $\tau_L = 3$ h; $\tau_P/\tau_D = 0.4$; $P_{max} = 0.65$; filling time of the maching $\tau_{fill} = 1$ h; 100 days of continuous operation with $L(0) = 10^{31}$ cm^{-2} s^{-1}.

negligible with any reasonable set of acceptance criteria. The rate of $\gamma\gamma$ events accepted within these criteria (and not affected by the helicity flip) can be kept so small that one can also forget about this problem.

For $A_{ch}^{\mu\mu}$ the situation is much more critical and it has already been discussed in Section 3.

7.7.2 Flavour tagging

It has been shown that A_{ch}^{pol} has several interesting properties and requires the identification of the final state. In the case of $q\bar{q}$, this implies flavour tagging as well as the distinction between q and $\bar{q}$. This problem is discussed in Ref. [32], has been reviewed in [57], and here we recall its main points.

We can now forget about the $t\bar{t}$ final state on the Z; we are thus left with three down-type (d, s, b) and two up-type (u, c) quark flavours. It is generally considered that the heavy quarks (c, and especially b) are relatively easy to isolate with useful efficiency and purity, whilst this is not the case for light ones. However, given the present situation of b physics, for which mixing will complicate the asymmetry measurement, it would be preferable to measure also this asymmetry for another down-quark, for instance the s.

Flavour tagging relies on the following:

i) The knowledge of quark fragmentation for each individual flavour.

For the time being, paradoxically this is measured more accurately for heavy quarks. In particular, not much is known about the strange quark: this is understandable since, at e^+e^- rings, the s-quark, because of its charge, plays only a minor role, whilst in deep-inelastic scattering, strangeness can be found only in the sea. The situation will change completely on the Z, where d-, s-, and b-quarks will be the most abundantly produced ($\sim$ 15% branching ratio): an exposure on the Z should, in principle, bring us much new information on s fragmentation, and we will discuss this later.

ii) A set of techniques allowing identification of specific properties of the final state.

Prompt leptons, with appropriate p and p_T cuts to improve their purity, are well-known and efficient candidates for flavour tagging. From their identification and measurement, we can go a long way towards the isolation of beauty.

These lepton measurements can be complemented by hadron identification, obtained either from dE/dx techniques in gaseous tracking devices or by the Cherenkov effect. Figure 72 summarizes the identification power of the Ring-Imaging Cherenkov (RICH) counter technique and gives preliminary results. Kaon/proton identification seems indispensable for most of the spectroscopic studies. In b physics, it is also a 'must' to identify the various sources of mixing and have access to some rare modes of the B particles. For flavour tagging, the purity of isolated samples can be substantially increased if hadron identification is added to the measurement of leptons.

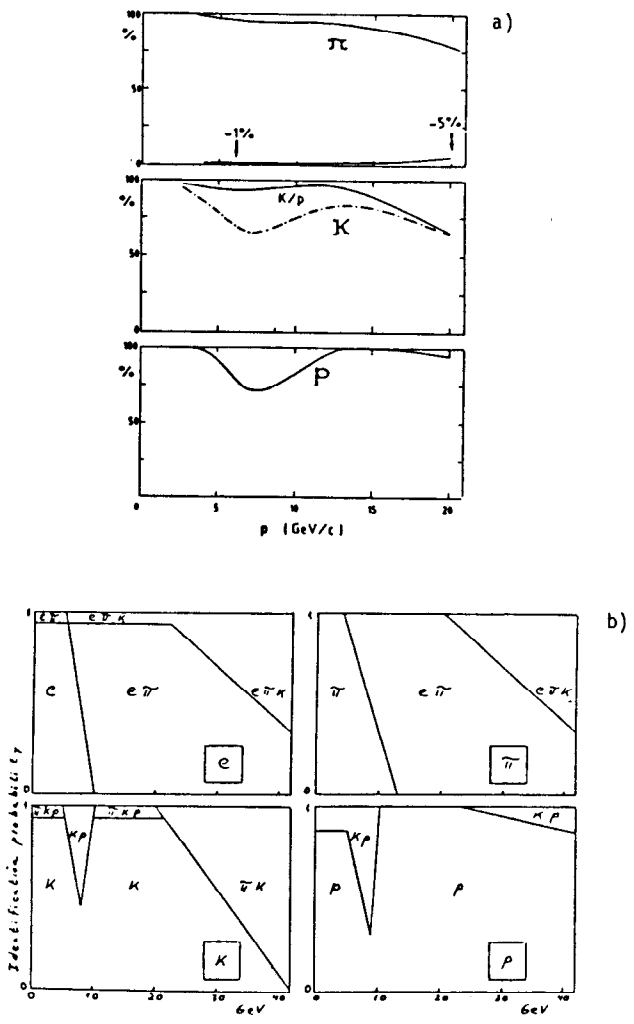

Fig. 72 Hadron identification by the RICH counters of DELPHI. a) Barrel RICH. The curves labelled π, K, p give the probability that the corresponding hadron is correctly identified. The rate of error is very small. b) Forward RICH.

Finally, the use of microvertex detectors to identify secondary vertices, and to unambiguously attribute to them subsets of the banks of reconstructed tracks, is the latest well-known method of flavour identification. It improves the accuracy of the measurement, decreases the combinatorial problems enormously, and provides information on the lifetimes. This has been well illustrated for LEP microvertex detectors [94]. However, the present limitations of such devices are well known, too: because of the large radius of the present beam pipe, the accuracy of extrapolation is not as good as it could be, and it is impossible to cover angles below $\sim$ 40°. All experiments are interested in improving this situation. This requires a reduction in the size of the vacuum pipe, and therefore a careful evaluation and rejection of background due to synchrotron radiation and lost particles, as we discussed previously.

Another limitation, and one that is difficult to overcome, is due to the fact that part of the uncertainty in flavour tagging comes from confusing q and $\bar{q}$ of the same flavour: in such a case it would seem—and can be demonstrated—that the microvertex information does not help much.

7.7.3 Methodology of flavour tagging

This is described in Ref. [32]. The successive steps are:

i) to define a signature for a given flavour; for instance

– $s\bar{s}$ candidates must have leading K on both sides,

– $b\bar{b}$ must have a (lepton-kaon) pair of like signs with adequate kinematical properties,

– $u\bar{u}$ candidates must contain a leading proton, etc.;

ii) to estimate the efficiency of the procedure and the uncertainty in the knowledge of this efficiency;

iii) to estimate the purity obtained and the uncertainty in the knowledge of this purity.

Formally, weights can be defined, such as

$G^{q\bar{q}}$ (the probability of being right),

$g^{\bar{q}q}$ (the probability of confusing q and $\bar{q}$),

$g^{f\bar{f},f\bar{f}}$ (the probability of selecting another flavour by mistake),

the sum of all weights being unity.

The g factors are obtained from a Monte Carlo program; the error on them, $\Delta g/g$, reflects the uncertainty in the knowledge of the fragmentation of the quarks. Globally, the true asymmetry can be expressed in terms of the measured one by

$$A_{\rm ch}^{\rm pol,d} = \frac{A_{\rm ch,exp}^{\rm pol,d}}{1-C} \ ,$$

where C is a linear function of the weights. We have already said that for b- and c-quarks the present information about fragmentation is satisfactory, whilst it is poor for the light quarks—especially the s.

A crucial point of the planned strategy of flavour tagging is that during the first phase of LEP physics, yielding several million Z, the various available Monte Carlo models—such as the different versions of the Lund Monte Carlo, the Webber parton shower model, etc.—can be accurately tuned so that they reproduce the results obtained for inclusive distributions of identified particles (or any other observable) in the Z final state. Indeed, with such Monte Carlos, there may be legitimate doubts about their predictive power when they are extrapolated from PEP/PETRA energies upward, and it is therefore important to feed them with experimental data from TRISTAN at present, and on the Z later.

Nevertheless, Figure 73 shows that in their present state the different models already agree very well; the uncertainty on fragmentation can, for the time being, be defined as the remaining divergence ($\Delta g/g \leq 0.2$). Figure 73 also exhibits the dominance of s ($\bar{s}$) as the source of leading K in the final state, illustrating the remark made above about the role of the strange flavour at the Z.

We have already mentioned that when the integrated luminosity is sufficient, the double-tag procedures—more demanding in statistics, but less prone to systematics—are very promising. We should not, however, underestimate the residual systematic error due to the uncertainty in the knowledge of the background. It seems that we will be able to devise procedures for measuring this background with the level of accuracy needed and, we are then allowed to expect that the errors will scale as $\sim 1/\sqrt{N}$.

Tables 3 and 9, which are explained in detail in Ref. [32], summarize the expected achievements in flavour tagging. According to these tables, the residual uncertainty associated with flavour tagging will not prevent some LEP experiments from reaching the accuracy on $A_{\rm ch}^{\rm pol}$ that is needed to get interesting physical information from this quantity.

7.8 Conclusion on Polarization

All studies made up to now lead to the conclusion that polarization on the Z, together with $m_{\rm Z}$ and $m_{\rm W}$, can be exploited to provide the most accurate test of the Standard Model through $A_{\rm LR}$ and $A_{\rm ch}^{\rm pol}$ measurements.

Such accurate measurements will allow us to obtain a hint of the value of the Higgs mass (mostly from $A_{\rm LR}$ once $m_{\rm Z}$ is given) and also of the t-quark mass (mostly from $m_{\rm W}$), if they are still unknown at that time.

New physics inside and outside the algebraic frame of the SM will be sought; the possibility of identifying its nature among all models, using the combination of various accurate measurements, is now firmly established. The physics outcome will not be obscured by complications in the theoretical description.

On the experimental side, the normalization problem should be overcome, and the best way of achieving this is by extending the SAT coverage to reach the angular acceptance already met by L3. The four-bunch scheme, which is unique to LEP, provides the absolute value of the polarimetry: the monitoring of the polarization will be done, with the required accuracy, by the transverse

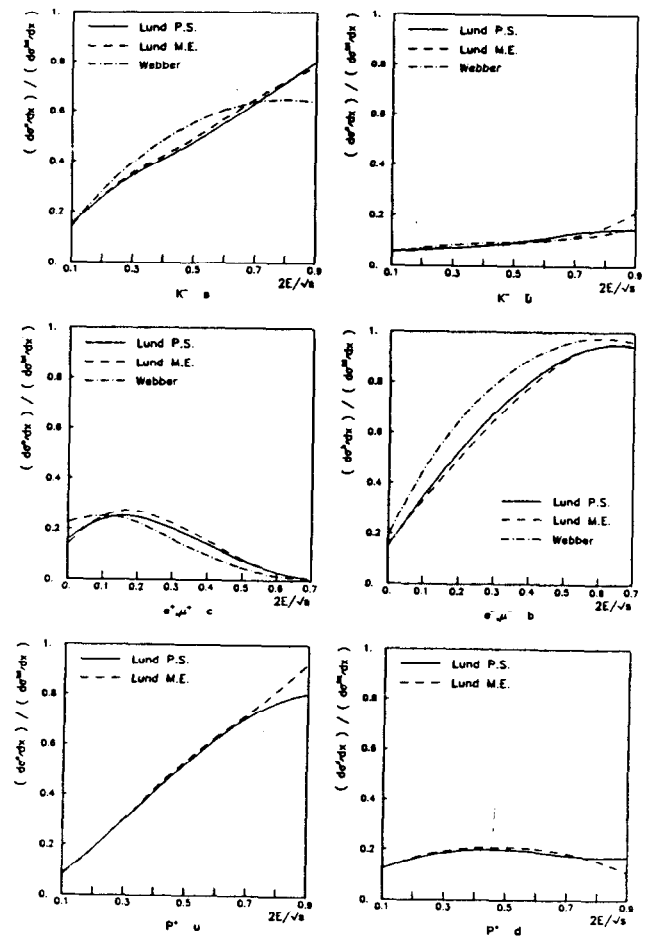

Fig. 73 The fragmentation of various quarks in different models available. The quantity plotted is the relative contribution of a given parent quark to a given inclusive particle as a function of fractional momentum.

polarimetry, probably cross-checked by another method involving quite different systematic errors.

Obtaining a useful level of longitudinal polarization at LEP is still considered difficult. However, several new facts concerning, for instance, optimized wigglers and the properties of straight-section rotators, as well as the way to correct machine imperfections, make the overall picture quite realistic and promising.

8 GENERAL CONCLUSION

The three options reviewed for the future of LEP have large and specific physics potentials.

Technically, the rise in energy and the multibunch option are strongly coupled and rely on the installation of RF SC cavities, in a sufficient number and with a high level of performance.

Polarization is not guaranteed from the machine point of view, since LEP characteristics are far from being optimal for that issue. What is important now is to keep the possibility open, by building the dedicated wigglers and pursuing work along the various sectors involved. One should also keep in mind that LEP offers two unique features: a high luminosity and the possibility of the four-bunch scheme, which solves the problem of the absolute measurement of polarization.

A very high luminosity at the Z is *a priori* quite promising. The on-going workshop on this subject should allow us to understand more deeply the experimental implications as well as the exact possibilities in the various physics sectors, for instance rare decays and B physics.

Various searches and measurements call for a higher energy. Multibunching can also increase the luminosity in this low cross-section domain, by a factor which depends on the installed RF power and decreases with $\sqrt{s}$. The strategy of energy rise should incorporate such a possibility.

Acknowledgements

I would like to thank J.E. Augustin and F. Pauss for a critical reading of the manuscript, and to express my appreciation of the competent and friendly help given by the CERN Scientific Editing and Text Processing Services.

I warmly thank the SLAC Summer Study organizers for their invitation to this stimulating meeting.

References

[1] J. Ellis and R. Peccei (eds.), Physics at LEP, report CERN 86–02 (1986).

[2] G. Altarelli, R. Kleiss and C. Verzegnassi (eds.), Proc. Workshop on Z Physics at LEP 1, Geneva, 1989 (CERN 89–08, 1989).

[3] A. Böhm and W. Hoogland (eds.), Proc. ECFA Workshop on LEP 200, Aachen, 1986 (CERN 87–08, ECFA 87/108, Geneva, 1987).

[4] G. Alexander et al. (eds.), Polarization at LEP, report CERN 88–06 (1988).

[5] J.D. Jackson, Classical electrodynamics, 2nd ed. (John Wiley and Sons, Inc., New York, 1975).

[6] M. Bassetti, Proc. 11th Int. Conf. on High-Energy Accelerators, Geneva, 1980 (Birkhäuser, Basle, 1980), p. 650.

[7] P. Bernard et al., *in* Ref. [3], vol. I, p. 29.

[8] B. Zotter, CERN LEP Note 528 (1985).

[9] E. Keil, *in* Ref. [3], vol. I, p. 17.

[10] E. Keil and R. Talman, Part. Accel. **14** (1984) 109.

[11] G. von Holtey, Note CERN/LEP–BI/88–52 (1988).

[12] D. Ritson and G. von Holtey, Note CERN/DELPHI 88–70 Gen 83 (1988).

[13] P. Roudeau, DELPHI internal note.

[14] M. Cvetič and B.W. Lynn, Stanford preprint SLAC PUB–3900 (1986) and Phys. Rev. **D35** (1987) 51.

[15] J.H. Kühn (ed.), Proc. Workshop on Radiative Corrections for e^+e^- Collisions, Ringberg Castle (FRG), 1989 (Springer, Berlin, 1989).

[16] P. Jenni, *in* Ref. [3], vol. II, p. 486.

[17] P. Roudeau et al., *in* Ref. [3], vol. I, p. 49.

[18] C.Y. Prescott, Stanford preprint SLAC PUB–3120 (1983).
B.W. Lynn and R.G. Stuart, Nucl. Phys. **B253** (1985) 216.

[19] A. Blondel et al., Univ. Montpellier preprint PM/87–14 (1987).

[20] MK II: Stanford preprint SLAC PUB–5124 (1989).

[21] ALEPH: Phys. Lett. **B231** (1989) 519.
DELPHI: ibid., p. 539.
L3: ibid., p. 509.
OPAL: ibid., p. 530.

[22] F. Dydak, Results from LEP and the SLC, Renew talk given at the Int. Conf. on High-Energy Physics, Singapore, 1990.

[23] Ya.S. Derbenev et al., Part. Accel. **9** (1980) 247.
D.B. Barber et al., Phys. Lett. **135B** (1984) 498.

[24] G. Burgers et al., *in* Ref. [2], vol. 1, p. 55.
F. Berends, *in* Ref. [2], vol. 1, p. 89.

[25] M. Böhm and W. Hollik, Nucl. Phys. **B204** (1982) 45.

[26] See in Ref. [4], vol. 1: B.W. Lynn, p. 24; W. Hollik, p. 83; H. Burkhardt et al., p. 145; B.A. Kniehl et al., p. 158; etc.

[27] F. Boudjema et al., Phys. Lett. **B202** (1988) 411 and **B214** (1988) 151; Nucl. Phys. **B314** (1989) 301.

[28] F. Pauss, preprint CERN–EP/89–93, Lectures given at the 28. Universitätswochen für Kernphysik, Schladming, 1989.

[29] W. Hollik, preprint CERN TH.5426/89 (1989).

[30] R.N. Cahn, Phys. Rev. **D36** (1987) 2666.

[31] M. Böhm and W. Hollik, *in* Ref. [2], vol. 1, p. 203.
G. Montagna et al., preprint CERN TH.5445/89 (1989).

[32] J. Drees et al., *in* Ref. [4], vol. 1, p. 317.

[33] See, for instance, W.W. Ash et al. (MAC Collab.), Stanford preprints SLAC PUB–3741 (1985) and SLAC PUB–4040 (1986).

[34] F. Boillot, Thèse de doctorat, Univ. Paris-VI (1987), unpublished.
S. Jadach and Z. Wąs, *in* Ref. [2], vol. 1, p. 235.

[35] S. Glashow, Phys. Lett. **187B** (1987) 367.
G.F. Giudice et al., Phys. Lett. **212B** (1988) 181.

[36] G. Feldman, SLAC MK II Note 2–24 (1987).

[37] G. Barbiellini et al., Phys. Lett. **106B** (1981) 414.

[38] L. Trentadue, *in* Ref. [2], vol. 1, p. 129.

[39] H. Band et al., Stanford preprint SLAC PUB–4990, presented at the Workshop on the Fourth Family of Quarks and Leptons, Santa Monica, Calif., 1989.

[40] P.J. Franzini and P. Taxil, *in* Ref. [2], vol. 2, p. 58.

[41] E.W.N. Glover and J.J. van der Bij, *in* Ref. [2], vol. 2, p.11.

[42] Higgs at LEP:
DELPHI CERN-EP/90-60(May 90) updated for Singapore.
L3 Preprint # 10 (June 90).
OPAL E/90-150 (Oct. 90).
ALEPH Higgs search: CERN-PPE/90-101 (July 90).

[43] G.F. Giudice, Phys. Lett. **208B** (1988) 315.

[44] J.F. Gunion, Univ. California (Davis) preprint UCD-89-10 (1989).

[45] H.J. Behrend et al. (CELLO Collab.), Phys. Lett. **B193** (1987) 376.

[46] M. Felcini, preprint CERN-EP/89-173 (1989).

[47] $H^{\pm}$ searches at LEP:
ALEPH, CERN-EP/90-34 and Phys. Lett. **B241** (1990) 623.
DELPHI, CERN-EP/90-33 and Phys. Lett. **B241** (1990) 449.
L3, Preprint # 19 (Sept. 90).
OPAL, CERN-PPE/90-116 (Aug. 90).

[48] OPAL, CERN-EP/89-154 (Nov. 89) and update for Singapore.

[49] A. Roussarie, talk at Singapore for the ALEPH Collaboration.

[50] E.J. Eichten et al., Phys. Rev. Lett. **50** (1983) 811.

[51] D. Bloch, Strasburg preprint CRN/HE 86-08 (1986).

[52] L.F. Abbott and E. Farhi, Phys. Lett. **101B** (1981) 69; Nucl. Phys. **B189** (1981) 547.

[53] D.W. Düsedau and J. Wudka, preprint MIT-CTP 1389 (1981).

[54] See D. Treille et al., *in* Ref. [3], vol. II, p. 414.

[55] C. Rubbia, preprint CERN-EP/88-130 (1988).

[56] J. Jowett, Note CERN-LEP-TH/89-17 (1989).

[57] Report on a High-Luminosity Version of LEP, to appear in 1991.

[58] G. Wormser, Stanford preprint SLAC PUB-4576 (1988), and references therein.
DELPHI, preprint CERN-PPE/90-123 (1990).

[59] R. Battiston et al., Perugia preprint DFUPG-13/89 (1989).

[60] W.S. Hou et al., Munich report MPI-PAE/PTh 55-88 (1988).

[61] E.W.N. Glover and J.J. van der Bij, *in* Ref. [2], vol. 2, p. 34.

[62] J.J. Gomez-Cadenas and C.A. Heusch, Univ. Calif. Santa Cruz preprint SCIPP 88/32 (1988).

[63] P. Roudeau, Orsay preprint LAL 89-21 (1989) and Ref. [57].

[64] C. de la Vaissière et al., Note CERN/DELPHI 89-5 Phys 35 (1989).

[65] K. Berkelman, Proc. SLAC Summer Inst. on Particle Physics—Probing the Weak Interaction: CP Violation and Rare Decays, Stanford, 1988 (SLAC Report No. 336, Stanford, 1989), p. 1.

[66] I. Bigi, *ibid*, p. 31.

[67] F.R. Cavallo, Note CERN/DELPHI 88-5 Phys 22 (1988).

[68] C. Defoix, Note CERN/DELPHI 90-40 Phys 67 (1990).

[69] H.G. Moser, MPI Preprint Exp. 209.

[70] G.J. Feldman et al., Report of the B Factory Subgroup (I: Physics and Techniques), *in* Proc. Summer Study on High-Energy Physics in the 1990s, Snowmass, Colo. (USA), 1988 (World Scientific, Singapore, 1989), p. 561.

[71] W.P. Atwood et al., Stanford preprint SLAC PUB–4544 (1988).

[72] E. Picasso, Talk given at the ECFA Open Meeting, CERN, 1989.

[73] E. Keil, private communication to the Polarization Working Group.

[74] By courtesy of R. Barbieri.

[75] J. Kalinowski et al., Warsaw preprint IFT/11/88 (1988).

[76] See in Ref. [3], vol. II: P. Igo-Kemenes et al., p. 251, and C. Dionisi et al., p. 380.

[77] M.L. Swartz, *in* Ref. [4], vol. 2, p. 163.

[78] A.A. Sokolov and I.M. Ternov, Sov. Phys.-Dokl. **8** (1964) 1203.

[79] A. Blondel and J.M. Jowett, CERN LEP Note 606 (1988).

[80] J.P. Koutchouk and T. Limberg, *in* Ref. [4], vol. 2, p. 204.

[81] B. Montague, Phys. Rep. **113** (1984), and references therein.

[82] R. Schwitters and B. Richter, SLAC PEP Note 87 (1984).

[83] A. Blondel and E. Keil, in Ref. [4], Vol. 2, p. 250.

[84] J. Buon and J.M. Jowett, CERN LEP Note 584 (1987).

[85] M. Placidi and R. Rossmanith, CERN LEP Note 545 (1985).

[86] A. Blondel, Phys. Lett. **B202** (1988) 145.

[87] G. Alexander et al., preprint CERN–EP/88–27 (1988) and *in* Ref. [4], vol. 2, p. 3.

[88] M. Placidi and R. Rossmanith, Nucl. Instrum. Methods **A274** (1989) 79.
M. Placidi, CERN/LEP–BI/89–09 (1989).

[89] G. Alexander et. al., *in* Ref. [4], Vol. 2, p. 83.

[90] See Vol. 3 of Ref. [2].

[91] J.F. Crawford et al., Nucl. Instrum. Methods **127** (1975) 173.

[92] J.Y. Hemery et al., CERN/LEP–BI/86–5 (1986).

[93] G. De Zorzi et al., *in* Ref. [4], vol. 2, p. 64.

[94] M. Burns et al., preprint CERN–EP/88–82 (1988).

Table 1

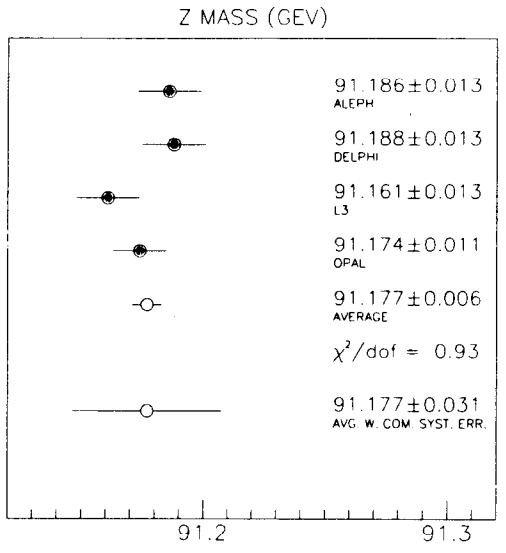

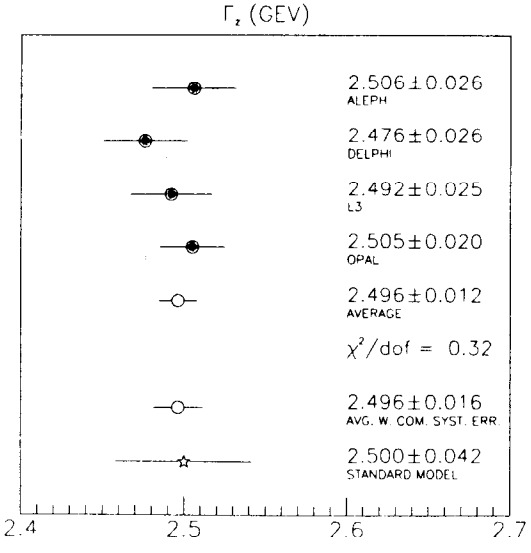

Table 2

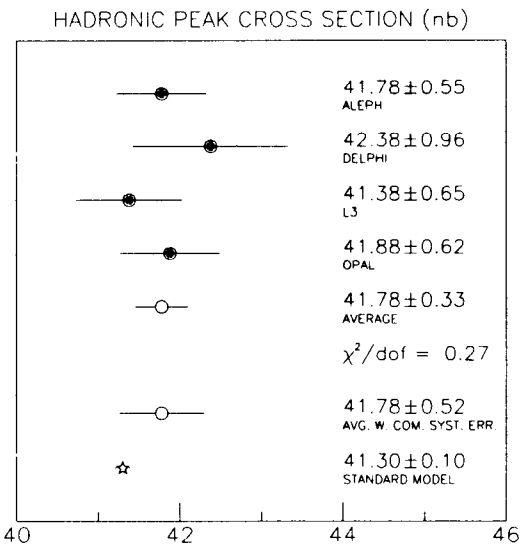

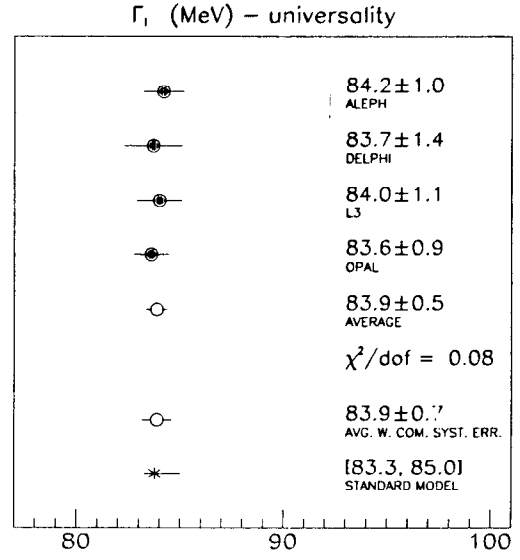

Table 3

a) Efficiencies and backgrounds of b, c, s, and u quark tagging, predicted value of $A_{FB,meas}$ for $\sin^2\theta_w = 0.23$, and statistical error, total error of $A_{FB,SM}$ including the systematic error, accuracy of $\sin^2\theta_w$. In the Born approximation $A_{FB} = 0.080$ for u, c and $A_{FB} = 0.112$ for d, s, b quarks. An integrated luminosity of 200 pb^{-1} is assumed.

	b	c	s	u
Efficiency %	11	4	6	1.4
Background %	11	34	45	30?
$A_{FB,meas}$	0.065	0.073	0.072	0.070
Statistical error	0.0026	0.005	0.004	0.008
Total error of $A_{FB,SM}$	0.0055	0.007	0.007	0.014
$\Delta\sin^2\theta_w$	0.0010	0.0015	0.0012	0.003

b) Results obtained so far on A_{ch}^{ff}

$A_{b\bar{b}}$	=	$[10.9 \pm 4.4\ (stat)] \times 10^{-2}$	L3
$A_{b\bar{b}}$	=	$[18.1 \pm 7.3\ (stat) \pm 5.9\ (syst)] \times 10^{-2}$	ALEPH
$A_{b\bar{b}}^{obs}$	=	$[1 \pm 8] \times 10^{-2}$	OPAL

c) P_τ measurement from ALEPH

Channel	Polarization
$e\nu\bar{\nu}$	$-0.24 \pm 0.16 \pm 0.07$
$\mu\nu\nu$	$-0.14 \pm 0.15 \pm 0.05$
$\pi\nu$	$-0.14 \pm 0.09 \pm 0.06$
ρ	$-0.17 \pm 0.06 \pm 0.05$
a_1	$-0.02 \pm 0.22 \pm 0.08$
Combined result $P_\tau = -0.157 \pm 0.055$	

Table 4

The merit of various measurements with and without polarization

Measurement	Corresponding precision in	
	A_{LR}	$\sin^2\theta_w$
νN scattering	0.048	0.006
νe scattering (CHARM II)	0.040	0.005
m_Z (LEP 1)	0.002	0.0003
$A_{FB}^{\ell^+\mu^-}$	0.014	0.0017
$A_{FB}^{s\bar{s}}$	0.010	0.0012
$A_{FB}^{c\bar{c}}$ (200 pb^{-1} at Z)	0.013	0.0016
$A_{FB}^{b\bar{b}}$	0.007	0.0009
p^τ	0.011	0.0014
m_W ($p\bar{p}$ collider)	0.017	0.0021
m_W (500 pb^{-1} at LEP 2)	0.005	0.0006
A_{LR} (SLC) (10^4 Z)	0.025	0.003
A_{LR} (LEP 1) (40 pb^{-1} with $P_L = 0.5$)	0.003	0.0003
$A_{FB,pol}^{\ell^+\ell^-}$ (LEP 1)	0.005	0.0006
$m_H = 10^{2\pm1}$ GeV/c^2	±0.009	±0.0011
$m_t = 110 \pm 20$ GeV/c^2	±0.005	±0.0006

Table 5

The partial width $\Gamma(Z \to q\bar{q}\ell^+\ell^-)$ in MeV. For the light quark masses one chooses $m_u = m_d = m_s = 0.3$ GeV/c^2, which represents the typical hadronic mass scale, whilst for the heavy quarks, we take $m_c = 1.5$ and $m_b = 4.5$ GeV/c^2. (From Ref. [41].)

	$u\bar{u}$	$d\bar{d}$ ($s\bar{s}$)	$c\bar{c}$	$b\bar{b}$
e^+e^-	0.71	0.23	0.57	0.14
$\mu^+\mu^-$	0.14	0.042	0.10	0.024
$\tau^+\tau^-$	0.051	0.013	0.020	0.003

Table 6

Scaling laws for compositeness tests

Contact terms: Magnitude $c \propto s/\alpha\Lambda^2$ Scale $\Lambda \propto \sqrt[4]{\int L\,dt}\sqrt[4]{s}$
Search for e^* from anomalous behaviour of $ee \to \gamma\gamma$: $(\text{Mass } e^*)^4 \propto \alpha\, s^{3/2}\sqrt{\int L\,dt}$ a)

a) The usual parameter λ in the Lagrangian is taken to be equal to 1.

Table 7

Accuracy on $\sin^2\theta_w$ from $A_{ch}^{\mu\mu}$ (for 1000 pb^{-1})

Error	ΔA (%)	$\Delta \sin^2\theta_w$
Statistical	0.1	
Systematic:		
$\Delta m_Z = \pm 20$ MeV/c^2	0.16	
Detection efficiency	0.1	
QED radiative correction	0.12	
Total	0.25	0.0012

Table 8

Accuracy on $\sin^2\theta_w$ from P_τ ($\tau \to \pi\nu$ channel only) (for 1000 pb^{-1})

Error	ΔP (%)	$\Delta \sin^2\theta_w$
Statistical	0.4	0.0005
Systematic:	0.65	0.0008
$\rho\nu$ channel		
+ radiative corrections		
+ ...		
Total	0.8	0.00095

Table 9

a) Accuracy on $\sin^2\theta_w$ from quark asymmetries $A_{ch}^{q\bar{q}}$ (25 $\times 10^6$ Z)

Type of quark	b	c	c (π of D^*)	s	u ?
Efficiency of tagging	0.11	0.04	0.15 a)	0.05	0.02
Stat. error on A_{ch}	0.0014	0.0026	0.0030	0.002	0.0036
Syst. error on A_{ch}	0.0028	0.0034	> 0.0021	0.004	0.004
$\Delta \sin^2\theta_w$ b)	0.00065	0.0011	> 0.00080	0.0008	0.0011

a) Signal/background = 1/5.

b) Without mixing.

b) Estimated error contribution to b and c charge asymmetry

Source of error	$b\bar{b}$	$c\bar{c}$
Flavour tagging	0.0020	0.0030
Beam setting	0.0004	0.0006
Detector (Delphi)	0.0002	0.0005
QED	0.0002	0.0002
QCD	0.0016	0.0013
Total syst.	0.0026	0.0034
Stat. error	0.0035	0.0070

c) Errors on the $b\bar{b}$ asymmetry $A_{ch}^{b\bar{b}}$ with mixing for two luminosities

L (pb^{-1})	200	2000
Genuine systematic error	0.0028	0.0028 a)
Statistical error (including the effect of mixing)	0.0045	0.0014
Total	0.0053	0.0031

a) Should be smaller in principle, since harder cuts are possible with high L.

Table 10

Typical conditions for obtaining $\Delta \sin^2 \theta = \pm 0.0003$ (experimental error) from A_{LR} measurement.
$L_{i,j}$ are luminosities registered with different spin configurations.

Integrated luminosity: $\int L\, dt = 50\ pb^{-1}$
Polarization: $\mathcal{P} \cong 50\%$
Uncertainty on $\mathcal{P}$: $\Delta\mathcal{P}/\mathcal{P} = 1\%$
Rate of Bhabha events: 4 × rate of Z events
Relative error on luminosity: $\Delta(L_i/L_j)_{syst.} = 1.5‰$

Table 11

Some characteristics of $Z \rightarrow b\bar{b}$ (Ref. [63])

Cross-section: $\sigma_{b\bar{b}} = 6.5$ nb.
Percentage, relative to the hadronic Z modes: $\sigma_{b\bar{b}}/\sigma_{had} = 0.22$.
Percentage, relative to the visible Z modes: $\sigma_{b\bar{b}}/\sigma_{vis} = 0.19$.
Population of various species, from 100 million Z: $15.5 \times 10^6\ B^0$ $15.5 \times 10^6\ B^+$ $4.5 \times 10^6\ B_s^0$ $1.7 \times 10^6\ \Lambda'_b$ $0.35 \times 10^6\ \Xi'_b$
Mean number of charged particles per B: ~ 5.
Mean number of charged particles at the primary vertex: ~ 10.
Mean flight path of B: ~ 2.2 mm.

Table 12

The percentage of well-classified events is 80.3 ± 0.9%. Example of a classification of 2000 $Z \rightarrow q\bar{q}$ events between four classes: L (q = u, d, s); C (q = c); B (q = b); T (q = t). Events are classified according to a 'class likelihood' derived from 15 variables, seven of which use the measurement of impact parameters given in the barrel region by the microvertex detector. (Ref. [64].)

	Class generated				
Classified	Purity	L	C	B	T
L	90.8%	1012	87	14	2
C	47.0%	173	187	38	0
B	87.4%	9	41	348	0
T	66.3%	14	4	12	59
Loss		16.2%	41.4%	15.5%	3.3%

Tagging of beauty on one arm
ϵ is the efficiency, A the percentage of the asymmetry effectively observable; G ($= A\sqrt{\epsilon}$) is the figure of merit (Ref. [63])

Process	ϵ (%)	A (%)	G (%)
Semileptonic decays	7	67	18
Exclusive D signals	3.5	84	16
Charge of the B	11	80	26
	30	64	35
Beam polarization ($\mathcal{P} = 45\%$)	63	45	36

Table 13

Vertex detector: present and future

Microvertex 1 (present one of DELPHI)			
R_1 (cm)			9
R_2 (cm)			11
σ (μm) (1 coordinate)			5
Si thickness (μm)			400
Al thickness of vacuum chamber (mm)			1
θ_{min} (°)			42
p (GeV/c)	3	4.7	14
Transverse accuracy (μm)			
without microvertex	136	90	41
with microvertex	54	41	27
σ along flight path (μm)			
(secondary vertex)		250	
Microvertex 2 (ideal)			
R_1 (cm)			5
R_2 (cm)			8
R_3 (cm)			11
σ (μm) (2 coordinates)			5
Si thickness (μm)			200
Be thickness of vacuum chamber (mm)			1
θ_{min} (°)			20
p (GeV/c)	3	4.7	14
Transverse accuracy (μm)	27	19	11.6
σ along flight path (μm)			
(secondary vertex)		150	

Table 14

The expected number of B mesons per 10^7 Z's is calculated with the theoretical values of the B branching fractions. No acceptance or efficiency factors are included. For D-meson and light-meson branching fractions, the Particle Data Group values are assumed, except for BR($D_s \to \phi\pi$) where 4% is used. [Branching fractions in %.]

Decay channel	ARGUS	CLEO	THEORY	No. B/10^7 Z
$B_d^0 \to D^{*-}\pi^+$ $D^{*-} \to \overline{D^0} + \pi^+$ $\overline{D^0} \to K^+\pi^-$	$0.35 \pm 0.18 \pm 0.13$	$0.16 \pm 0.12 \pm 0.10$	0.15	100
$B_d^0 \to D^+\pi^-$ $D^- \to K^+\pi^-\pi^-$	$0.31 \pm 0.13 \pm 0.10$	$0.16^{+0.32+0.15}_{-0.28-0.12}$	0.58	550
$B_u^+ \to \overline{D^0}\pi^+$	$0.19 \pm 0.10 \pm 0.06$	$0.51^{+0.17+0.11}_{-0.15-0.07}$	0.37	170
$B_s^0 \to D_s^-\pi^+$ $D_s^+ \to \phi\pi^-$ $\phi \to K^+K^-$			0.5	30
$B_d^0 \to J/\psi + \overline{K^{*0}}$ $J/\psi \to \ell^+\ell^-$ $\overline{K}^{*0} \to K^+\pi^-$	0.33 ± 0.18	0.06 ± 0.03	0.39	430
$B_u^+ \to J/\psi + K^+$ $J/\psi \to \ell^+\ell^-$	0.07 ± 0.04	0.05 ± 0.02	0.09	150
$B_s^0 \to J/\psi + \phi$ $J/\psi \to \ell^+\ell^-$ $\phi \to K^+K^-$			0.3	70

Table 15

Comparison of B-factory techniques (from Ref. [70])

Factor	Case				
	Asymmetric T(4S)	Symmetric T(4S) +	$\sqrt{s}$ = 16 GeV	Z P = 0	Z P = 0.9 (P = 0.45)
$b\bar{b}$ cross-section (nb)	1.2	0.3	0.11	6.3	6.3
Fraction of B^0	0.43	0.34	0.35	0.35	0.35
ψK_S reconstruction efficiency	0.61	0.61	0.61	0.46	0.46
Tagging efficiency (and method)	0.48 (ℓ, K)	0.48 (ℓ, K)	0.30 (ℓ, D)	0.18 (ℓ, D)	0.61 (A_{FB})
Wrong tag fraction	0.08	0.08	0.08	0.08	0.125 (0.27)
Asymmetry dilution	0.71	0.63	0.52	0.52	0.71
$\int L\,dt$ needed for 3σ effect (10^{40} cm^{-2})[a]	0.3-12	2.2-78	14-490	0.5-19	0.1-3.6 (0.3-9.6)
Relative $\int L\,dt$ needed	1.0	6.4	40	1.5	0.3 (0.8)

a) The peak luminosity needed in units of 10^{33} cm^{-2} s^{-1} for 10^7 seconds of fully efficient running at peak luminosity.

Table 16

(From E. Picasso, ECFA meeting, Dec. 1989)

Number of cavities for different collision energies

Number of SC cavities	8	32		64		128		192	
Date installed		1992		1993				1994	
Acc. gradient (MV/m)	5	5	7	5	7	5	7	5	7
Total accelerating voltage	68	272	381	545	760	1090	1520	1635	2280
Beam energy (3 mA current)									
SC cavities alone	36.3	51.3	55.8	64	69.5	76	82.6	84.1	91.4
SC and Cu cavities	58.75	64.3	66.8	73.4	77.2	82.2	87.6	88.9	95.2

Table 17

Scaling laws in the case where the beam-beam tune shift ξ_Y is made constant

Stored beam current	Luminosity	Beam size	$Q^3 J_x$
Constant	$\propto \gamma$	$\propto 1/\sqrt{\gamma}$	$\propto \gamma^3$
$\propto \gamma$	$\propto \gamma^2$	Constant	$\propto \gamma^2$

Table 18

The sample of W pairs at LEP 2

$\int L\,dt$ =	500 pb^{-1}
$\sqrt{s}$ =	190 GeV
m_W =	80.3 GeV
$\sin^2\theta$ =	0.229

produced ⟶	W → $\ell\nu$ ⟶ selection (ℓ = e, μ)	e, μ
7150 WW	2000	1600

Table 19

Systematic uncertainties in relative luminosity measurement in L3

Parameter at IP	Typical value	Known to	Absolute change in ‰ for typical value	Systematic uncertainty (‰)
$\langle x \rangle$	100 μm	15 μm	0.1	0.10
σ_x	300 μm	10 μm	1.5	0.05
$\langle y \rangle$	100 μm	5 μm	0.1	0.03
σ_y	12 μm	1 μm	0.06	0.01
$\langle z \rangle$	1 mm	0.7 mm	0.1	0.11
σ_z	33 mm	0.5 mm	1.5	0.08
$\langle x' \rangle$	0	2 μrad	0	0.01
$\sigma_{x'}$	175 μrad	5 μrad	0.05	0.01
$\langle y' \rangle$	0	10 μrad	0	0.04
$\sigma_{y'}$	175 μrad	5 μrad	0.05	0.01
Total (errors added linearly)				0.4

Table 20

Integrated luminosities needed under various assumptions. (Estimated number of 10^6 Z events needed to measure A_{LR} with $\Delta A_{LR} = 3$‰.) $\Delta(L_i/L_j)_{syst}$ is the systematic error on the relative luminosity measurement of bunch i to bunch j; γ is the ratio of Bhabha events to Z events; 10^6 Z events are obtained with $\sim 40\ pb^{-1}$.

P (%)	$\Delta(L_i/L_j)_{syst}$ (‰)	$\gamma = 1$	$\gamma = 4$	$\gamma = 15$
50	0.5	1.5	0.9	0.8
	1.0	1.6	1.0	0.8
	1.5	1.9	1.2	1.0
	2.0	2.7	1.7	1.5
30	0.5	6.2	3.9	3.3
	1.0	9.3	5.8	4.9
	1.5	48.0	30.0	25.5